2002

# Development and Structural Testing of FRP Reinforced OSB Panels for Disaster Resistant Construction

Eric Dana Cassidy

# DEVELOPMENT AND STRUCTURAL TESTING OF FRP REINFORCED OSB PANELS FOR DISASTER RESISTANT CONSTRUCTION

Eric Dana Cassidy

B.S. University of Maine, 2000

A THESIS

Submitted in Partial Fulfillment of the

Requirements for the Degree of

Master of Science

(in Civil Engineering)

The Graduate School

The University of Maine

December, 2002

Advisory Committee:

William G. Davids, Assistant Professor of Civil Engineering, Advisor

Habib J. Dagher, Professor of Civil Engineering

Douglas Gardner, Professor of Wood Science and Technology

# DEVELOPMENT AND STRUCTURAL TESTING OF FRP REINFORCED OSB PANELS FOR DISASTER RESISTANT CONSTRUCTION

By Eric Dana Cassidy

Thesis Advisor: Dr. William G. Davids, P.E.

An Abstract of the Thesis Presented
in Partial Fulfillment of the Requirements for the
Degree of Master of Science
(in Civil Engineering)
December, 2002

The resistance of conventionally constructed wood-framed structures to extreme events such as earthquakes and hurricanes depends in large part on the strength and energy absorption characteristics of the shear walls. These shear walls are often sheathed with oriented strand board (OSB) panels, and their performance is primarily a function of the nailed sheathing-to-framing connections at the panel edges. A new sheathing panel called Advanced OSB (AOSB) has been developed at the University of Maine's Advanced Engineered Wood Composites Center. The AOSB panel integrates glass fiber-reinforced polymer (GFRP) reinforcing into regions of the OSB panel that have been observed to fail under hurricane or earthquake loading. Structural testing of both single nail connections and full scale shear walls have shown that AOSB has great potential for increasing the energy dissipation capacity and lateral load resistance of wood-framed structures subjected to extreme wind and seismic events.

The GFRP reinforcement increases the lateral resistance of conventional wood-framed shear walls by improving the strength and ductility of the sheathing-to-framing nail connections. AOSB changes the primary failure mode of the sheathing-to-framing nails from a shear out type failure where the nail tears through the edge of OSB to a more ductile and energy absorbent failure mode where the nails exhibit double curvature and are withdrawn from the framing.

The results of monotonic tests on single-nail connections show that the strength of an individual nailed connection can be increased by about 39% and the energy dissipation capacity can be more than quadrupled through the use of AOSB. Results of cyclic connection tests with AOSB compared to those of plain OSB specimens indicate that the AOSB panels are less sensitive to damage accumulation from repeated load cycling.

Standard size (8ftx8ft) shear wall specimens sheathed with AOSB panels tested in accordance with ASTM E564 were able to maintain at least 80% of their peak load up to a drift of approximately 5.5 in. compared to approximately 4.0 in. for walls sheathed with conventional OSB. When tested cyclically, the conventional OSB sheathing panels were extensively damaged due to edge tear of nails, however very little damage of the AOSB panels was observed. This, coupled with the fact that failure of the AOSB walls was driven primarily by nail fatigue and nail pullout, indicates that AOSB sheathing panels provide as much capacity as the framing and the nails will allow.

A finite element model of two panel AOSB shear walls was developed using the commercial software ANSYS. The primary goal of this model was to capture the

complex load sharing behavior of the AOSB shear wall system to aid future design improvements of AOSB shear wall systems. The model results are in good agreement with the results of the static wall tests.

AOSB panels appear to have great potential for increasing the energy dissipation capacity and lateral load resistance of wood-framed structures subjected to extreme wind and seismic events. Ongoing research efforts at the University of Maine will help to further refine and optimize the AOSB technology.

## ACKNOWLEDGEMENTS

I would like to thank all of the members of my graduate committee. Initial thanks go to Bill for not only being accommodating, generous with his time, and a great person to work with, but also for being a good friend. I would also like to thank Habib, whose inexplicable confidence in my abilities and perpetually optimistic attitude has been truly inspiring. Thanks to Doug for all of the input on aspects of this research that deal more with polymer science than structural engineering.

On a more personal note I would like to thank all of the lifelong friends that I have made here at the University of Maine. I would also like to thank Matthew Richie and Kyle Wentworth, for the countless hours of work that they put into this project. My greatest thanks go out to my parents and my long time girl friend for all of their support throughout this experience.

Finally I would like to acknowledge the National Science Foundation for providing the funding for this research.

## TABLE OF CONTENTS

## LIST OF TABLES

## LIST OF FIGURES

# Chapter 1

# INTRODUCTION

## 1.1 Background

According to recent United States Census Bureau data, the in-place value of housing constructed during 1998 was $189 billion, which represents 28% of the total value of all 1998 building construction (http://www.census.gov/pub/const). The vast majority of new homes are built using conventional, stick-built lumber construction (AF&PA 1995). In recent years, the U.S. has sustained many expensive weather-related disasters, totaling $90 billion in damages between August 1992 and May 1997 (http://www.fema.gov). As such, increasing the disaster resistance of wood-framed residential construction is a critical research need.

A sufficiently strong, ductile and energy-dissipating lateral force-resisting system (LFRS) is crucial for adequate building performance in extreme wind or seismic events. In housing construction, the LFRS typically consists of interconnected vertical and horizontal diaphragms. In stick-built construction, these diaphragms are generally fabricated from Oriented-Strand Board (OSB) or plywood sheathing panels, which are nailed to lumber framing. OSB use continues to increase at the expense of plywood, and today OSB has taken a significant portion of the plywood market for sheathing and flooring applications.

When built properly, wood buildings generally perform well in earthquakes and hurricanes. However, connection failures and noncompliance with good construction

practices or building codes have generally been responsible for most structural failures (Yancey *et al.* 1998). Inadequate nailing of plywood or OSB sheathing reduces the building's resistance to lateral load and often results in shear wall failure. When adequate nailing is provided no failures are typically observed.

## 1.2 Research Objective

The objective of this study was to develop an optimized synthetic fiber-reinforced OSB panel, which significantly improves the disaster resistance and lowers ownership cost of conventional wood-frame construction. It is well known that the performance of wood-framed shear walls (vertical diaphragms) with panelized sheathing is highly dependent on the nail spacing at the panel edges. This thesis details research efforts into the development and structural testing of an Advanced OSB (AOSB) panel that have been conducted over the past two years. The AOSB panel is selectively reinforced with fiber-reinforced polymer composites (FRPs) at the panel edges to increase the lateral resistance of conventional wood-framed shear walls by improving the strength and ductility of the sheathing-to-framing nail connections. The AOSB panel is a sandwich panel consisting of thin outer sheets (1/4" thick) of OSB with an FRP composite sandwiched between OSB panels at the edges. The reinforcement has been designed specifically to (see Figure 1.1):

1) *Reduce nail edge-tear failures around the sheathing panel perimeter*. Shear wall failures are often precipitated by inadequate panel perimeter nail edge distance or a larger than allowed perimeter nail spacing. This leads to edge splitting of the

sheathing panel around the nails, or "edge tear", preventing the full shear capacity of the panel from being developed.

2) *Reduce nail-head pull-through failures.* Nail heads pulling through the sheathing panels has been observed in laterally loaded shear walls as well as roof diaphragms subject to negative pressure from high wind loading.

3) *Improve energy dissipation capacity under load cycling.* The tests of Shenton *et al.* (1997) showed that enlarging of nail holes due to localized crushing of panel fibers reduces the energy dissipation capabilities of shear walls after the initial load cycle.

4) *Meet or exceed the weather exposure requirements of conventional OSB.* Sheathing panels used in shear wall and horizontal diaphragm applications are not typically classified as exterior exposure, however they may be exposed to inclement weather during construction. Specific attention has been paid to the strength and water resistance of the adhesive bond between the OSB and FRP, to ensure this bond performs as well or better than the internal flake-to-flake bond of the OSB itself.

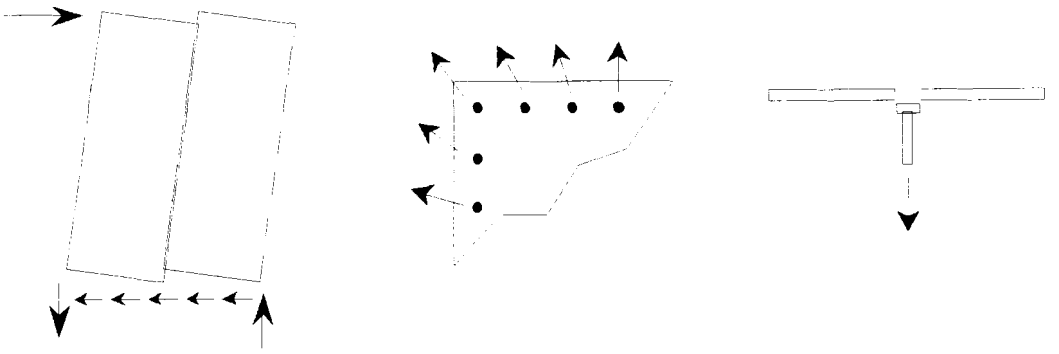

Loaded Shear Wall  Edge Tear  Nail Head Pull-Through

**Figure 1.1 Deformed Shear Wall and Critical Failure Modes.**

5) *Look the same and install the same*. Attempts to market products that require specialized construction techniques are typically met with considerable resistance from the construction community. AOSB has been designed so that it can be installed using standard construction practices.

## 1.3 Research Approach

The research program was divided into the tasks shown below.

1) Screening and Selection of Reinforcing Materials

2) Connection Tests

   a. Monotonic tests of single nail connections

   b. Cyclic tests of single nail connections

c. Nail head pull-through tests

3) Shear Wall Tests

a. Static Shear Wall Tests

b. Cyclic Shear Wall Tests

4) Computer Modeling of Shear Walls

This thesis has been organized according to the tasks listed above, the order of which coincides with the order that the research was performed. To provide adequate background information on each task, a literature review covering each topic is provided in Chapter 2. Discussion of the experimental work performed in this study begins with Chapter 3, with methodology and results of connection level testing of AOSB specimens. Three types of connections tests were performed: monotonic tests of nailed connections, cyclic tests of nailed connections and nail head pull-through tests. Control specimens built with 7/16 in. thick OSB were also tested to provide a baseline for comparison. The methodology and test results used for screening and selection of reinforcing materials for AOSB is documented seperately in Cassidy *et al.* (2002). Structural testing of shear walls is the topic of Chapter 4. Similarly to the connection tests, both control and AOSB walls were tested to allow for comparison and quantification of the benefits of AOSB sheathing panels. Both static and cyclic shear wall tests were performed.

Chapter 5 describes the development of a two-dimensional finite element model of two panel AOSB shear walls with 4 in. perimeter nail spacing. The model was developed

using the computer program ANSYS 5.7 (ANSYS 2000). The model has 15,749 degrees of freedom and employs a small displacement nonlinear analysis to model the monotonic load-deflection response of the shear wall test specimens discussed in Chapter 4. The computer results correlate reasonably well with the experimental data from the static wall tests. Chapter 6 presents a summary of the research conducted in this study, and gives conclusions and recommendation for further research.

# Chapter 2

## REVIEW OF RELEVANT LITERATURE

Plywood panels with fiberglass skins have been used for many years for numerous applications including truck, trailer and van bodies, intermodal and reusable shipping containers, concrete forming, sewage treatment tanks, walk-in coolers, railcar linings and siding panels (APA 1972, 1992, 1998). However, the use of wood-based structural panels that are selectively reinforced with FRP in shear wall and horizontal diaphragm applications is a relatively new idea. To the best of the authors knowledge the University of Maine is one of only two Universities performing research in this area. The other is Brigham Young University in Provo, Utah. The research at Brigham Young has been and continues to be performed under the direction of Fernando S. Fonseca, PhD, P.E. Fonseca and his graduate research staff have published results of two pilot studies. Since these studies are highly relevant to the development of AOSB and disaster resistant construction in general, a detailed discussion of the methods and results of these studies is provided in this chapter.

Published literature pertaining to testing and modeling of full-scale shear walls and intra-component connections has become quite prevalent in recent years. Much of this literature was reviewed in the process of developing and testing AOSB. The purpose of the literature review was to ensure that pertinent issues were being addressed in the design of AOSB and that the testing facilities and procedures used were representative of the current standards and trends of the progressively evolving field of wood-frame shear

wall research. The literature survey provided guidance in the design of the experimental testing program as well as valuable insight used in the development of a finite element model of two panel AOSB shear walls described in Chapter 5. The topics of the literature reviewed include monotonic and cyclic testing of both nailed connections and full-scale shear walls, as well as computer modeling of shear walls.

## 2.1 GFRP and Reinforced Plywood Panels

The methods and results of the two studies performed at Brigham Young University are presented in this section. The first study investigated the advantages of hybrid diaphragms consisting of both plywood panels and glass fiber reinforced polymer (GFRP) panels. The second study addressed the behavior of plywood shear walls with fiberglass edge reinforcement.

### 2.1.1 Hybrid Diaphragms

Judd and Fonseca (2002) investigated the advantages of diaphragms using plywood and GFRP sheathing (hybrid diaphragms). Both coupon tests and full-scale diaphragm tests were performed. The sheathing materials used included 3/8 in. plywood and 1/4 in. retail GFRP sheathing panels. The GFRP panels had a uni-directional fiber orientation and were manufactured by Strongwell Inc. These panels consist of a combination of glass fiber and isophthalic resin (EXTREN Series 500). The mechanical properties of the GFRP panels are published by the manufacturer in the EXTREN Design Manual (1998). The modulus of elasticity parallel to the fiber direction is 2,601,977 psi, the shear modulus is 425,251 psi and the material has a Poisson's ratio of 0.33. Nominal

2x4 Douglas Fir-Larch No.2 framing members were used for both the connection and full-scale diaphragm tests.

#### 2.1.1.1 Connection Tests

Both monotonic and cyclic connection tests were performed. The monotonic loading was similar to the ISO Standard 6891-1983, where a ramp load is applied at a rate of 0.1 in. per minute until failure (ISO 1983). The cyclic loading was a modified form of the proposed ISO (1997) lateral loading procedure. This loading consists of a series of quasi-static fully reversed cycles. Multiple blocks of three fully reversed cycles at constant displacement amplitude are performed followed by three cycles of increased amplitude. This pattern continues until failure.

Three sizes of common nails were considered in the connection tests: 8d, 10d and 16d. Preliminary tests of connections with 12d common nails were also performed. The reason for the preliminary study was to investigate the effect of nail length; as the only difference between 10d and 12d common nails is the length. Three tests were performed and no significant differences between 10d and 12d nails were observed, so no further investigation of 12d nails was performed.

The GFRP panels were oriented with the fibers parallel to the studs and perpendicular to the applied load. The grain of the framing members was also oriented perpendicular to the applied load. The most commonly observed failure modes were nail withdrawal and splitting of the framing (see Table 2.1). Withdrawal was most common for GFRP connection specimens fabricated with 8d nails, however splitting of the wood became the most common failure when larger diameter nails (10d and 16d) were used.

No tests of connections with plywood sheathing were performed in this study. The GFRP connection test results were compared to the results of previous tests performed by Dugan (1995) using a similar specimen configuration and loading protocols. The specimens tested by Dugan consisted of 3/8 in. CDX structural grade plywood and 8d common nails. The failure mode of all plywood specimens was in the form of the nails tearing through the sheathing edges.

**Table 2.1 Monotonic Connection Response (after Judd & Fonseca 2002).**

| Connection Type | Primary Failure Mechanism (as a Percent of Total Specimens) | | | |
|---|---|---|---|---|
| | Nail Withdrawal | Nail Fatigue | Sheathing Failure | Wood Splitting |
| PLY-8d | --- | --- | 100 | --- |
| GFRP-8d | 56 | --- | --- | 44 |
| GFRP-10d | 17 | --- | --- | 83 |
| GFRP-16d | 11 | --- | --- | 89 |

The most common failure mechanism observed in the cyclic tests for 8d and 10d nailed connections was nail fatigue (See Table 2.2). All of the GFRP-8d specimens and 62% of the 10d specimens exhibited nail fatigue failure. Splitting of the framing was the second most common failure mode for GFRP-10d specimens. No nail fatigue failures occurred for specimens connected with 16d nails. Wood splitting was the most common failure mode followed by nail withdrawal for the 16d nail connections. Half of the plywood specimens tested by Dugan failed by nail fatigue while the other half exhibited sheathing failure.

For comparison of the results, the monotonic load-displacement curves and cyclic envelope curves were idealized with a mathematical equation originally developed to model the response of reinforcing steel in concrete beams (Menegotto and Pinto 1973; Stanton and McNiven 1979). The nonlinear equation, which consists of an initial asymptotic line or initial stiffness joined to a second asymptotic line (secondary stiffness) using a varying transition curvature, was said to provide an accurate description of monotonic and cyclic envelope load-displacement curves characteristic of sheathing to framing connections (Judd & Fonseca 2002; Fonseca 1997).

**Table 2.2 Cyclic Connection Response (Judd & Fonseca 2001).**

| Connection Type | Primary Failure Mechanism (as a Percent of Total Specimens) | | | |
|---|---|---|---|---|
| | Nail Withdrawal | Nail Fatigue | Sheathing Failure | Wood Splitting |
| PLY-8dc | --- | 50 | 50 | --- |
| GFRP-8dc | --- | 100 | --- | --- |
| GFRP-10dc | 8 | 62 | --- | 30 |
| GFRP-16dc | 25 | --- | 17 | 58 |

Respective monotonic strength increases of 47%, 81% and 125% over Dugan's plywood specimens were produced with GFRP connections using 8d, 10d and 16d common nails. Cyclic strengths were increased by 53% for 8d connections and 115% for 10d and 16d nailed connections. Strength and stiffness degradation of GFRP connections was found to be less than that of plywood connections.

GFRP connections using 8d nails were found to be approximately twice as stiff under monotonic loading as 8d nailed plywood connections. The energy absorption of each connection type was calculated as the area underneath the idealized load-displacement curves up to the maximum displacement. Plywood connections absorbed between 50 and 100% less energy than GFRP connections.

The connection test results were compared to the theoretical strengths calculated using general dowel equations (American Wood Council 1999). On average the theoretical strengths were found to be 93% of the measured strength for GFRP connections. Given this result it was concluded that dowel equations may be used to evaluate connections using different sheathing materials, thicknesses, mechanical fasteners and wood framing.

#### 2.1.1.2 Diaphragm Tests

Two tests of 24 x 12 ft. diaphragms were performed. First a conventional diaphragm with 3/8 in. structural grade A-C exterior plywood sheathing, 8d common nails and 2x4 joists spaced at 24 in. o.c. was tested. The nailing schedule included nails spaced at 4 in. o.c. along the diaphragm boundary and along continuous panel edges, 6 in. o.c. along non-continuous panel edges and a 12 in. nail spacing in the field. After testing the conventional diaphragm, the hybrid diaphragm was assembled by replacing the damaged corner plywood panels of the previously tested conventional diaphragm with GFRP sheathing panels.

Damage of the conventional diaphragm was concentrated in the corner plywood sheathing panels. Sheathing failure was caused by nails tearing through the edges of the

sheathing along the diaphragm perimeter. The nails remained essentially undeformed suggesting to the authors that the nails remained largely in the linear elastic range and were not loaded to capacity. This being the case, the plywood sheathing limited the strength of the diaphragm.

The plywood sheathing sustained most of the damage in the hybrid diaphragm. The nails tore through the edges of the plywood panels, similar to the test of the conventional diaphragm. The GFRP panels in the diaphragm corners were undamaged.

The hybrid diaphragm exhibited a 34% strength increase over the conventional diaphragm. The hybrid diaphragm also showed a 25% increase in initial stiffness and absorbed 46% more energy than the conventional diaphragm. The authors suggested that the strength increase may represent a lower-bound on the capacity of a hybrid diaphragm since the plywood panels used were already damaged from the previous test.

The results of the diaphragm tests were compared to the strength predicted by summing the contributions from individual sheathing-to-framing connections resisting the load-namely the perimeter connections transverse to the applied load. The actual diaphragm unit shear was compared to the unit shear predicted by this approximation. The measured diaphragm unit shear was consistently 83% of the predicted value for both conventional and hybrid diaphragms.

### 2.1.2 Plywood Shear Walls with Fiberglass Edge Reinforcement

Six 8x8 ft. shear walls with the sheathing panels oriented vertically were tested in this study. All but one wall was tested cyclically following the Sequential Phase Displacement Loading Protocol (SPD) developed by the Structural Engineers Association

of Southern California (SEAOSC) Ad Hoc Committee. The other wall was tested statically according to ASTM 564 (ASTM 1998a).

The wall specimens consisted of nominal 2x4 framing with two 4x8 ft. plywood sheathing panels. The framing material was No. 2 Douglas Fir-Larch. Both the top and bottom plates of the wall were doubled to provide enough clearance so that the sheathing panels could rotate freely without bearing on the testing machine. The wall frame was assembled with gun driven 10d nails manufactured by Halsteel. The nails were 3 inches long and 0.131inch diameter. The plywood panels were three-ply A-C Group 1 exterior grade with a thickness of 11/32 in.. The sheathing was attached to the framing with hand driven 8d common nails. Nail spacing around the perimeter of the panels was 6 in. and a 12 in. spacing was used in the field. Advanced Connector Systems AHD15A hold-downs were connected to the end studs in both bottom corners of the walls.

Woven fiberglass tape was used as panel edge reinforcement. The tape was a plain weave (0/90) fabric weighing 9-ounces per square yard. The reinforcing strips were 1-1/2 in. wide and 0.012 in. thick. The glass tape was bonded to the plywood panels with an isophthalic polyester resin. The application of the reinforcing was performed with a wet lay up procedure, meaning that the fabric was set in place and saturated with resin. The reinforcement was allowed to cure under pressure at room temperature for 24 hours before constructing the walls.

One conventional (unreinforced) wall was tested monotonically under displacement control. This wall exhibited failures typical of conventional shear walls. Nails tearing through the edge of the sheathing and nail heads pulling through the

sheathing were the primary failure mechanisms. A rapid progression of these failures was observed along the left edge of the left panel. This failure progression is commonly referred to as "unzipping" meaning that the panel separates from the framing due to sheathing failures localized at the nail locations.

Similar failure modes were observed in the three conventional walls that were tested cyclically. Nail fatigue failures were also prevalent in the walls tested cyclically. The nail fatigue failures are likely a result of the SPD loading protocol. The SPD loading has since been criticized because nail fatigue failures are not typically observed in earthquake reconnaissance studies. However, at the time of this study, SPD was the most widely accepted cyclic loading protocol.

Two reinforced walls were tested cyclically. The wall behavior was improved by the addition of the fiberglass edge reinforcement. Edge tear failures were eliminated entirely and the occurrence of nail-head pull-through was reduced. The authors note that the fiberglass reinforcement may increase shear wall capacity more than the test results indicate. Their rationale for this conclusion centers on the numerous occurrences of nail fatigue failures observed in the tests of both conventional and reinforced walls. Once the nails have sheared, the reinforcement becomes useless. Since sheared nails are rarely observed during earthquakes, the test results may not be indicative of the true benefit provided by the reinforcing (Fonseca *et al.* 2001).

## 2.2 Sheathing-to-Framing Connections

Intra-component connections such as sheathing-to-stud connections, subfloor-to-joist connections, etc. provide the bulk of the energy dissipation within a lateral-force-

resisting-system. Salenikovich (2000) states that "It is well known that yielding of nails between sheathing and framing is the main source of ductility in typical shear walls. When other means of connection are used, such as screws and/or adhesive, the ductility and the failure mode can change significantly." They also play a critical role in developing maximum shear wall capacity, since shear wall failures are often governed by connection strength. A number of tests have been conducted over the years to determine the static strength of individual fasteners; generally these tests follow the criteria outlined in ASTM D1761 (ASTM 1998b).

In the past, investigation of nailed connections has been focused on monotonic racking performance because the design codes of North America are based on the monotonic performance of shear walls (Dolan & Madsen 1992a). Recognizing the need for better models, capable of predicting the response of timber structures to dynamic loads, researchers began to study the cyclic response of shear walls and nailed connections in the mid 1980s. Unfortunately no standard test method exists for cyclic testing of timber joints or cyclic testing of shear walls for that matter. Despite the recognized need for standardization to facilitate comparison of results, cyclic connections test results provide a good indication of the energy dissipating capability as well as strength and stiffness degradation properties of individual sheathing-to-framing connections. While reversing cyclic loads are not representative of the random loads experienced during an earthquake they provide an adequate means of quantifying the hysteretic behavior of sheathing-to-framing connections (Dolan & Madsen 1992b).

Published studies of the monotonic and cyclic behavior of nail connections are reviewed in this section. Most of the experimental studies in the literature have been performed with either plywood or waferboard sheathing. The dissertation of Salenikovich (2000) is the only publication that the author is aware of where OSB was used as the sheathing material.

### 2.2.1 Numerical Modeling of Nonlinear Load-Slip Relationship

Most often, the primary motivation for experimental testing of nailed sheathing-to-framing connections has been to quantify the "average" load-slip relationship for inclusion in computer models of larger shear wall systems. For this reason it is desirable to approximate the load-displacement curve with a mathematical function, which allows for closed-form mathematical solutions (Salenikovich 2000). Several empirical models have been proposed to model the monotonic load-displacement relationship of nailed connections. One of the earliest and most often cited models was originally developed by Foschi (1974). Foschi studied the load-slip characteristics of nails, considering that the nail yields in bending and the wood under the nail fails in bearing. The model proposed by Foschi represents a nail on an elastic-plastic foundation and is expressed by Equation 2.1.

$$F_n = (P_0 + K_1\delta)\left[1 - \exp(\frac{-K_0\delta}{P_0})\right] \qquad 2.1$$

The meaning of the constants $K_0$, $K_1$ and $P_0$ are illustrated in Figure 2.1. $K_0$ is the initial stiffness, $K_1$ is the secondary stiffness and $P_0$ is the load-intercept of the secondary stiffness asymptote. Dolan (1989) modified the Foschi equation to include a linear descent for excursions beyond peak load. The modified equation is as follows:

$$F_n = (P_0 + K_1\delta)\left[1 - \exp(\frac{-K_0\delta}{P_0})\right] - K_2(\delta - \delta_{peak}) \qquad 2.2$$

In equation 2.2, $K_2$ defines the slope for deformations greater than $\delta_{peak}$ as is shown in Figure 2.2.

Chui and Ni (1997) proposed modifying the Foschi equation to take into account strength degradation effects. A presentation of the proposed modifications is beyond the scope of this text. However, the basic premise consists of adding an additional term to the equation which subtracts from the nail force at displacements above $\delta_{peak}$.

As stated previously several other empirical models have been developed to provide a closed form approximation of the monotonic load-slip relationship of nailed sheathing-to-framing connections. The Foschi model is the only one presented here as it is the most often cited. For more information on other models that have been proposed see Salenikovich 2000.

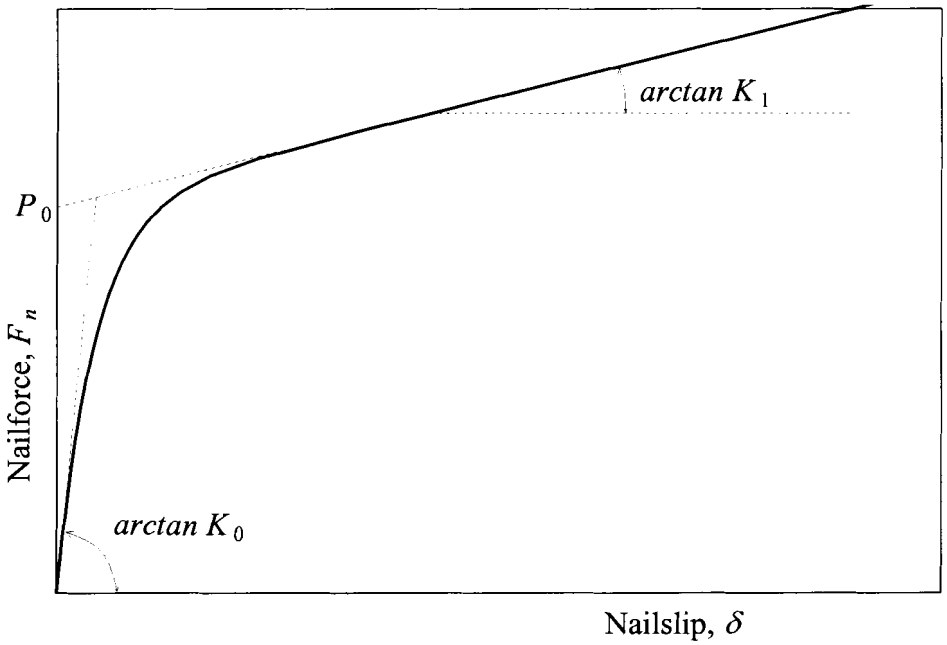


**Figure 2.1 Foschi load-slip curve (Salenikovich 2000).**

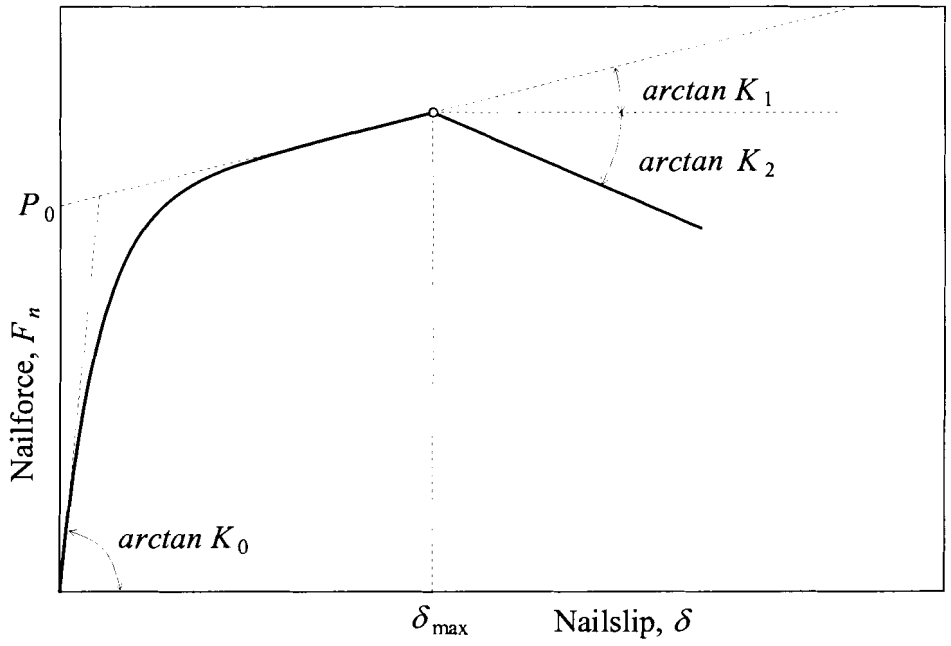


**Figure 2.2 Dolan-Foschi load-slip curve (Salenikovich 2000).**

The cyclic load-displacement response of nailed connections is typically modeled following the approach of Dolan and Madsen (1992b). In this approach, the hysteresis loop is defined by four segments. Four equations are used to define the four segments. Each segment is defined by four boundary conditions: $K_0$, $P_0$, $K_2$, $P_1$, $K_4$, where $K_0$, $P_0$, $K_2$ are as defined previously in Figure 2.2. $K_4$ and $P_1$ describe the pinching portion of the loop where $K_4$ defines the stiffness and $P_1$ is the load intercept. Variations of this approach, which requires fitting parameters to the experimental data, have been employed by several researchers (e.g. Chui and Ni 1997, Folz and Filliatrault 2001). More complex finite element models of individual connections which assume that the connection behaves essentially as an elastoplastic pile (steel nail) embedded in a layered nonlinear foundation (sheathing and framing material) have been developed by various researchers (e.g. Foschi, 1974, 2000; Chui *et al.* 1998). While these models are capable of capturing the detailed cyclic response, they are generally regarded as being too computationally demanding for inclusion in shear wall models (Folz and Fillitrault 2001).

### 2.2.2 Experimental Studies

Dolan and Madsen (1992a) performed monotonic and cyclic tests of both plywood and waferboard nail connections. The tests were part of a larger study aimed at investigating the behavior of timber shear walls subjected to earthquakes. The average nonlinear load-deflection curves were used with two finite element models to predict the behavior of full-size shear walls.

The monotonic test data were analyzed using a least squares regression method to fit the data to the Foschi equation. Since the shear wall specimens being modeled used a minimum of 100 nails, an average load-displacement curve was considered a sufficient means of modeling the sheathing-to-framing connections. "The wall specimen, as a whole, will experience the 'average' nail behavior." (Dolan & Madsen 1992a).

The materials used in this study included SPF framing, 3/8 in. three-ply Canadian softwood plywood and solid exterior grade waferboard. The sheathing was attached to the framing with 8d common nails.

In addition to modeling input, the connection test results were used to address four other issues:

1. Comparison of the performance of plywood and waferboard sheathing in shear walls.
2. Determine if the load-displacement curves were dependent on the grain orientation of either the sheathing or the framing materials.
3. Investigate the effect of load rate on connection response.
4. Confirm or deny the hypothesis that the hysteretic response of nailed connection is contained within an envelope defined by the monotonic load-displacement curve.

Plywood connections were found to be less stiff and weaker than waferboard connections. This was attributed to different failure modes of the two types of connections. Plywood specimens were observed to fail by nail-head pull-through while the waferboard specimens usually failed by either the nail breaking or pulling out of the framing material.

For plywood specimens, the face grain orientation was found to affect the secondary stiffness of the connection load-displacement curve, however, initial investigation of this parameter using the numerical models developed in Dolan's 1989 dissertation showed no effect on the predicted behavior of the shear walls. (Dolan & Madsen 1992a) Waferboard connections did not exhibit any dependency on the orientation of the sheathing. This was presumed to be due to the homogeneous nature of waferboard as opposed to the orthotropic properties of plywood. Further, testing speed was found to have no significant impact on the connection response. A similar conclusion that displacement rate does not affect the joint characteristics was made by Lhuede (1988).

Dolan and Madsen concluded that the nail properties are the primary factor in determining the load-displacement behavior of sheathing-to-framing connections. Dependence of the connection response on sheathing and framing orientation was said to be negligible when being included in a model of a full-size shear wall.

The test results confirmed the idea that the hysteresis response for nail connections is contained within an envelope defined by the monotonic load-displacement curve. Although not discussed by Dolan & Madsen, in general the results of cyclic connection tests have shown that the monotonic envelope provides a good approximation of the cyclic response in the early cycles. As cycling progresses and damage accumulates, the cyclic response deviates from the monotonic envelope. At higher amplitude cycles the connection response is marked by a significant degradation of strength and stiffness. The post peak cyclic response shows less ductility than the

monotonic curve, presumably due to the accumulation of damage incurred by repeated load cycling.

After several cycles the load displacement response is characterized by pronounced pinching of the hysteresis loops. The reason for the so called "pinching" effect is perhaps best described by Chui and Ni (1997):

> "On the first loading the wood fibers around the fastener are compressed and crushed. Upon displacement reversal (unloading), the fastener is initially still in contact with the wood. This accounts for the high value of initial stiffness. After a certain distance of travel, the fastener leaves the compressed wood behind and moves almost freely in the reversed direction until it contacts wood again on the opposite side. This behavior explains the low unloading stiffness and near-zero load intercept of the loops.... The loading segment is the reverse phenomenon. After a certain distance of free travel in the loading direction, the fastener bears on the wood again on the opposite side, which accounts for the sharp increase in stiffness."

The study of the load-embedment response of timber to reversed cyclic load published by Chui and Ni (1997) revealed that strength degradation occurs under both monotonic and cyclic loading for solid wood. However, no strength degradation was observed in plywood under either monotonic or reversed cyclic load. The degree of strength degradation for solid wood was found to increase with any increase in loading rate, wood density, fastener diameter, and the presence of preloading history. These results support the idea that a group of small diameter fasteners perform better than a group of large diameter fasteners under reversed cyclic loading conditions (Chui & Ni 1997). The results also present the possibility that the high density of Southern Pine lumber used predominantly in the Southeastern United States may have a negative impact of the performance of nailed timber joints. The strength degradation effects were thought

to be related to the onset of cracking. The lack of strength degradation in plywood was attributed to the presence of glue planes making it less susceptible to cracking.

Chou and Polensek (1987) investigated the effect of gaps developing between the contact surfaces of wood joints due to in-service drying of wood members. This is often the case on the West Coast where Douglas-fir components are usually assembled into structures in green or semi-seasoned condition and then dry while in service (Chou & Polensek 1987). The effect of these gaps was evaluated through cyclic-load tests of single nail connections constructed with 2x4 Douglas-fir studs and 19/32 in. thick plywood sheathing, fastened together with 6d box nails. The study focused on frictional damping along contact surfaces (slip damping). The results showed that there is a reduction in the damping ratio of joints constructed with green lumber and then dried to the expected in-service equilibrium moisture content (EMC). Joints assembled and tested green had an average damping ratio of 0.28 while joints assembled green and dried to 12% moisture content had a damping ratio of approximately 0.15. Based on these results the authors concluded that design values could be overestimated by a factor of two if this effect were not taken into account (Chou & Polensek 1987).

### 2.2.3 Edge Distance Effects

One important parameter affecting the performance of individual sheathing-to-framing fasteners is the location of the nail relative to the edge of the sheathing (edge distance). A study of nailed OSB connections performed by Salenikovich (2000) found that reduced edge distance effectively reduces the deformation capacity of the connections. This indicates that the minimum allowable edge distance requirements

might not be sufficient to provide the desired ductile response of shear walls under racking loads (Salenikovich 2000).

Salenikovich conducted three series of monotonic tests of nailed OSB connections with 10 replicate specimens in each series. Each series of specimens was constructed with a different edge distance. The three edge distances studied were 2 in., 3/4 in. and 3/8 in. The materials used were 7/16 in. OSB, 2x4 SPF studs and 8d gun driven nails manufactured by SENKO®. The effect of the framing grain orientation with respect to the applied load was also studied, however the framing orientation was found to have no significant effect on the results.

Although the connection strength appeared to be unaffected by reductions in edge distance, Salenikovich (2000) showed that deformations at peak load and at failure were reduced more than 40% when the edge distance was reduced from 3/4 in. to 3/8 in and by 100% when the edge distance was reduced from 2 in. to 3/8 in.

The typical failure modes observed by Salenikovich (2000) are illustrated in Figure 2.3. Nail heads pulling through the sheathing was characteristic of connections with 2 in. edge distance . Connections with 3/8 in. failed predominately by nails tearing through the edge of the sheathing. Connections with ¾ in. edge distance exhibited a combination of both failure modes (Salenikovich 2000).

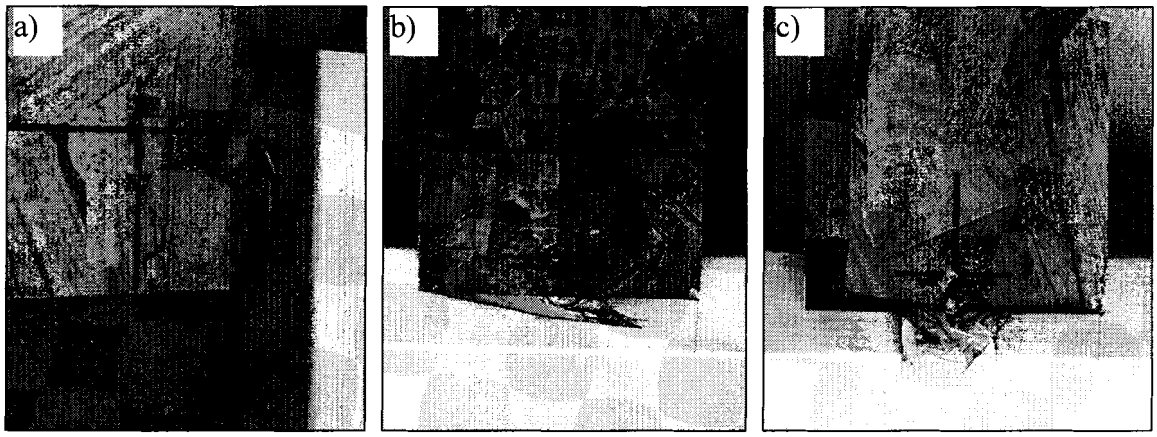


**Figure 2.3 Typical Failure Modes Observed by Salenikovich (2000): a) 2 in. edge distance, b) 3/4 in. edge distance, c) 3/8 in. edge distance (Salenikovich 2000).**

A study of edge distances for plywood shear walls was published by the Douglas Fir Plywood Association (1948). The study consisted of 650 monotonic nailed connection tests. Douglas Fir plywood was used as sheathing and Douglas Fir lumber for framing. Test variables included nail size, panel thickness, wood moisture content, grain orientation, and edge distances relative to both the panel and the studs. No consistent difference in strength was found for loads applied parallel, perpendicular, or at 45 degrees to the face ply grain. The strength of the connections was, however, found to decrease as edge distance was decreased.

## 2.3 Shear Wall Testing

Numerous experimental studies of timber shear walls have been published since panelized sheathing began to be used for shear walls in the late 1940s. The majority of these studies have followed ASTM E72 (ASTM 1998c) which was developed in the early 1940s to compare the performance of plywood sheathed walls with traditional board sheathed walls with "let in" corner or diagonal bracing. Tests of plywood sheathed walls

following ASTM E72 conducted by Tissel and Elliot (1986) and Adams (1987) were used as the basis for allowable shear capacities presented in the United States building codes. Given the fact that ASTM E72 was never intended for investigation of overall shear wall behavior, ASTM E564 was adopted in 1976 (ASTM 1998a). A comparative study using the procedures of both ASTM E72 and ASTM E564 was made by Griffiths (1984). Griffiths found that ASTM E72 overestimated stiffness and strength due to the use of two steel rods at ends of the specimen. During the past twenty years, most experimental studies have followed the procedures of ASTM E564. This standard is more versatile and accommodates a wider range of test variables (e.g. size of specimen, type and location of anchorage, and wall openings).

More recently, researchers have begun to investigate the response of timber shear walls to cyclic loads. No standard cyclic loading protocol exists although several have been proposed and used in past studies by various researchers. The Sequential Phased Displacement (SPD) loading protocol adopted by SEAOSC was originally thought by many to have the most potential for standardization and is still used frequently. However, this protocol and similar ones have been repeatedly criticized for inducing low cycle nail fatigue and nail fracture failures which are not commonly observed in post earthquake investigations. A more recent protocol developed by the Consortium of Universities for Research in Earthquake Engineering (CUREE) appears to be gaining wide spread acceptance at this time (Krawinkler *et al.* 2000).

A fairly comprehensive review of past and present shear wall testing programs is provided in Yancey *et al.* (1998). Also an excellent summary of research conclusions

from years of shear wall research is published in the dissertation of Salenikovich (2000). Dolan and Madsen (1992b) recommend reading Peterson (1983), which provides an extensive bibliography on historical timber shear wall research. The research observations and conclusions that are relevant to the development and testing of AOSB sheathing panels are discussed in this section. Rather than extend the literature survey, the reader is referred to the three previously mentioned references for additional information.

A summary of the observations and conclusions made by various researchers from past experimental studies of timber shear walls is presented in this section. The discussion is broken down into sub-sections corresponding to the shear wall components of interest.

### 2.3.1 Sheathing-to-Framing Connections

Shear wall damage is typically concentrated at the sheathing-to-framing nails. Damage observed in static monotonic tests is typically characterized by the sheathing pulling away from the framing, localized sheathing failure at the location of the perimeter nails, extraction of the sheathing nails and splitting of the bottom plate at the nail line. Damage due to reversed cyclic loading is most often characterized by fatigue and shearing of the sheathing nails, however pull out of sheathing nails is also observed frequently. Since nail failures are not consistent with the findings of earthquake reconnaissance observations they are thought by most researchers to be a result of the cyclic loading protocol used.

Numerous studies provide evidence indicating that sheathing-to-framing connections are the predominant parameter governing the overall shear wall behavior. Fasteners such as nails and staples provide high ductility and energy dissipation while screws and adhesives exhibit high stiffness and brittle failure (Salenikovich 2000). It is generally accepted that the performance of sheathing connections is dependent on nail diameter, sheathing thickness and framing penetration.

Dolan and Madsen (1992b) explained the difference in hysteretic behavior of individual nail connection and full size shear walls without considering any parameters other than the sheathing-to-framing connections. It was shown by Dolan and Madsen (1992a) that the load intercept for a single connector remains constant during cyclic displacements. Intuitively this leads to the expectation that shear walls should exhibit the same behavior. However, this is not the case; the hysteretic response of walls typically shows an increase in the load intercept with increased racking displacement. This behavior can be explained by the shear wall deformation pattern and the resulting load distribution among the sheathing nails. For small racking displacements the nails located near the panel corners are the only ones that are stressed enough to cause inelastic behavior. As the wall racks further more nails will exhibit inelastic behavior. This means that more nails will follow the hysteresis curves and will have a nonzero load intercept. Dolan and Madsen (1992b) concluded that the load intercept of the wall should be equal to the sum of all individual load intercepts. In the author's opinion, these findings provide a very convincing argument that the sheathing-to-framing connections

are the primary factor governing the wall response and that these connections are therefore the most important connection in the shear wall system.

### 2.3.2 Anchorage and Intercomponent Connections

Engineered shear walls typically include the use of overturning restraints such as tension hold downs to provide a direct load path to transfer tension in the end stud to the foundation. Although they are used less frequently, steel angles, straps or similar types of connections are used to reinforce stud-to-plate connections. Various other connectors are used to connect different portions of wood-frame structures such as floors, roofs and foundations. Formerly, effects of intercomponent connections were underestimated or neglected. Experimental studies and computer modeling results have shown that their effect is far from negligible. It is now acknowledged that these connections are one of the most important, and the least understood, links in the load path (Foliente 1995, 1997).

Anchorage conditions strongly affect response of shear walls by providing higher strength and stiffness (Salenikovich 2000). The strong influence of anchorage is easily illustrated by comparing the deformation patterns of fully-anchored walls to that of walls with shear anchorage only. The test results of Dolan and Madsen (1992a) showed that overturning restraint and top corner framing connections were required to facilitate proper load transfer among shear wall components and to prevent the wall from rotating as a rigid body rather than in a panel racking fashion. The sheathing nails do not provide an adequate means of load transfer between horizontal and vertical framing members. The lack of proper anchorage and intercomponent connections causes the most highly

loaded sheathing nails (in the panel corners) to fail at low loads, thus limiting the capacity and ductility of the wall.

The effect of foundation anchorage on shear wall deformation is illustrated in Figure 2.4 and Figure 2.5. In actual wood-framed buildings, partitions, floors, roofs, and ceilings provide significant restraint. Several researchers have expressed concerns that laboratory test set-ups may not provide an accurate reflection of these conditions, especially for isolated narrow walls. Damage or failure of wood-framed buildings during earthquakes and hurricanes is frequently due to failure of intercomponent connections (Yancey *et al.* 1998). Despite this fact, intercomponent connections have been the topic of only a very limited number of experimental and analytical studies.

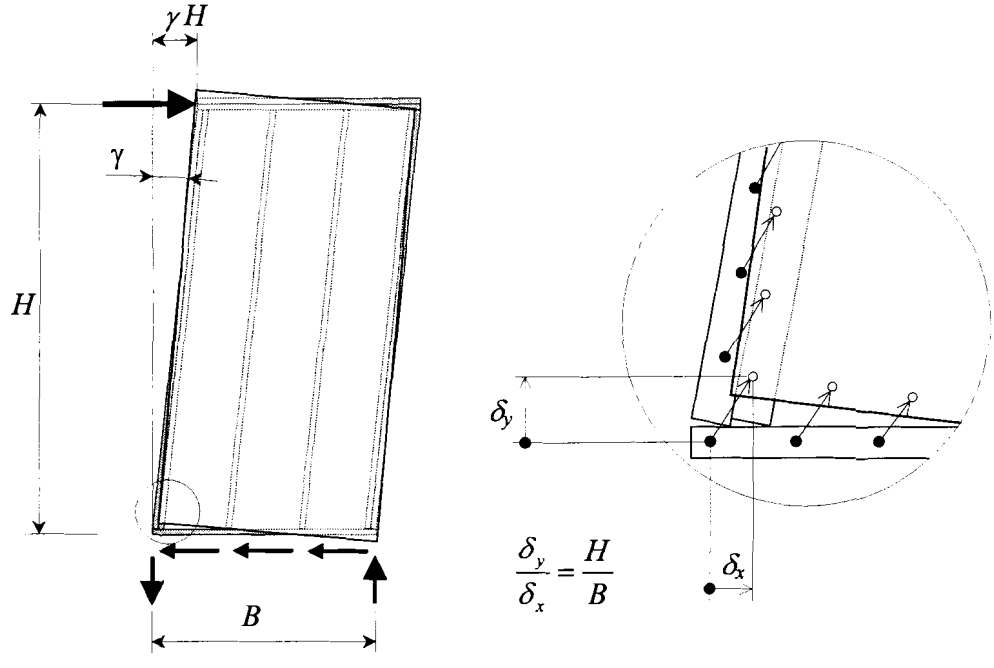


**Figure 2.4 Deformation of fully-anchored shear wall (Salenikovich 2000).**

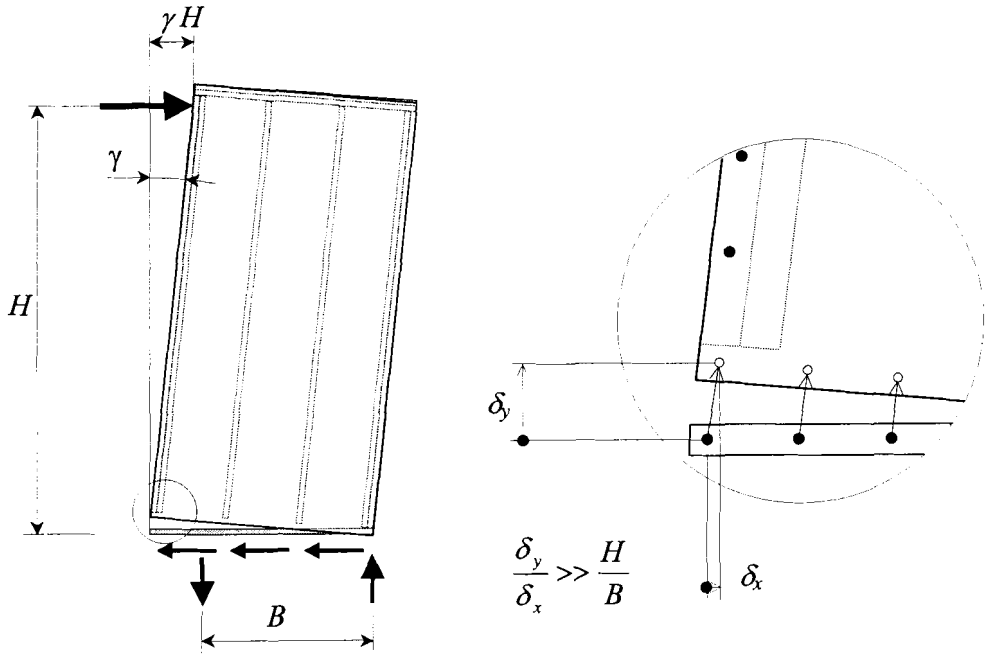


**Figure 2.5 Deformation of non-anchored shear wall (Salenikovich 2000).**

### 2.3.3 Shear Wall Geometry

It is accepted that the racking resistance and stiffness of timber shear walls under monotonic loading is proportional to wall length if the height-to-length aspect ratio is 2:1 or less. Bending of the vertical studs contributes to story drift (total lateral displacement for the building story of interest) for walls with larger aspect ratios. The effect of wall openings for doors and windows is known to alter lateral load path and affect the strength, stiffness, ductility and failure mechanisms. The effect is dependent on the size and configurations of the openings and is not well studied (Salenikovich 2000). Design and analysis calculations are typically based on the nominal capacity of a fully sheathed wall multiplied by an empirical reduction factor.

He *et al.* (1999) investigated the effect of wall openings on walls sheathed with both standard and oversized OSB panels. The results showed that both nail failure and panel failure contribute to the strength of walls with openings. Buckling of panels was observed mainly in the corner regions of the openings due to large stress concentrations. Given this observation, further investigation of localized panel reinforcement for walls with openings was recommended.

Simpson Strong-Tie introduced their Strong Wall™ series of nailed wood panel shear walls in June of 1998. The walls are engineered to provide improved performance at high aspect ratios. Strong Walls push the limits of what has been considered acceptable in maximum aspect ratio for wood-framed shear walls. As required by the *Acceptance Criteria for Prefabricated Wood Shear Panels* (ICBO ES AC130), Strong Wall ratings are derived from static reversed cyclic testing in accordance with the SPD protocol. Acknowledging that cyclic testing cannot predict dynamic response, dynamic testing and nonlinear dynamic analysis of high aspect ratio nailed wood shear walls is currently being conducted under the "Earthquake 99 Project". The Earthquake 99 Project has been designed and managed by TBG Seismic Consultants in collaboration with the University of British Columbia. Although much of the development is proprietary - "in cooperation with the CUREE-Caltech Woodframe project, all data for nonproprietary systems collected in the Earthquake 99 Project will be released to further the understanding of the performance of light-framed structures subjected to seismic excitation." (Pryor *et al.* 2000). Preliminary shake table test results of full-scale structural systems indicate that the Strong-Wall system experienced substantially less

permanent drift than the traditional Code wall system. The work of Simpson Strong-Tie and the research being performed under the Earthquake 99 Project suggest that prefabricated engineered high aspect ratio shear walls may provide a promising method of improving seismic performance of wood-framed buildings while reducing shear wall area at the same time.

## 2.4 Finite Element Modeling of Shear Walls

Several finite element models of shear walls have been developed over the past 25 years by various researchers. Some of the models have been produced with commercial finite element programs such as NONSAP and ANSYS while others were developed with original computer code written by the researchers themselves. A review of most of the finite element models that have been developed is provided in this section. Discussion of the models focuses on the elements and numerical methods employed as well as the conclusions and recommendations of the developers. Many closed form analytical and empirical models have also been proposed. Since no analytical or empirical modeling of shear walls was performed in the development of AOSB, no literature review of this topic is provided here.

Polensek (1976) presented a finite element model to predict the response of stud walls subjected to flexural and compressive loading. I-beam-column elements were used to represent the framing and the sheathing was modeled with plate elements. The stiffness of the fasteners was assumed to be distributed along the nail lines. The model provided accurate predictions of deflections and stresses at both service and ultimate

loads. Polensek noted that the accuracy of his solution was highly dependent on the accuracy of the nail load-slip relationship and the material properties.

Another model developed by Foschi (1977) consisted of two-dimensional linear orthotropic plane stress elements with twelve nodes to represent the sheathing, linear beam-column elements for framing members, and nonlinear springs for the sheathing-to-framing connections. The springs representing the sheathing-to-framing connections were grouped at the nail lines to reduce the computational complexity of the model. The model results compared well with experimental results of a 20x26 ft. board sheathed wall with overlaid plywood tested at Oregon State University.

Easley *et al.* (1982) developed a two-dimensional finite model of a three panel shear wall for the purpose of verifying proposed numerical formulas for wood-frame shear wall analysis. The model was made using the program POLO-FINITE. The sheathing panels were modeled with eight-node plane stress elements having a quadratic displacement field. These elements were assumed to be isotropic and have a linear elastic stress-strain relationship. The framing elements were also modeled with the eight-node element as linear and isotropic. Stud to plate connections were pinned to release moment and allow shear and axial force transfer. Two orthogonal springs (extending parallel and perpendicular to the axis of the framing members) were used to represent the sheathing nails. The spring elements were of zero length in the undeformed position of the wall since they were connected to coincident nodes of the sheathing panels and framing members.

The boundary conditions applied in the model consisted of zero displacement at the framing nodes along the base of the wall and restriction of vertical displacement for all top plate nodes. The vertical restriction of the top plate was meant to approximate conditions in an actual building. However, in preliminary analyses, allowing vertical displacements along the top plate was found to have a negligible effect on the nail forces and shear deformations. To reduce computational complexity the model was substructured so that the linear panel elements were ignored during tangent stiffness updates. The Newton-Raphson procedure was used for obtaining nonlinear solutions. The results compared well with experimental data and the results of the analytical formulas proposed by Easley *et al.* (1982).

Another model that employed perpendicular spring pairs to connect the sheathing and framing nodes was developed by Itani and Cheung (1984). Linear beam elements were used to model the framing and 4-node quadrilateral plane stress elements represented the sheathing. The program NONSAP was modified by Itani and Cheung to incorporate the nonlinear spring pairs. Reasonable agreement was found between the model predictions and experimental results of three-panel plywood shear walls tested by Easley *et al.* (1982). Itani and Cheung (1984) cited the properties of nailed joints as the main factor governing shear wall performance.

Itani and Robledo (1984) incorporated a shear wall model into a computer program called PANFRA (Panel and Frame Analysis). The model was similar to those developed by Easley *et al.* (1982) and Itani and Cheung (1984) except that constant strain

triangular elements were used to model the sheathing panels. The model was said to provide accurate results for walls with and without openings.

Gutkowski and Castillo (1988) incorporated compression only springs to model contact between sheathing panels. The model was capable of providing good predictions for both single and double sheathed walls. Falk and Itani (1989) simplified their previous model by developing a "transfer element" used to account for the stiffness of individual fasteners through the use of nonlinear spring pairs. The number of degrees of freedom was reduced by 40% from their earlier model. Parametric studies indicated that nail spacing had a greater effect than the nail load-slip relationship.

Kasal (1992) and Kasal and Leichiti (1992) developed a detailed three dimensional model for walls subjected to flexural and compressive loading using the commercial software package ANSYS. A simplified single degree of freedom version of the model was incorporated as a substructure element into a model of a complete building. The detailed model consisted of two dimensional linear rectangular shell elements with six degrees of freedom per node to represent both the framing and sheathing. A set of three one-dimensional springs were used to model each sheathing to framing fastener (one for out of plane withdrawal and two for in-plane shear resistance). Gap elements between sheathing panels were also included.

Dolan and Foschi (1991) developed a finite element program called SHWALL that included bearing between panels and out-of-plane bending of the sheathing elements. Three independent one-dimensional springs were used to model the sheathing to framing connectors. Similar to the model of Kasal (1992) one spring was used to resist out-of-

plane withdrawal and two springs oriented perpendicular to each other were used to resist the components of the in-plane shear force. The properties of the connector springs were developed from experimental nailed connection test data and fitted to the Dolan-Foschi load-slip model described in section 2.2.1. The sheathing element used was a three-dimensional four-node plate element with a cubic displacement field in each direction. This sheathing element had 12 degrees of freedom at each node. A bilinear spring was used to represent bearing of adjacent sheathing panels. The stiffness of the spring was essentially infinite in compression and nearly zero in tension. The element was used to prevent overlapping of the sheathing elements and did not provide any resistance to relative in-plane or out-of-plane movement perpendicular to the connector.

SHWALL employed a direct stiffness approach to assemble the global stiffness matrix and used the iterative Newton-Raphson solution method. The ultimate load capacity of the wall was well predicted by the computer results. However, the stiffness matrix would become ill-conditioned causing numerical singularities when modeling post-peak response (Dolan and Foschi 1991).

White and Dolan (1995) developed a program entitled WALSEIZ by modifying the SHWALL and DYNWALL programs developed by Dolan (1989) and Dolan and Foschi (1991). The modifications resulted in a reduction of degrees of freedom. WALSEIZ was capable of both monotonic and time dependant dynamic analysis. The sheathing-to-framing connectors were modeled with two one-dimensional independent nonlinear springs rather than three (out of plane withdrawal was not accounted for). A two dimensional eight degree of freedom rectangular plane stress plate element was used

to model the sheathing. The same sheathing-bearing element that was used in SHWALL was used for WALSEIZ. Operation of the sheathing-bearing elements utilized a penalty parameter approach. The displacement of adjacent sheathing panel nodes was checked within each equilibrium iteration. The effect of bearing was included if the nodes overlapped and neglected otherwise. The Newton-Raphson solution method was used for monotonic analysis and the Newmark-beta was used for dynamic analysis.

More recently Folz and Filiatrault (2000,2001) developed a program called CASHEW (Cyclic Analysis of Shear Walls). The model geometry is defined via an input file allowing for versatility in wall geometry. The model predicts the load-displacement response and energy dissipating characteristics of wood shear walls under arbitrary (user defined) quasi-static cyclic loading. Formulation of the model was based on a balance of model complexity and computational overhead (Folz and Filiatrault 2000).

For simplification, the framing was modeled with rigid pin connected elements. The common method of using two independent mutually orthogonal springs to model the sheathing to framing nails was employed in the CASHEW program. In the process of verifying the computer results, it was discovered that the use of two springs over predicted the amount of energy dissipated by the wall. The connector spacing was adjusted so that the monotonic load-displacement response agreed, in terms of energy absorbed, with the model prediction based on using only one nonlinear spring to model each sheathing-to-framing connector (Folz and Filiatrault 2001). This result raises a very important point as noted by Folz and Filiatrault (2000):

" ...the use of two orthogonal uncoupled springs is only structurally equivalent, in terms of resultant force and stiffness, to one spring if each spring is linear elastic with the same stiffness."

Remarkably, given the numerous models that have used two uncoupled nonlinear springs to model each connector, this result has not been discussed previously in other research studies.

Another unique feature of CASHEW is the displacement control solution strategy employed. Similar to previous models, CASHEW uses the Newton-Raphson solution method. However, as discussed previously, this method fails when the global tangent stiffness matrix is nonpositive definite. To overcome this limitation Folz and Filiatrault introduced an artificial spring at the top of the wall. The stiffness of the artificial spring was set equal to the initial stiffness of the wall. The result is that the combined tangent stiffness matrix of the shear wall and the spring remains positive definite over the entire cyclic loading protocol. The force developed in the spring is removed at the end of each load step to obtain the real force at the top of the shear wall.

A summary of the finite element models of shear walls that have been developed over the years is given in Table 2.3. It is important to point out that despite the recognized importance of tension hold-downs and other anchorage devices used to resist global overturning, the effect of such restraints has been neglected more often than not in past finite element models.

**Table 2.3 Summary of Shear Wall Models (after Yancey *et al.* 1998).**

| Reference | Program Name | Static | Dynamic | Comments |
|---|---|---|---|---|
| Polensek (1976) | | x | | Walls were subjected to flexure and compression |
| Foschi (1977) | | x | | |
| Easley *et al.* (1982) | POLO-FINITE* | x | | |
| Itani and Cheung (1984) | NONSAP* | x | | |
| Itani and Robeldo (1984) | PANFRA | x | | |
| Gutkowski and Castillo (1988) | WANELS | x | | Gap elements used to model bearing between sheathing panels |
| Falk and Itain (1989) | | x | | |
| Dolan (1989) | SHWALL DYNWALL | x | x | Model include sheathing bearing elements |
| Kasal (1992) | ANSYS* | x | | Detailed 3-D shear wall model |
| Kasal (1992) | ANSYS* | x | | Simplified model used for analysis of a complete structure |
| White and Dolan (1995) | WALSEIZ | x | x | |
| Folz and Filiatrault (2000) | CASHEW | x | | Monotonic and Cyclic Loading |

*Commercial software

# Chapter 3

# CONNECTION TESTS

Following a rigorous and highly iterative testing program consisting of monotonic tests of single-nail sheathing–to-framing connections per ASTM D1761 (ASTM 1998b) and compression shear tests of OSB panels with various types of FRP reinforcing following ASTM D1037 (ASTM 1998d), the best performing FRP was selected as the reinforcing for AOSB. The material screening and selection process is documented separately in Cassidy *et al.* (2002). The selected reinforcing materials and fabrication parameters are also described in detail in Cassidy *et al.* (2002).

After selecting appropriate reinforcing materials and fabrication parameters, connection tests were conducted to quantify the benefits of AOSB on individual nail connections. Three types of connection tests were performed: 1) monotonic tests of single nail connections according to ASTM D1761 (ASTM 1998b); 2) cyclic testing of single nail connections following the recommendations for the Cal-Tech Wood Frame housing project developed by CUREE (Krawinkler *et al.* 2000) and 3) nail head pull-through tests following ASTM D1037 (ASTM 1998d). The methods and results of these tests are discussed in this Chapter.

## 3.1 Reinforced Panel Fabrication

Based on the test results of the material screening and selection process documented in Cassidy *et al.* (2002), a panel consisting of two ¼" thick sheets of OSB sandwiching a narrow ( approximately 1/16 in. thick) internal layer of FRP was

determined to have the best combination of durability, ductility and strength Details of the chosen FRP laminate and fabrication details are documented separately in Cassidy et al. (2002).

A thermosetting resin that is typically slow cured under ambient conditions was selected for the fabrication of AOSB. Since the resin is a thermoset, it was possible to accelerate the curing reaction with heat. After testing several sets of process parameters (refer to Cassidy *et al.* (2002) for a complete listing of the parameters tested and the results of these tests), the fabrication procedure that produced the highest quality product with the shortest fabrication time was selected.

Connection test specimens were cut from small, 2ftx2ft panels fabricated in a hydraulic hot press of the same size. The hot press fabrication process is illustrated in Figure 3.1

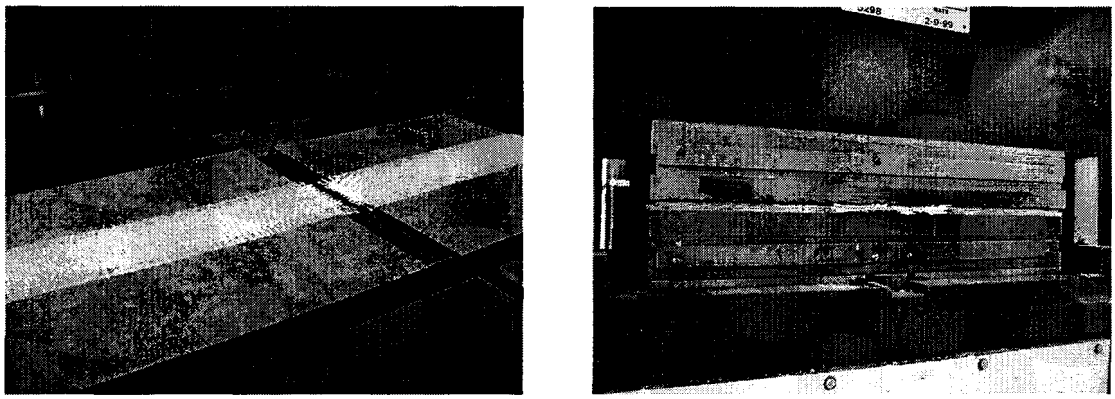

**Figure 3.1 Wet lay-up and hot-pressing of 2x2ft. AOSB panels.**

The panels were fabricated as shown Figure 3.1, with a strip of reinforcing placed in the center of the panel. After fabrication the panels were cut in half along the centerline of the reinforcing strip. Ten single nail connection specimens could be cut

from each half of the panel. The cutting pattern is illustrated in Figure 3.2. Only the reinforced portion of the panel was used for nail head pull through tests, and the remainder of the panel was discarded. The width of the reinforcing strip varied depending on the width of the reinforcing fabric, which was purchased in both 6in. and 8in. wide tapes. The unreinforced portions of the panels were bonded with exterior exposure Liquid Nails® purchased at a local hardware store. The decision to use Liquid Nails® was made after initial attempts to bond the unreinforced portion of the panels with the same adhesive used for the FRP produced weak bonds prone to frequent delamination despite a relatively heavy adhesive spread rate of 50 pounds per thousand square feet of glue line (MSGL). It is recognized that the use of Liquid Nails® or a similar construction adhesive is not a feasible means of commercial fabrication of AOSB. However since this study was more of a pilot study to address the feasibility the AOSB technology this bonding method was considered acceptable for characterizing the structural performance of AOSB connections.

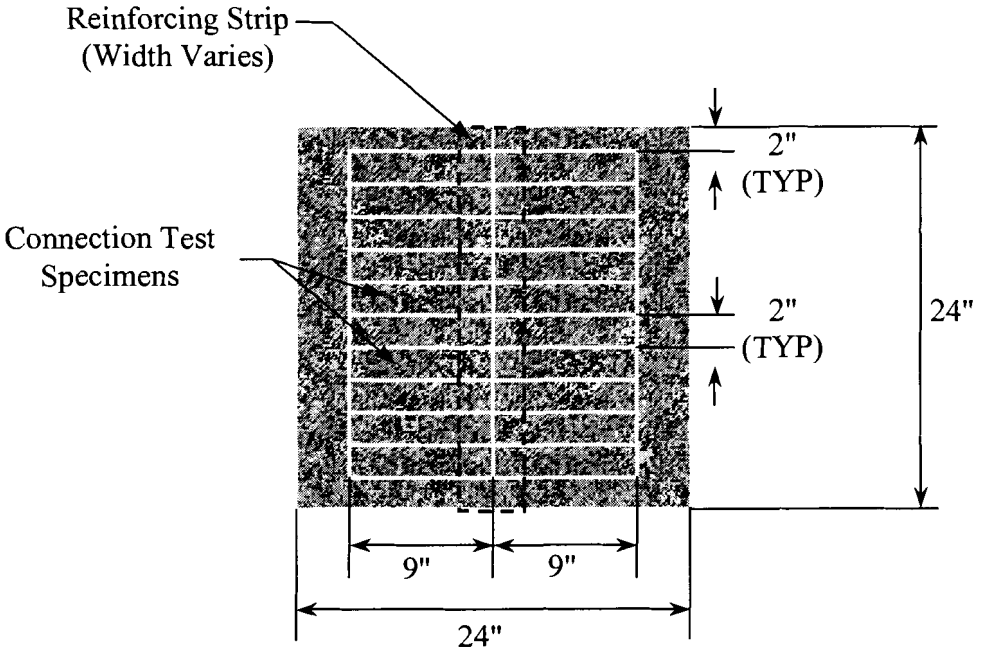


**Figure 3.2 Cutting Pattern for Monotonic and Cyclic Connection Test Specimens.**

## 3.2 Monotonic Connection Tests

Since shear wall performance is primarily driven by the sheathing-to-framing connections, quantifying the monotonic connection strength and failure modes of nailed connections was of significant importance. Single nail connection specimens built with No. 2 southern pine framing were tested monotonically following the procedure of the lateral nail resistance test described in ASTM D1761 (ASTM 1998b). The average load-displacement curves from the monotonic tests were used as constitutive input for a finite element model of 8ft.x 8ft. shear walls, which is the topic of Chapter 5. The methods and results of the monotonic connection tests are described in this section.

### 3.2.1 Experimental Methods

To provide a means of comparison monotonic tests of both conventional and FRP reinforced OSB (AOSB), single nail connections were conducted. A total of 15 control specimens were tested, however the sample size was reduced to 10 specimens for AOSB for the purpose of conserving material and expediting the testing program. The control tests (conventional OSB) used 7/16" thick OSB sheathing manufactured by Louisiana Pacific. The FRP reinforced specimens were manufactured at the University of Maine according to the fabrication parameters described in the previous section.

The connection specimens were made with a single nail driven flush at a distance of 3/8" from the edge of the sheathing coupon. This is the minimum edge distance allowed by most building codes (e.g., BSSC 1998). The nails were driven pneumatically with a Stanley Bostitch® Industrial Framing Nailer (Stick Nailer). The nails were 8d smooth shank nails, also manufactured by Stanley Bostitch®. The nails were 0.120 in. in diameter and 2 ½ in. long with 28° notched heads.

The specimens were oriented so that the load was applied parallel to the grain of the framing member. Both the *National Design Specification for Wood Construction*, NDS, (AF&PA 1997) and Salenikovich (2000), state that there is no appreciable difference in performance of nailed connections loaded parallel- and perpendicular- to-grain. Based on this, testing of connections specimens with other grain orientations was deemed unnecessary for the purpose of determining the lateral load-deformation response of sheathing-to-framing connections.

The specimen dimensions were modified from those given in ASTM D1761 to accommodate the limited stroke of the servo-hydraulic actuator. The actual specimen dimensions are shown in Figure 3.3.

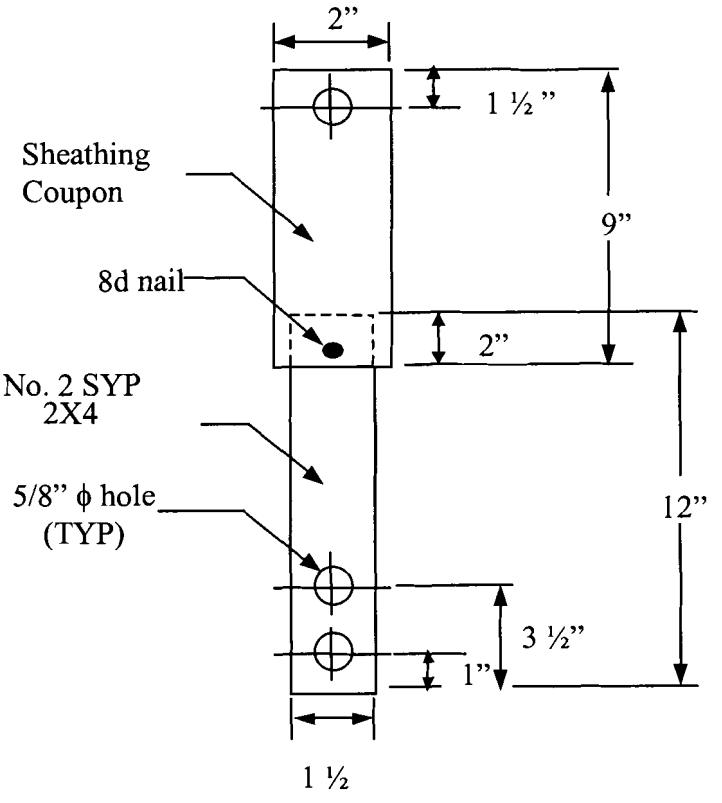


**Figure 3.3 Monotonic Connection Test Specimen Dimensions.**

To simulate shear wall boundary conditions, the sheathing was not restrained against out of plane movement. A steel plate of roughly the same thickness as the OSB was connected to the framing member with two ½" diameter bolts (see Figure 3.4). The reason for the thick steel plate was to simulate actual shear wall loading conditions by creating a concentric load path along the axis of the sheathing coupon.

Real-time load-displacement curves were obtained for each monotonic test. Load and displacement readings were collected at a rate of 1 sample per second. The data were collected and recorded via a PC based data acquisition system equipped with Lab View Software and a National Instruments data acquisition card (PCI-MIO-16XE-50). Two direct current linear variable differential transducers (DCDTs) were used to measure slip at the nail. One DCDT was mounted on each side of framing member (See Figure 3.4). The two DCDT readings were averaged to cancel out any in-plane rotation of sheathing relative to the framing.

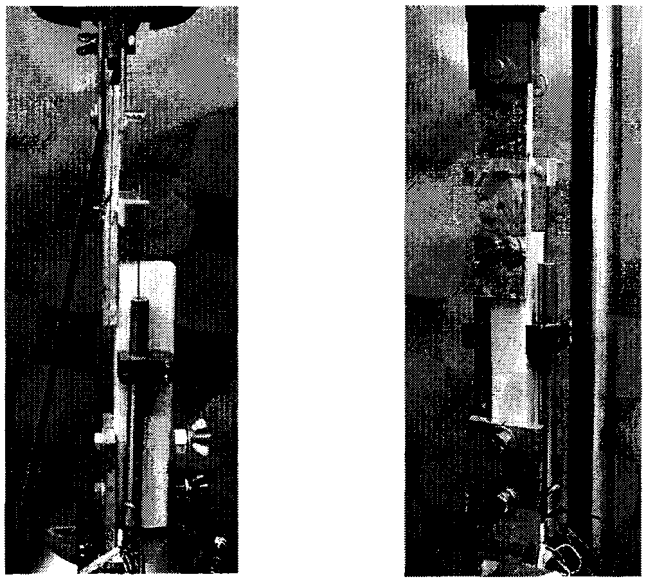

**Figure 3.4 Monotonic Connection Test Set-up.**

### 3.2.2 Reduction of Monotonic Connection Test Data

To allow for a better comparison of the load-displacement response of conventional OSB and AOSB, all of the individual load-displacement curves from each

test set were compiled into one average load-displacement curve resulting in two average curves (one for conventional OSB and one for AOSB).

The curves were averaged using a routine written in Matlab (Matlab 2000). The computer program uses linear interpolation to find load values at identical discrete displacements for each test. This results in a new array of load and displacement for each experimental data file. Becasue these new arrays all have the same displacements, they can simply be averaged together to form a matrix corresponding to the average load-displacement curve.

The Matlab program can only perform the linear interpolation if the load-displacement data is monotonic. To overcome this problem, the curves were smoothed before linear interpolation by taking a moving average of the data. The number of points required for the moving average varied depending on how monotonic the data were. To provide the best representation of the data, the smallest moving average interval possible was used for each reinforcing system. Finding the minimum moving average interval was an iterative process. Moving average intervals were increased by an interval of five points until the entire data set was monotonic. If the moving average was too small, Matlab would return an error message stating that it could not perform linear interpolation because the data were not monotonic. The same moving average interval was used for every replicate specimen in each test set.

The experimental data files were modified slightly to account for the differences in the failure modes observed in individual connection tests. There is a large increase in displacement if the specimen failure is controlled by the nail pulling out of the stud. Total

displacements are much less when the nails tear through the edge of the OSB. AOSB exhibited a combination of the two failure modes. This became problematic when trying to develop an average load-displacement plot, because the displacement range of the average plot is limited by the test with the smallest total displacement. To obtain a complete average load-displacement curve rather than a partial curve that stopped at the smallest maximum displacement observed in the experimental tests, an extra line of data was added to each data file. This line of data consisted of a zero load reading and the DCDT displacement readings of the specimen with the largest maximum displacement. This allowed for linear interpolation of each experimental load-displacement curve throughout the entire displacement range observed in the testing.

Note that the experimental averages for peak load and displacement at peak differ slightly from values read off the average load displacement curves. This inconsistency is because of the computational method used to develop the average load-displacement curves. Because the peak values occur at different locations (load or displacement) for each specimen tested and the Matlab routine uses linear interpolation to find average load values at given displacements, values determined from the average load-displacement curves are always less than the average experimental values.

### 3.2.3 Monotonic Results

Figure 3.5 shows the smoothed average connector load-displacement response of the AOSB specimens and the unreinforced control specimens. All of the experimental load-displacement curves are shown in Figure 3.6 and Figure 3.7 for control and AOSB specimens, respectively. Note that these curves have been smoothed with a moving

average for clarity of presentation. The raw (not smoothed) load-displacement curves for each specimen tested are provided in Appendix A. Results and failure modes of individual specimens are also provided in Appendix A. The experimental averages (see Table 3.1) show a 39% increase in ultimate load, along with increased ductility and a 351% increase in energy dissipation. The displacement at maximum load increased from an average value of 0.279" for conventional OSB to 0.505" for the AOSB specimens.

The conventional and AOSB connections exhibited very different failure modes. The failure mode of the conventional OSB specimens was characterized by the nails tearing through the edge of the sheathing. The initial yield mode of the conventional OSB connections was characterized by rotation of the nail into the OSB and a plastic hinge forming in the nail at the interface of the sheathing and framing members. This corresponds to a Mode IIIs failure as defined by the 1997 NDS (AF&PA 1997).

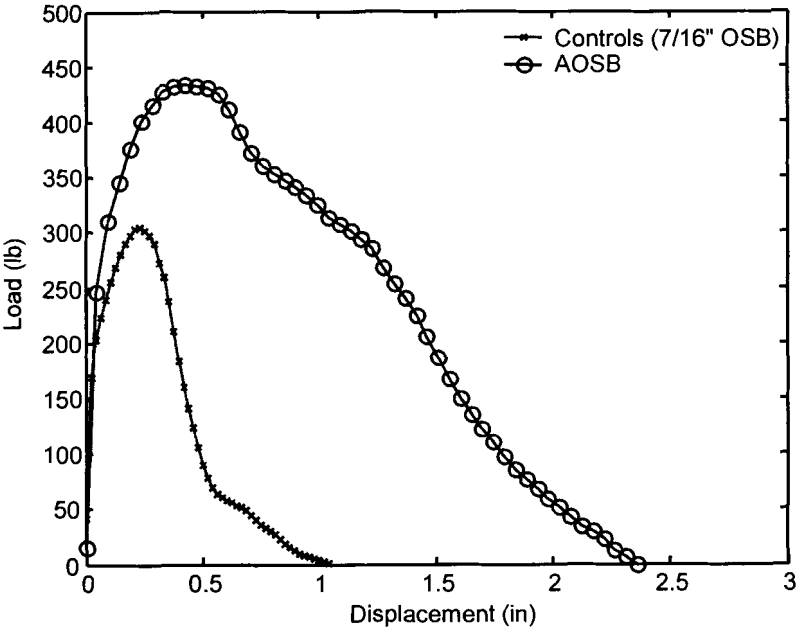


**Figure 3.5 Average Monotonic Load-Displacement Curves.**

**Table 3.1 Average Experimental Results of Monotonic Connection Tests.**

| Results | Controls (7/16" OSB) | | | | AOSB | | | |
|---|---|---|---|---|---|---|---|---|
| Statistics | Peak Load (lb) | Displ. @ Peak Load (in) | Total Displ. (in) | Energy Absorbed (lb-in) | Peak Load (lb) | Displ. @ Peak Load (in) | Total Displ. (in) | Energy Absorbed (lb-in) |
| Average | 327.2 | 0.279 | 0.619 | 128 | 454.8 | 0.505 | 1.901 | 580.0 |
| St. Dev. | 45.4 | 0.117 | 0.165 | 52.2 | 77.2 | 0.243 | 0.350 | 170.8 |
| COV(%) | 14% | 42% | 27% | 41% | 17% | 48% | 18% | 29% |

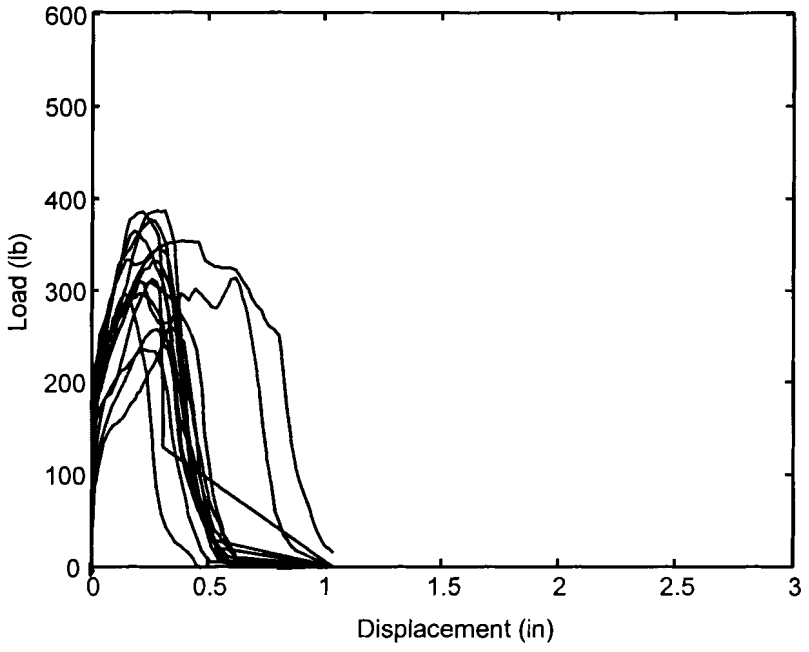


**Figure 3.6 Experimental Load-Displacement Curves for Control Specimens.**

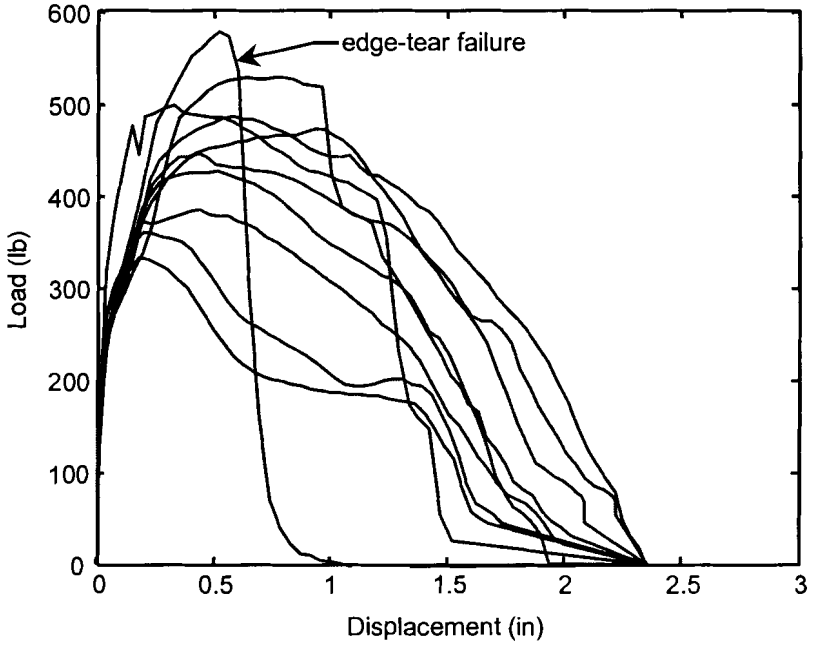


**Figure 3.7 Experimental Load-Displacement Curves for AOSB Specimens.**

OSB;
edge tear

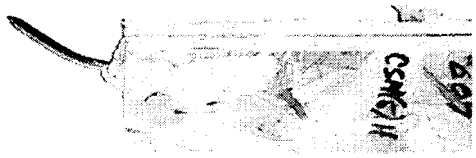

AOSB;
nail pull-out

**Figure 3.8 Monotonic Connection Failure Modes.**

For the AOSB specimens, the failure was typically in the form of the nail pulling out of the framing. Nine out of the ten specimens tested exhibited nail pull-out failure. In the other one, the nail tore through the edge of the sheathing, but the failure exhibited increased load and occurred at a much larger displacement than was observed in any of the conventional OSB connection tests. Initial yielding of the AOSB connections occurred as bending of the nail at the interface of the FRP and the OSB layer adjacent to the framing. Further yielding occurred as local crushing of the stud around the nail followed by the formation of a second plastic hinge of the nail in the framing member. The formation of two plastic hinges in the nail is classified as a Mode IV failure by the NDS. All reinforced specimens exhibited a Mode IV failure. In the case of nail pullout, the OSB layer adjacent to the framing coupon was damaged, but little or no visible damage to the FRP or the surface layer of OSB was observed. The AOSB held the nails

more rigidly, preventing the head of the nail from rotating into the sheathing and changing the location at which initial bending occurred in the nails.

## 3.3 Cyclic Connection Tests

Cyclic connection tests were performed with a slightly modified version of the same test rig used for the monotonic tests. Ten tests of both OSB and AOSB connections with No. 2 southern pine framing were conducted for a total of twenty tests. The loading protocol was developed using the recommendations of the CUREE wood-framed housing project for the control specimens. Both the conventional OSB and AOSB specimens were subjected to the same loading protocol to allow easy comparison of damage accumulation. The methods and results of these tests are discussed in this section.

### 3.3.1 Experimental Methods

The monotonic test jig was modified slightly for cyclic testing (See Figure 3.9). For monotonic testing the sheathing was connected to the top grip of the testing frame with two steel plates and a clevis pin. The sheathing coupon was in effect pinned at both ends, which caused it to behave as a linkage when subjected to compressive loading. To fix this problem, the two steel plates were extended further down along the sides of the sheathing to allow enough room for another bolt. The two in-line bolts prevented rotation at the top, which eliminated the linkage action. The bolts were tight fitting and were fully torqued to prevent slippage between the test jig and the connection specimen.

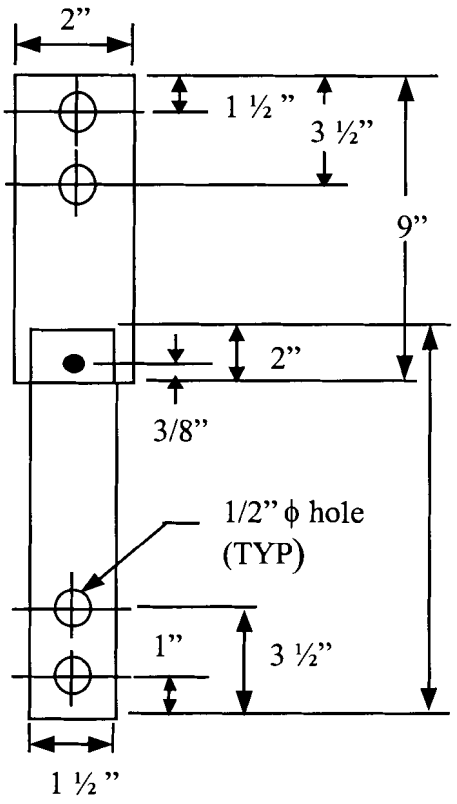


**Figure 3.9 Cyclic Connection Test Rig.**

The connection specimens were loaded according to the Quasi-Static Deformation Controlled Cyclic Test Protocol developed by CUREE (Krawinkler *et al.* 2000). This protocol was developed by using time-history analysis of actual earthquake records in the Los Angeles area. The loading is intended to simulate ordinary ground motions in the Los Angeles area whose probability of exceedance in 50 years is 10% (475 yr. return period). The protocol consists of 43 total cycles of varying amplitude.

At the time these tests were performed, the CUREE protocol was quite new and the Sequential Phased Displacement (SPD) test procedure developed by the Structural Engineers Association of Southern California (SEAOSC) was perhaps the most widely

accepted cyclic loading protocol found in the literature. The CUREE protocol was selected over SPD after noting the common occurrence of nail fatigue failures with SPD. Dinehart and Shenton (1998) and He *et al.* (1999) note that the nail fatigue failures are likely a result of the large number of high amplitude cycles imposed by the testing program and that the occurrence of nail fatigue is not consistent with the findings of damage surveys conducted following actual seismic events. Although the occurrence of nail fatigue failures is also possible with the CUREE loading procedure, it is less likely given that there are only 43 total cycles compared to the 72 cycles in the SEAOSC standard. Another reason for selecting the CUREE protocol over SPD was related to the definition of the reference deformation. The SPD uses the first major event (FME) or yield slip, while CUREE uses the ultimate slip. It is difficult to reach agreement on the definition of the yield slip because of differences in national standards (ISO 1997). In the CUREE publication, the investigators argue that the response of components of wood frame buildings rarely exhibit characteristics that can be associated with a yield point or any other break-point in the force-deformation response (Krawinkler *et al.* 2000). Conversely, the ultimate displacement is a property that is easily determined and which is defined with reasonable agreement throughout the world (ISO 1997).

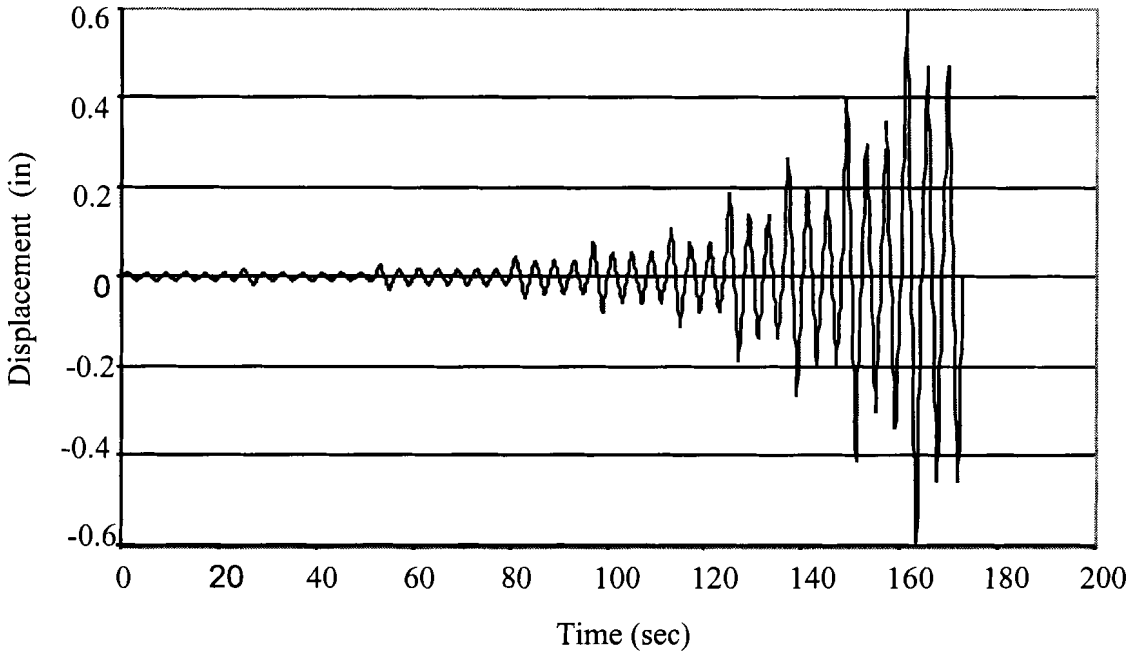


**Figure 3.10 Cyclic Connection Test Displacement History.**

A test speed of 0.25 Hz was chosen so that the speed for all cycles would fall within the range of 0.004 and 0.4 in/sec (0.1 to 10 mm/sec), which is the range recommended by the proposed ISO standard for cyclic testing of mechanically fastened timber joints , ISO/DIS 16670, and cited by CUREE.

The reference deformation that the cyclic loading protocol was based on was obtained from the average load-displacement response of the conventional OSB connections in the monotonic tests. CUREE recommends defining the reference deformation as a specific fraction of the monotonic deformation capacity ($\Delta_m$), where $\Delta_m$ is defined as the point at which the applied load drops, for the first time, below 80% of the maximum load that was applied to the specimen (see Figure 3.11). A value of 0.6 $\Delta_m$

is suggested by CUREE. The 0.6 factor is intended to account for the difference in deformation capacity between monotonic and cyclic testing (Krawinkler *et al.*, 2000).

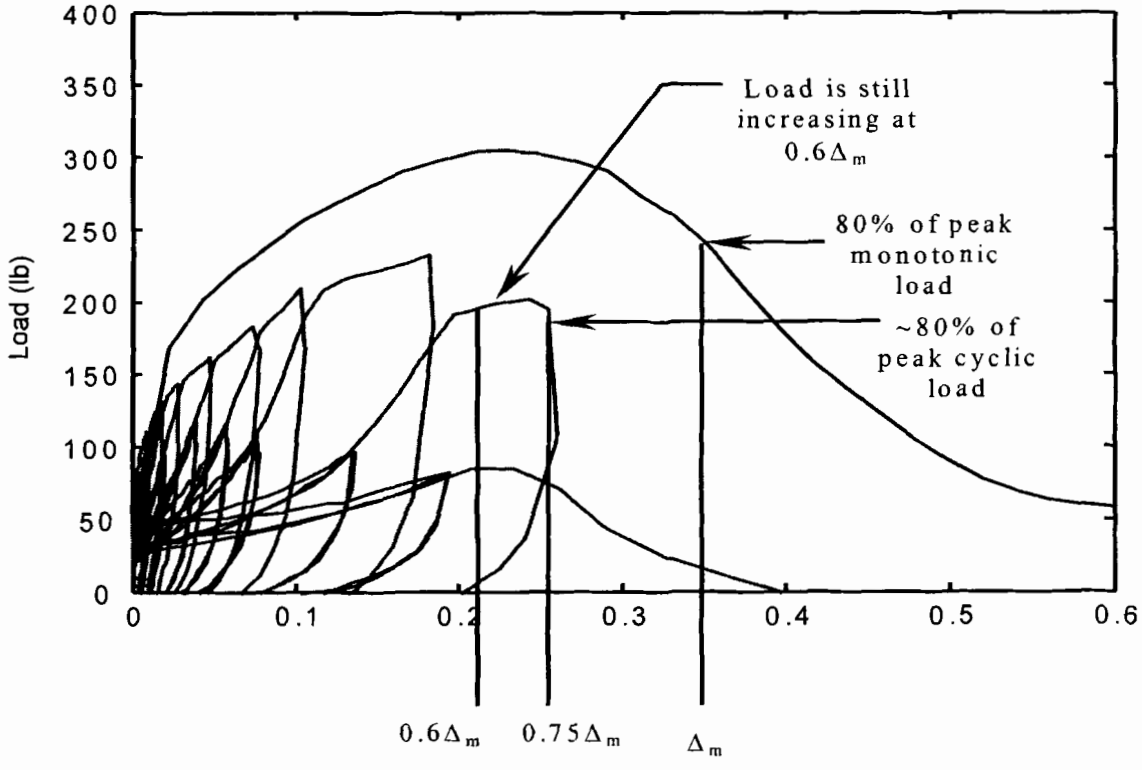


**Figure 3.11 Selection of Reference Deformation from Preliminary Test Data.**

Since the CUREE protocol is intended for shear wall testing, preliminary tests were performed to determine if the suggested reference deformation of 0.6 $\Delta_m$ was applicable to connections. Based on the results of these preliminary tests, a value of 0.75 $\Delta_m$ was found to more accurately account for the difference in deformation capacity between the monotonic and cyclic tests, and was chosen as the reference deformation for the cyclic connection tests (refer to Figure 3.11).

The AOSB connection specimens were subjected to the same identical cyclic deformation history as the conventional OSB connections. The reason for doing this

rather than developing a separate deformation history based on the monotonic data for AOSB, was to provide a direct comparison between the performance of AOSB and OSB when subjected to the same loading. Because the AOSB connections have a much larger ultimate displacement than the control specimens, they did not fail after being subjected to the same number of cycles that caused failure of the control specimens. To quantify the remaining capacity of the AOSB connections, they were loaded monotonically to failure at a rate of 0.4 in/sec following completion of the CUREE protocol. Data were recorded at a rate of 30 samples per second for all cyclic connection tests with the same PC based data acquisition system used for the monotonic tests.

### 3.3.2 Cyclic Results

The failure of all conventional OSB specimens subjected to cyclic loading was a Mode IIIs edge tear failure. The most common failure mode (80%) of the AOSB specimens was a Mode IV nail withdrawal failure similar to the failure observed in the monotonic tests. The failures of the other two AOSB specimens occurred as splitting of the framing and nail fatigue.

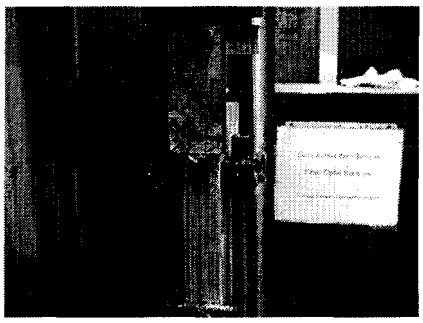

OSB;
edge tear

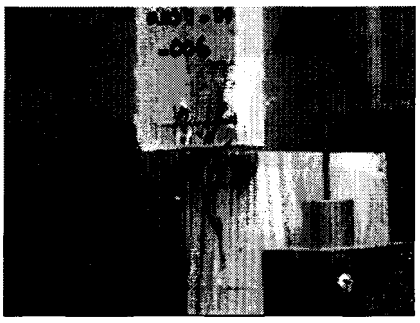

AOSB;
nail pull-out

**Figure 3.12 Cyclic Connection Failure Modes.**

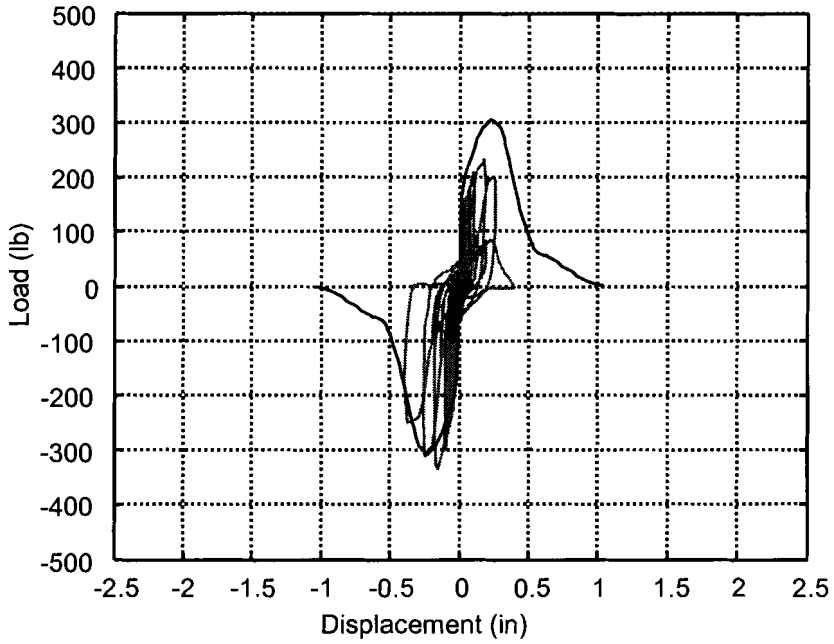


**Figure 3.13 Typical Cyclic Load-Displacement Curve and Monotonic Envelope for Conventional OSB Connections.**

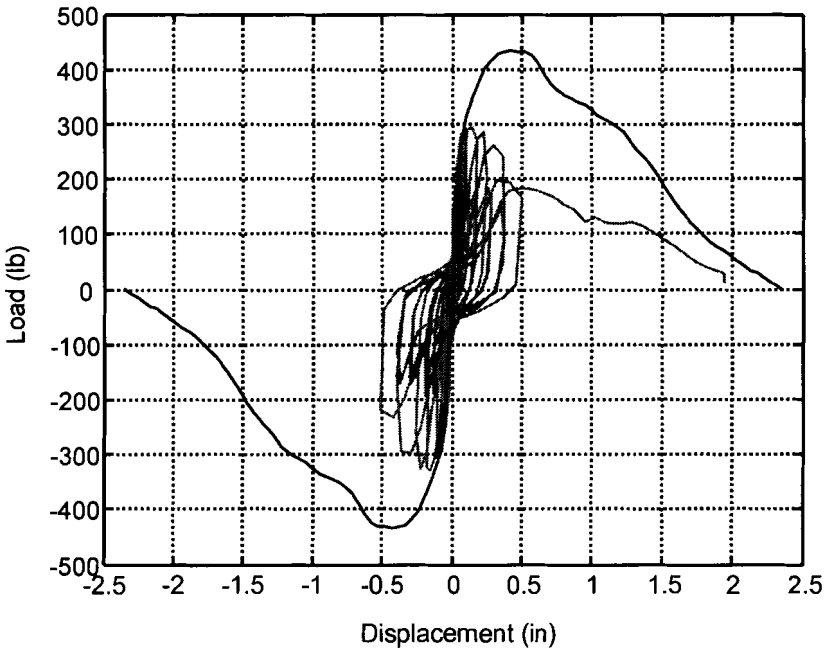


**Figure 3.14 Typical Cyclic Load-Displacement Curve and Monotonic Envelope for AOSB Connections.**

For the control specimens, the monotonic curve accurately predicts the cyclic response for the first few small amplitude cycles, however after repeated cycling, continual stiffness reductions are observed (see Figure 3.13). The cyclic response is also characterized by rapid strength degradation due to cumulative damage. In the compressive direction, where the edge distance is effectively unlimited, the failure is a ductile bearing failure as opposed to the lower strength and more brittle edge tear failure mode observed when tensile loading is applied. From the typical hysteretic curves shown in Figure 3.15 and the values given in Table 3.2, it can be seen that AOSB has not significantly changed the ultimate compressive loads or the displacement at which the maximum load occurs. However, under tensile loading, where the edge distance is minimal (3/8 in.), AOSB provides a marked improvement in both strength and displacement capacity over conventional OSB connections.

Dolan and Madsen (1992b) found that the cyclic response of nailed plywood connections is contained within an envelope defined by the monotonic load-displacement response. AOSB connections were also found to follow this behavior (see Figure 3.14). Similar to the results for conventional OSB connections, the monotonic curve provides a good prediction of the cyclic response in the early cycles, but the monotonic and cyclic response are very different after continued load cycling. The AOSB specimens show a less dramatic decrease in strength and stiffness in the latter cycles, indicating that the AOSB connections are more resistant to damage accumulation incurred by load cycling.

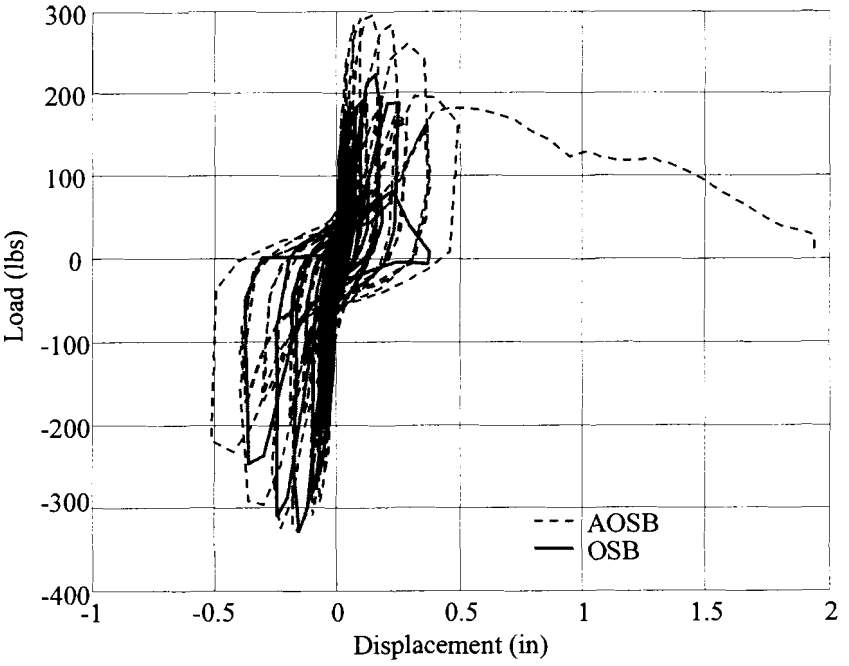


**Figure 3.15 Typical Measured Hysteresis Curves.**

**Table 3.2 Average Results of Cyclic Connection Tests.**

| Results | Controls (7/16" OSB) | | | AOSB | | |
|---|---|---|---|---|---|---|
| Statistics | Max Load (lb) | Disp @ Max Load (in) | Energy Absorbed (lb-in) | Max Load (lb) | Disp @ Max Load (in) | Energy Absorbed (lb-in) |
| Average | 261.9 | 0.192 | 584.3 | 312.9 | 0.334 | 1177.3 |
| St. Dev. | 56.6 | 0.077 | 139.6 | 63.8 | 0.266 | 178.4 |
| COV (%) | 22% | 40% | 24% | 20% | 80% | 15% |

Note: This data is based on the CUREE loading history only and does not include the residual capacity of the AOSB specimens during the monotonic drive to failure.

When subjected to the same cyclic loading history, the reinforced specimens exhibited an average increase of 20% in maximum tensile load and a 74% increase in the displacement at maximum load. The total energy dissipated was approximately twice

that of conventional OSB connections. Tabulated results of and hysteresis plots for individual specimens are given in Appendix A.

The AOSB specimens did not fail after being subjected to the same loading history that caused failure in all control specimens. To quantify the residual capacity of the AOSB connections, the specimens were monotonically driven to failure, immediately following the completion of the CUREE loading protocol. On average the reinforced specimens retained 45% of their ultimate load capacity and 60% of their monotonic energy dissipation capacity after cyclic testing. After being subjected to all 43 load cycles, the reinforced specimens exhibited a residual energy absorption capacity which was more than three times that of the average monotonic energy absorption of the conventional OSB connections. A comparison of the average residual load-displacement response of AOSB with the average monotonic curves of both conventional and reinforced OSB is shown in Figure 3.16.

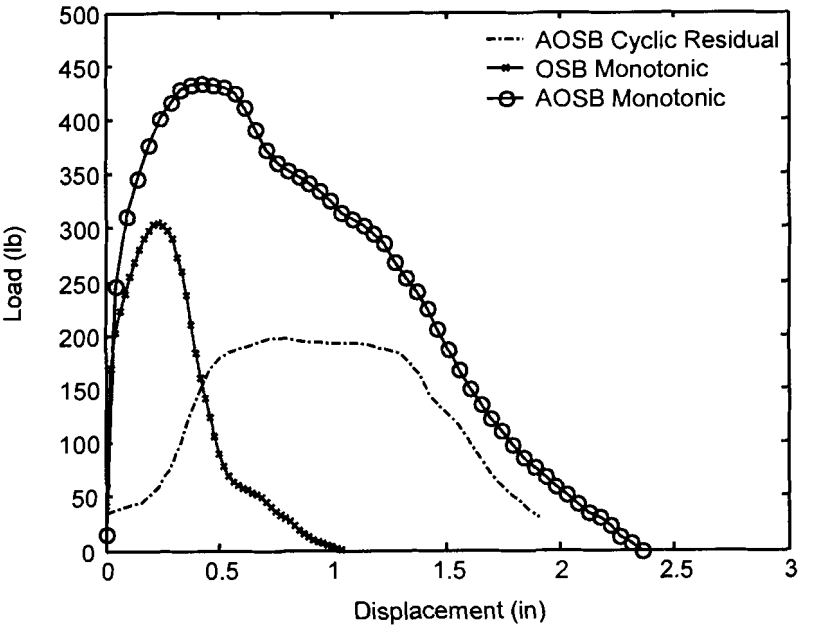


**Figure 3.16 Residual Capacity of AOSB Connections after Cyclic Loading vs. Monotonic Response of OSB and AOSB Connections.**

## 3.4 Nail Head Pull-Through Tests

Nail-head pull-through tests were conducted on both AOSB and conventional OSB specimens. The tests follow the procedures outline in ASTM D1037 (ASTM 1998d). Twenty specimens of each were tested; half of them were tested dry and the other half were soaked in water at approx 68 °F for 24 hours according to ASTM D1037 prior to testing. For the wet specimens the nails were driven prior to soaking specimens in the water. The average results are listed in Table 3.3. Detailed results of individual specimens are provided in Appendix A.

**Table 3.3 Average Results of Nail Head Pull-Through Tests.**

| OSB Type | Ultimate Load (lbs) | Initial Stiffness (bs/in) |
|---|---|---|
| 7/16" OSB Dry | 297 | 2173 |
| AOSB Dry | 673 | 4666 |
| 7/16" OSB Wet | 208 | 938 |
| AOSB Wet | 541 | 2374 |

As shown in Table 3.3, the ultimate load required to pull the head of the nail through the AOSB specimens was more than twice that of the conventional OSB specimens. The initial stiffness was also increased significantly. It is also important to note that the AOSB specimens that were soaked in water for 24 hours exhibited more strength and stiffness than the conventional OSB specimens that were tested dry.

# Chapter 4

# SHEAR WALL TESTS

For this initial study of AOSB, shear wall specimens with two vertical panels and no openings were tested. Static and cyclic tests of both conventional OSB and AOSB shear walls built with southern pine framing were conducted. The sheathing was attached to the framing with pneumatically driven 8d nails. Nail spacings of both 4 in. and 6 in. at the panel edges were investigated and all nails were driven at 3/8 in. from the panel edge. The methods and results of these tests are discussed in this Chapter.

## 4.1 Fabrication of AOSB Sheathing Panels

Full size (4x8ft.) AOSB sheathing panels were fabricated by sandwiching an 8 in. wide strip of FRP between two thin (1/4 in.) sheets of OSB at the panel edges. The 8 in. width was used for ease of fabrication and because the reinforcing fabric had been purchased previously in 8 in. wide rolls. Further research is needed to determine the optimal width of the reinforcing strip, however connection test results indicate that a 2 in. strip will provide equivalent structural performance. The same fabrication parameters described in Cassidy *et al.* (2002) for fabrication of AOSB connection test specimens were used to manufacture full size panels. The fabrication process, which involved a wet lay-up of the FRP composite followed by hot pressing under a pressure of 10 psi (measured over a 4x8 ft. area) for 30 minutes is illustrated in Figure 4.1 through Figure 4.3. The finished product is shown in Figure 4.4. The plies placed in contact with the

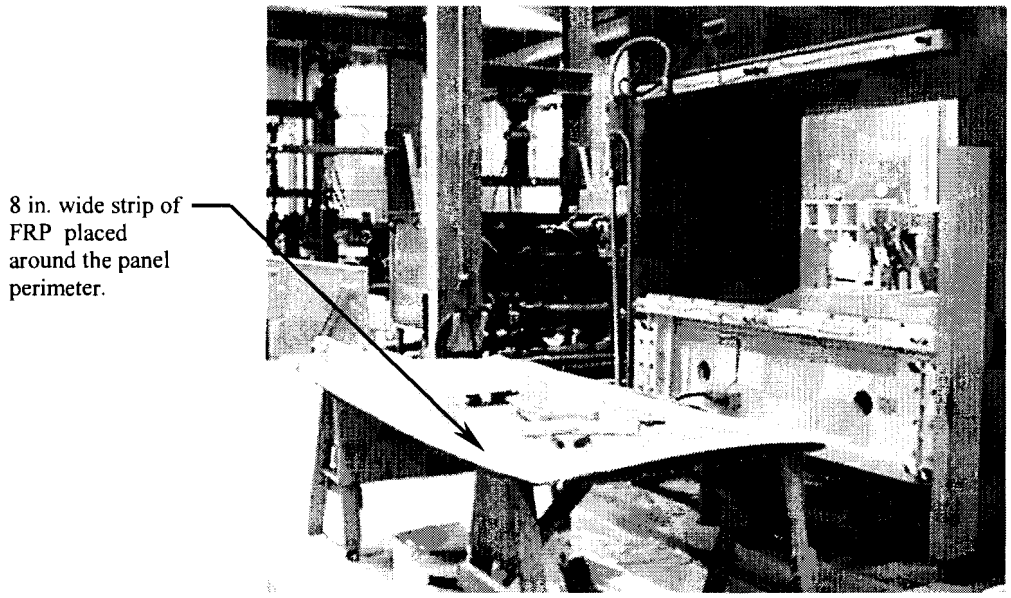


**Figure 4.1 Fabrication Set-Up.**

OSB were highly absorbent, which promoted good bonding between the FRP and the OSB. The resin was applied to the fabric by hand with paint rollers. Each of ply of fabric was wetted individually to ensure complete fabric wet-out. The wet-resin-to-fabric weight ratio was maintained at approximately 1:1.

During fabrication trials it was noted that the resin tended to squeeze out of the fiber glass and migrate toward the interior of the AOSB panels when pressure was applied, resulting in a poorly performing resin starved composite. To prevent this a resin barrier was created by placing a double-sided sealant tape, used for SCRIMP® and vacuum bagging applications, at the edge of the composite (see Figure 4.2). The sealant tape prevented the resin from migrating into the interior of the panels resulting in higher quality FRP composite.

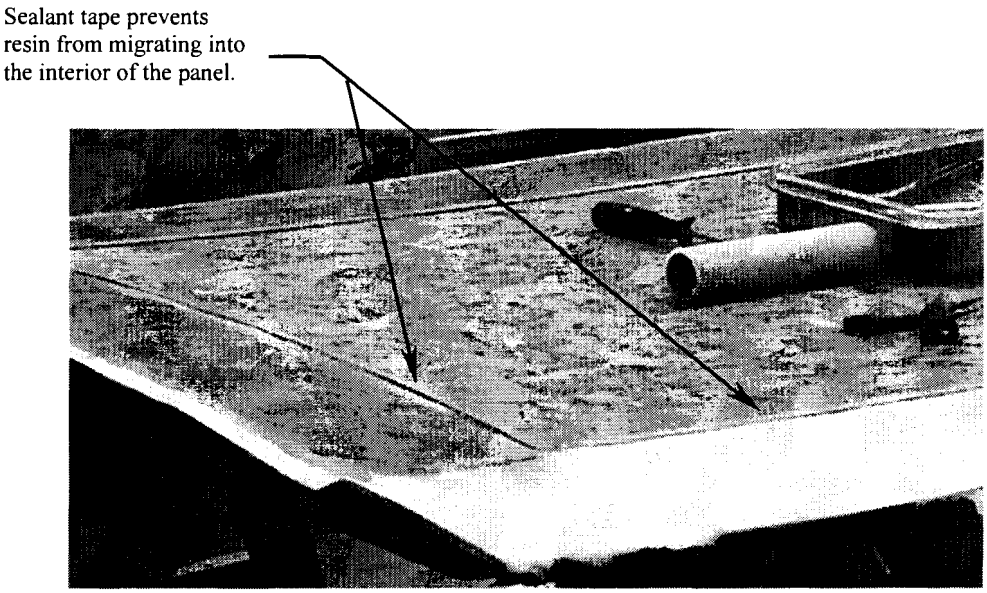


**Figure 4.2 Wet Lay-up of AOSB Panel.**

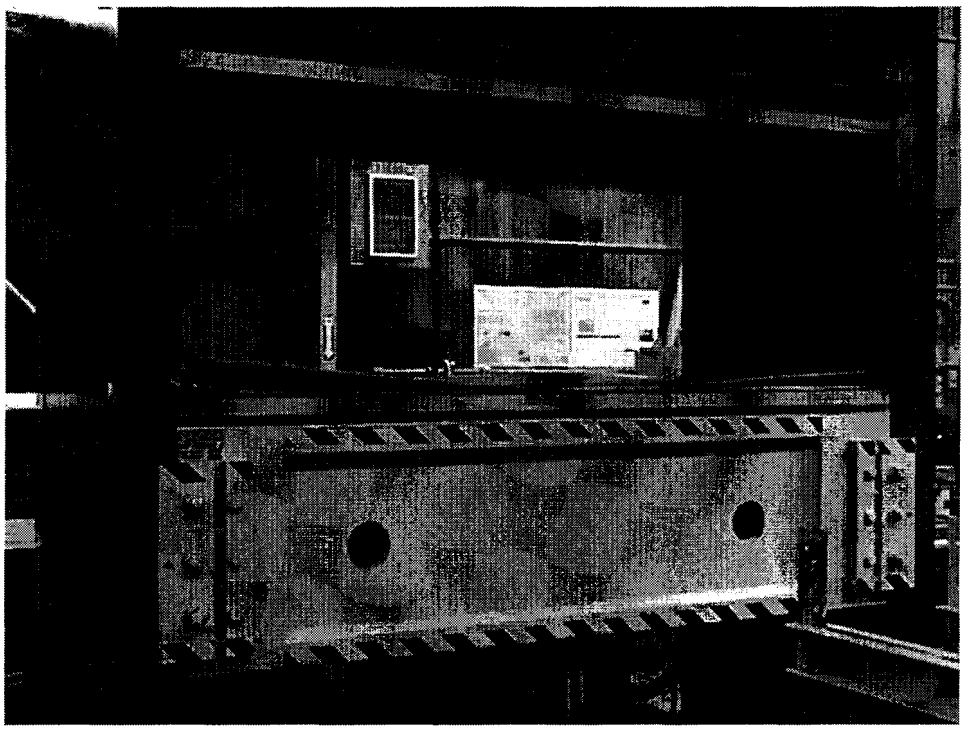

**Figure 4.3 Hot Pressing of AOSB Panel.**

Because of the relatively high cost and poor OSB-OSB bonding performance of the resin used to fabricate the FRP, the unreinforced, interior sections of the panels were bonded together with Liquid Nails®, an exterior exposure construction adhesive. As noted in Chapter 3, this is not considered a feasible means of commercial fabrication for this product, however for this pilot study the interior bond only had to be strong enough to prevent the two outer sheets of OSB from pulling away from each other and buckling individually. For commercial fabrication it may be possible to introduce the FRP reinforcing within the OSB production line, which would eliminate the need for an additional adhesive to join the center of the panels as was necessary in the secondary fabrication technique used here.

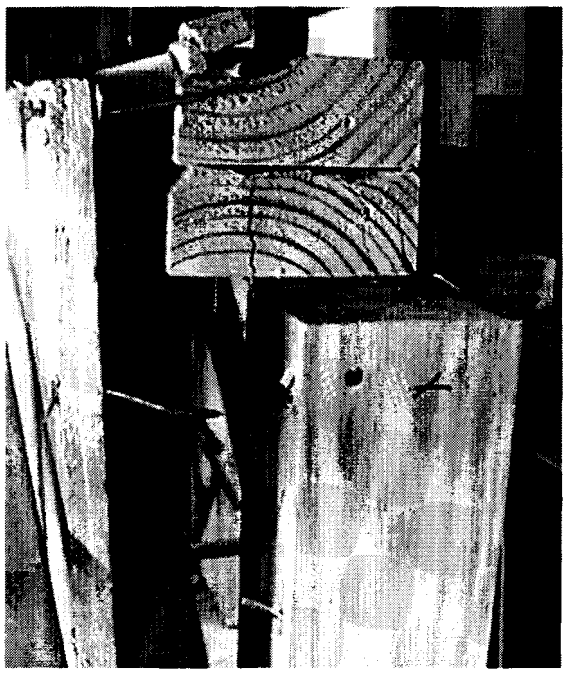

**Figure 4.4 Finished Product in Action.**

## 4.2 Shear Wall Test Rig

The shear wall test rig consisted of a 55 kip servo-hydraulic actuator attached to a reinforced concrete reaction wall on one end and a steel load distribution beam on the other (see Figure 4.5). The actuator was pin supported at both ends to avoid rotational and/or torsional restraint. Although supported by the reaction wall on one end, only the loading beam resting on the top plate of the shear wall test specimen supported the other end of the actuator. This allowed the end of the actuator to translate freely in the vertical direction with increased racking deflection of the shear wall specimen. Steel safety cables, which were slack during testing, attached the front of the actuator to the reaction wall. The cables were only present to prevent the actuator from being damaged in the event that the test specimen collapsed. A truss made of steel angle members was used to support the front of the actuator when no test specimen was in place or the load distribution beam had been detached.

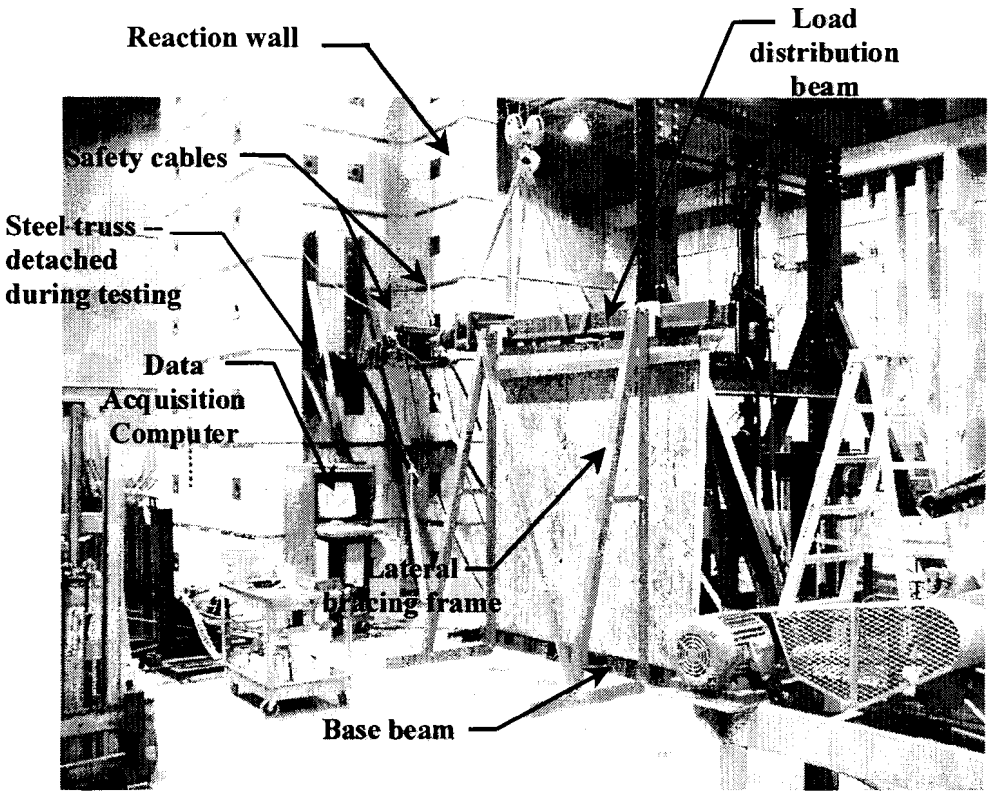


**Figure 4.5 Shear Wall Test Rig.**

The load distribution beam provided the load path from the actuator to the top plate of the wall. The beam, which was constructed of welded plates and tube sections, weighed approximately 75 lb/ft and rested on four small steel tube sections that were placed along the top plate of the shear wall specimen. The heavy weight of the beam was designed to produce dead load in the plane of the wall. Four bolts measuring ¾ in. in diameter and 8 in. in length secured the loading beam to the top plate of the wall. Square steel plate washers measuring 3 in. on a side and ¼ in. thick were placed between the under side of the wall top plate and the nut. The bolts were tight fitting to minimize slip between the loading beam and the top plate of the wall.

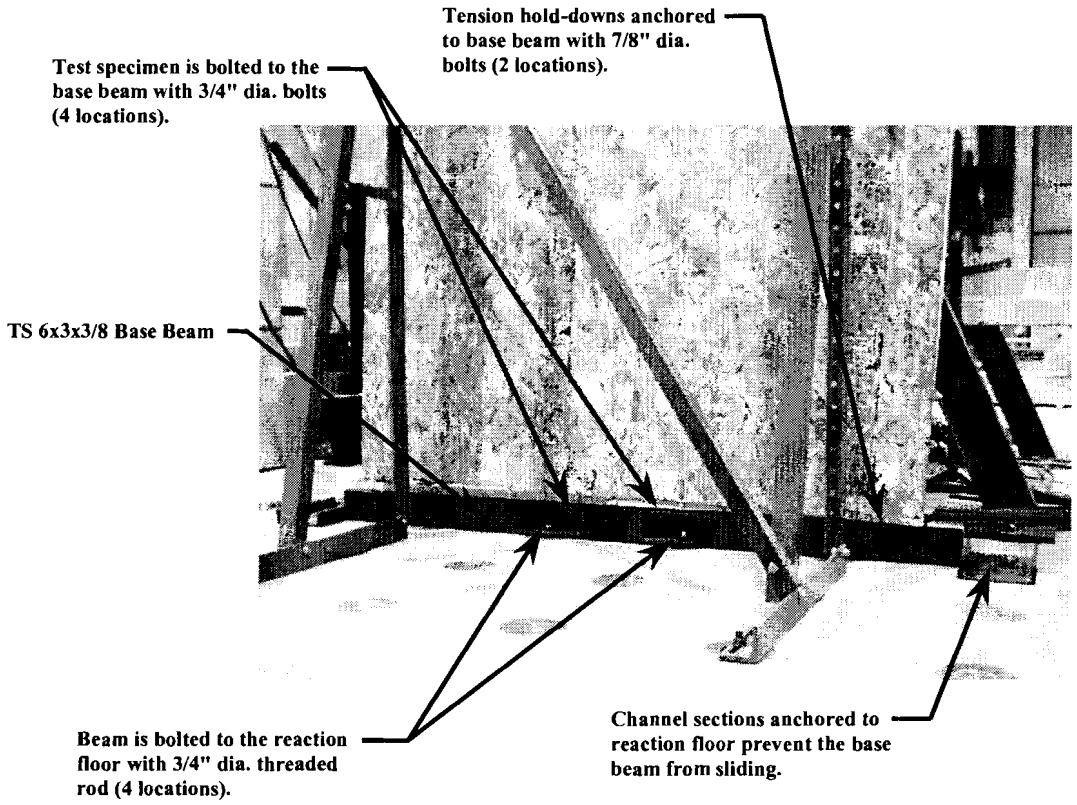


**Figure 4.6 Close-Up View of Base Beam.**

The bottom plate of the shear wall test specimen rests on a steel base beam made from a 6x3x3/8 in. steel tube section. The base beam was bolted through the 2½ ft. thick reaction floor with 1 in. diameter threaded rod in four locations. The test walls were attached to the top of the base beam with four ¾" diameter bolts. The bolts were tight fitting in the holes to minimize slip between the bottom plate of the wall and the base beam. Steel channel sections, anchored to the reaction floor, were placed at either end of the base beam to prevent the beam from sliding along the floor.

The load distribution beam was laterally braced by frames on each side (see Figure 4.5). The bracing frames, which were constructed from steel angles joined by bolts, were attached to the reaction floor with ¾ in. diameter threaded rods. Sections of wood blocking with an attached strip of high density polyethylene were used to guide the load distribution beam as the test walls were racked by the actuator. The high density plastic strip was placed in contact with the steel beam to minimize the amount of frictional resistance while preventing out-of-plane movement of the beam and the top of the specimen.

## 4.3 Instrumentation

Load and displacement readings were recorded during the tests with a PC based data acquisition system. Data were collected at a rate of 10 samples per second for the static wall tests and 50 samples per second for cyclic tests.

The instrumentation plan is illustrated in Figure 4.7. The applied load was recorded from the actuator load cell and displacements were measured with either DCDTs or string potentiometers powered by a +/-15 volt power supply. DCDTs with a range of +/-2 in. were used to measure uplift and horizontal slip at the base of the wall. For the static wall tests, the translation at the top was measured with a +/-10 in. DCDT. A flexible rod connected to the DCDT core was attached to an angle bracket that was mounted to the double top plate of the walls with screws. The hole in the bracket where the rod passed through was slotted vertically to prevent bending of the rod. Unfortunately, the slotted hole did not prevent the rod from bending. Concerns that bending of the rod may produce inaccurate displacement readings and possibly damage

the DCDT prompted the replacement of this DCDT with a steel cable string potentiometer ( "string pot"). The string pot, which had a 20 in. range, was used for all cyclic wall tests.

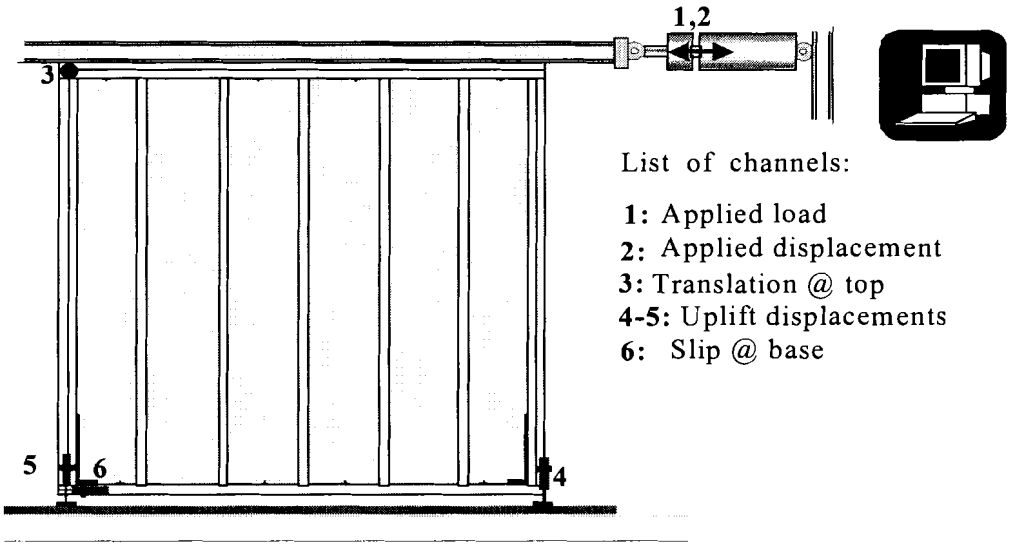


**Figure 4.7 Instrumentation of Shear Wall Test Specimen.**

(Note: This figure was adapted from Salenikovich 2000)

## 4.4 Wall Construction

Normal construction practices were followed, with No. 2 southern pine framing consisting of nominal 2x4 studs spaced at 16 in. on center, a double top plate and a single sole plate. All nailing was done with a Stanley Bostitch® nail gun The studs were attached to the single bottom plate and the double top plate with two 16d (0.131in. $\phi$ x 3.5in.) power driven nails at each end.

The sheathing panels were oriented vertically and unblocked. A single layer of sheathing was attached to one side of the framing with power driven 8d smooth shank nails, measuring 0.120 in. in diameter and 2.5 in. in length. Nails driven along the sheathing panel edges were driven at an edge distance of 3/8 in.

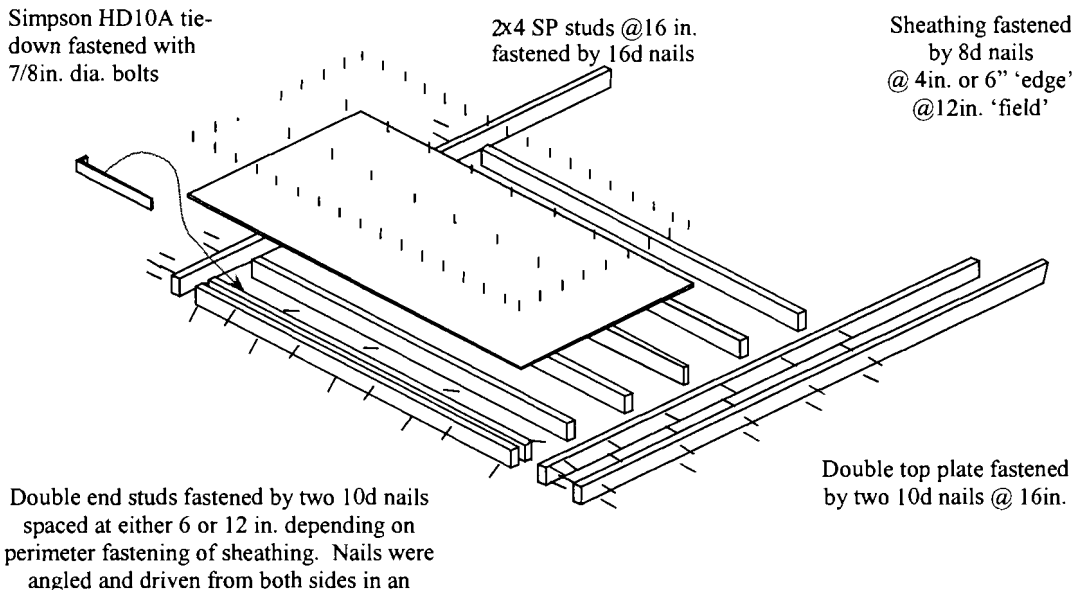


**Figure 4.8 Shear Wall Assembly.**

**(Note: This figure was adapted from Salenikovich 2000)**

End studs consisted of two 2x4s fastened by two 10d (0.120 in. $\phi$ ×3.0 in.) nails every 12 in. for walls with 6 in. perimeter nail spacing and every 6 in. for walls built with 4 in. nail spacing at sheathing panel edges. The nails were angled and driven in from either side in an alternating staggered pattern (see Figure 4.8). These nail spacings were

chosen after conducting a preliminary static wall test with AOSB sheathing attached to the framing with a 4 in. perimeter nail spacing. In this test, failure of the wall was controlled by buckling of the double 2x4 compression stud. The two 2x4s that comprised the end stud, which were nailed together with two 10d nails spaced at 12 in. on center, pulled apart and appeared to be acting as two slender 2x4 columns rather than a single built up column.

The theoretical Euler buckling load was calculated assuming that this built up column was fully composite and therefore behaved like a solid sawn piece of dimension lumber. The Euler buckling load for a solid sawn column measuring 3in. x 3.5 in. with pinned ends and an unbraced length of 8 ft. is approximately 15,200 lbs. In the test wall, the stud buckled when the lateral load reached 9,339 lb. Note that since the aspect ratio of the walls is 1:1, the force in the compression stud is approximately equal to the applied lateral load. With an upper bound buckling load of 15,200 lbs, it was expected that buckling could be prevented by doubling the number of nails tying the two studs together. The nail spacing was reduced to 6 in. for all walls tested with 4 in. perimeter nail spacing, and no more buckling failures were observed. Buckling of the compression stud was not expected to occur in walls with 6 in. perimeter nail spacing since these walls have less strength capacity, so the nail spacing was kept at 12 in. for construction of the double end studs of these walls.

Prior to testing, the wall specimens were stored in the laboratory for at least two weeks to allow for wood relaxation around the nails, which better simulates as-built condition in actual light-frame wood structures.

## 4.5 Loading

The static wall tests were conducted in load control following ASTM E-564 (ASTM 1998a), while the cyclic tests were performed under displacement control following the CUREE protocol (Krawinkler *et al.* 2000). Details of the loading protocols used for static and cyclic tests are discussed separately in this section.

### 4.5.1 Static Loading

Higher test loads than those recommended in ASTM E-564 were used (ASTM 1998a). The higher loads were necessary to exceed the design allowable load of the wall before the third half cycle. The use of higher loads is consistent with the test procedure used by the APA (Tissel 1993). These higher loads were also used by Dinehart and Shenton (1998) for tests of both plywood and OSB shear walls.

The loading consisted of three half cycles. In the first half cycle, the specimen was loaded at a rate of 20 lb/sec to a peak load approximately equal to the design load, and then unloaded to zero load at the same rate. The second half cycle consists of loading the specimen to approximately two times its design load and then unloading to zero again. Following the second unloading, the wall was loaded to failure.

The design loads were calculated for conventional OSB shear walls from the load tables given in NER-272 (NES 1997), which list allowable shear loads in pounds per foot for wind or seismic loading of walls fabricated with pneumatically driven nails of the type and size that were used to construct the wall test specimens. Values that were slightly higher than the calculated design values were used to be consistent with loads

used by other researchers for walls built with common nails (see for example: Dinehart and Shenton 1998). The calculated allowable loads and the test loads used are listed in Table 4.1.

**Table 4.1 Static Loading vs. Allowable Design Loads.**

| Nail Spacing at Panel Edges (in) | Design Allowable (lbs) | 1st Cycle Peak Load (lb) | 2nd Cycle Peak Load (lb) | 3rd Cycle Peak Load (lb) |
|---|---|---|---|---|
| 6 | 1760 | 2000 | 4000 | load to failure |
| 4 | 2600 | 3000 | 6000 | load to failure |

Since the design loads as well as the ultimate loads were unknown for AOSB shear walls, these walls were subjected to same loading as the conventional OSB shear walls. Using identical loading for static tests of both OSB and AOSB walls provided a direct means of comparing the performance of the two wall systems.

### 4.5.2 Cyclic Loading

The specimens were loaded according to the Quasi-Static Deformation Controlled Cyclic Test Protocol developed by CUREE at a rate of 0.4 in/sec, which is the highest loading rate recommended by CUREE (Krawinkler *et al.*, 2000) . Refer to Figure 3.10 to see the shape of the CUREE waveform.

Since the monotonic displacement capacities of AOSB walls were significantly larger than that of conventional OSB walls (see Table 4.2), two separate loading histories were developed (one for OSB and one for AOSB). This differs from the loading used for

**Table 4.2 Monotonic Displacement Capacities.**

| Control Specimens | $\Delta_m$ (in) | AOSB Specimens | $\Delta_m$ (in) |
|---|---|---|---|
| Static_4C_1 | 3.26 | Static_4R_001 | 5.10 |
| Static_4C_2 | 4.78 | Static_4R_002 | 6.08 |
| Static_4C_3 | 4.51 | Static_4R_003 | 5.35 |
| Static_6C_1 | 3.9 | Static_6R_001 | 5.45 |
| Static_6C_2 | 3.95 | Static_6R_002 | 5.76 |
| Static_6C_3 | 3.62 | Static_6R_003 | 5.35 |
| Average | 4.01 | Average | 5.52 |
| $\Delta = 0.6\ \Delta_m$ | 2.40 | $\Delta = 0.6\ \Delta_m$ | 3.31 |

the cyclic connection tests discussed in Chapter 3, where the AOSB specimens were subjected to the same loading as the control connections. One reason for performing the connection tests in this manner stemmed from the fact that no wall tests had been performed at that time, which left some uncertainty as to whether or not the increased displacement capacity of the AOSB connections would correspond to an increased displacement capacity of shear walls built with AOSB. Furthermore, it was not certain if the nails in the wall would undergo the same displacements as those imposed by the connection tests. However, since the results of the static wall tests did show that AOSB walls had a larger displacement capacity than conventional OSB walls, which could change the wall response to seismic excitation, parameters for the load histories were developed separately for OSB and AOSB walls.

No significant difference could be found between the monotonic displacement capacity of walls built with 4 in. and 6 in. perimeter nail spacing for either OSB or AOSB. Given this, data from the static tests of walls built with both perimeter spacings were used to develop parameters for the cyclic tests, and walls of both spacings were subjected to identical cyclic loading.

CUREE recommends defining the reference deformation as a specific fraction of the monotonic deformation capacity ($\Delta_m$), where $\Delta_m$ is defined as the point at which the applied load drops, for the first time, below 80% of the maximum load that was applied to the specimen. In contrast to preliminary connection test results, a preliminary cyclic wall test indicated that the reference value of $0.6\Delta_m$ recommended by CUREE did provide an accurate description of the difference in ultimate displacement capacity between walls tested statically and cyclically. Given this result, $0.6\Delta_m$ was used as the reference deformation ($\Delta$) for all cyclic wall tests. The monotonic displacement capacities computed from each static wall test and the resulting reference deformations ($\Delta$) for both control and AOSB specimens are listed in Table 4.2. Note that AOSB walls exhibited an average increase in monotonic displacement capacity of 38% over the control walls.

## 4.6 Static Shear Wall Test Results

The test matrix consisted of walls with both 4 in. and 6 in. perimeter nail spacings. Three specimens of each configuration were tested for a total of 12 static tests (see Table 4.3).

**Table 4.3 Static Shear Wall Test Matrix.**

| Specimen Type | 4in. Nail Spacing | 6in. Nail Spacing |
|---|---|---|
| Control | 3 | 3 |
| AOSB | 3 | 3 |

The overall load-displacement response of the AOSB specimens was characterized by a substantial increase in ductility over the control specimens. On average, walls built with AOSB panels were able to maintain at least 80% of their peak load up to a drift of nearly 5.5 in. compared to approximately 4.0 in. for the control walls. The AOSB walls with 4 in. perimeter nail spacing exhibited a 24% strength increase over the controls on average. No statistically significant difference was found in the strength of AOSB and control walls with a 6 in. perimeter nail spacing. The load-displacement curves for each wall configuration are shown in Figures 4.9 thru 4.12. Table 4.4 and Table 4.5 summarize average results for all tests. Tabulated results of all static wall tests are provided in the Appendix B. Pictures illustrating typical failures are also provided in Appendix B.

Moisture contents of the framing members were not recorded for the static wall tests. The lumber arrived with moisture contents ranging from 9 to 12%, and remained

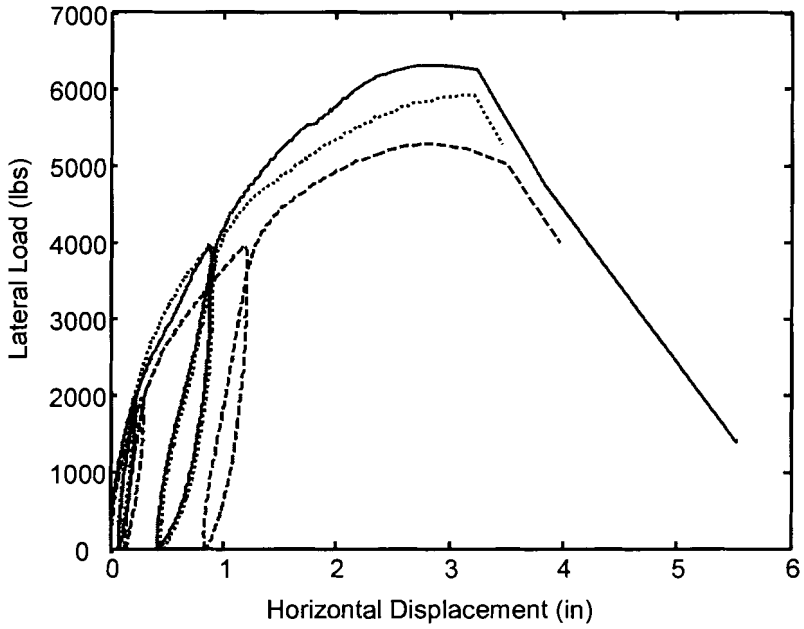


**Figure 4.9 Load-Displacement Curves for Control Walls with 6 in. Perimeter Nail Spacing.**

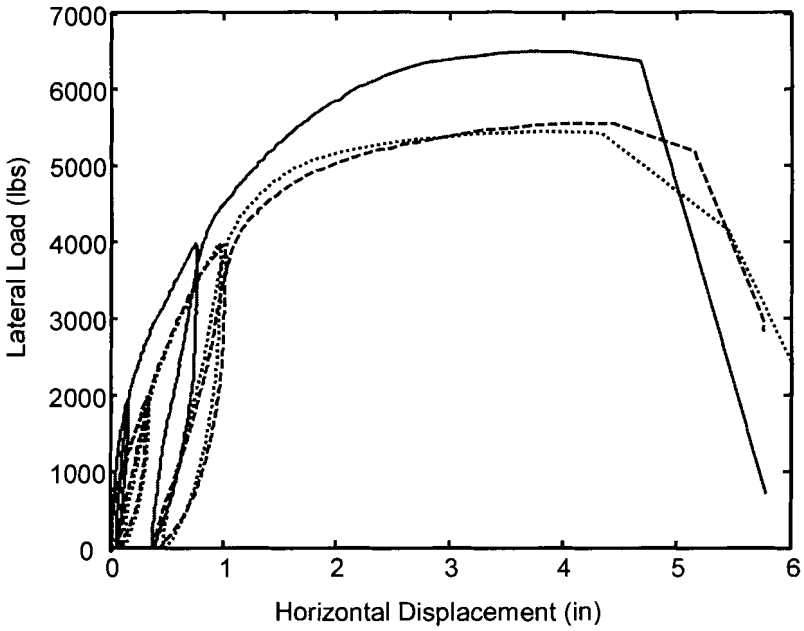


**Figure 4.10 Load-Displacement Curves for AOSB Walls with 6 in. Perimeter Nail Spacing.**

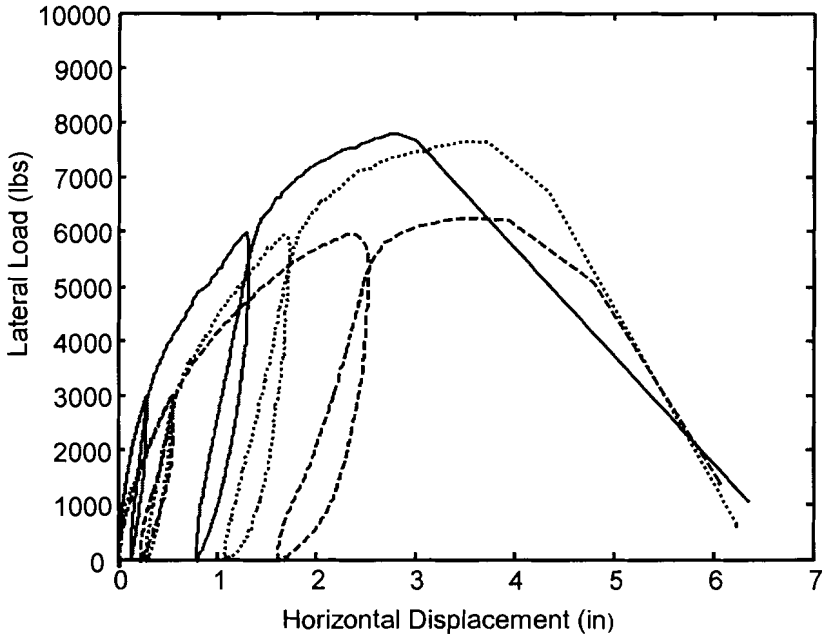


**Figure 4.11 Load-Displacement Curves for Control Walls with 4 in. Perimeter Nail Spacing.**

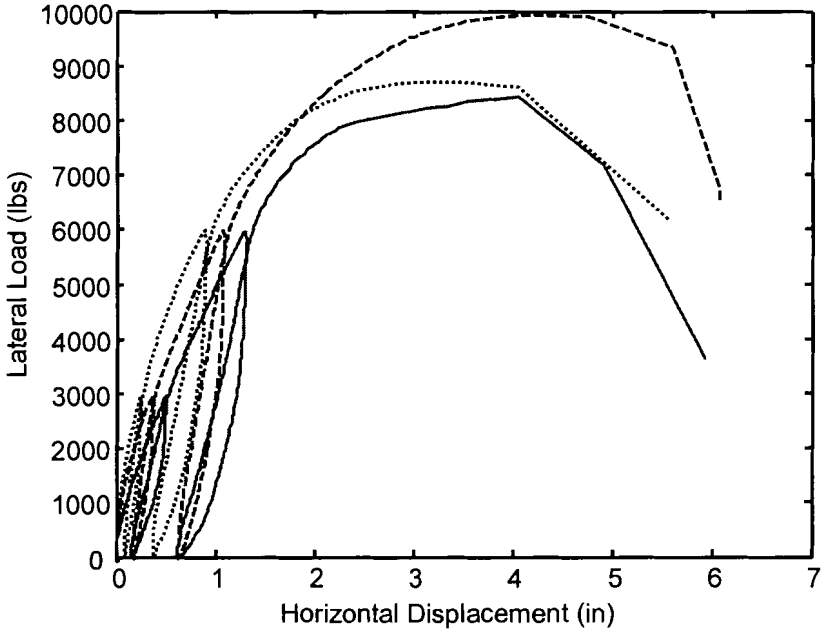


**Figure 4.12 Load-Displacement Curves for AOSB Walls with 4in. Perimeter Nail Spacing.**

**Table 4.4 Average Test Results of Walls with 6 in. Perimeter Nail Spacing.**

| Sheathing Type | Peak Load (lb) | Displ @ Peak Load (in.) | %Nails Failed | %Edge Tear | %Pull Through | %Pull Out |
|---|---|---|---|---|---|---|
| Control | 5908 | 3.09 | 56 | 43 | 54 | 3 |
| AOSB | 5872 | 3.93 | 30 | 11 | 0 | 89 |

**Table 4.5 Average Test Results of Walls with 4 in. Perimeter Nail Spacing.**

| Sheathing Type | Peak Load (lbs) | Displ @ Peak Load (in.) | %Nails Failed | %Edge Tear | %Pull Through | %Pull Out |
|---|---|---|---|---|---|---|
| Control | 7317 | 3.30 | 40 | 41 | 53 | 6 |
| AOSB | 9070 | 3.80 | 22 | 20 | 0 | 80 |

essentially unchanged throughout the summer months that these walls were built and tested. Since the moisture contents did not change very much due to the temperature and relative humidity at the time, shrinkage or expansion of the framing was expected to be minimal, which negated the need to document moisture contents at the time of building and testing.

The tests were stopped when the actuator reached a preset displacement limit of 6 in. Note that two of the control walls with 6 in. perimeter nail spacing (see Figure 4.9) were stopped at a displacement of approximately 4 in. The reason for stopping these tests prematurely was due to malfunctioning of the actuator. The load control gain settings were too high, which caused the servo valve to become unstable once the walls reached

their strength capacity and the load could no longer be increased. Once the servo valve became unstable, the actuator was uncontrollable and the hydraulics had to be shut off immediately for safety reasons. The proportion, integral and differential gain settings were adjusted following these two tests. The new settings, which allowed the actuator to move through the entire 6 in. without instability of the servo valve, were used for all subsequent tests.

The predominant nail failure modes for all of the control walls were edge tear and nail-head pull-through. In the AOSB walls, nail pullout was the most common failure mode, and no nail-head pull-through failures were observed. A small percentage of edge tear failures were noted, however the nails were substantially withdrawn from the framing before tearing through the edge of the sheathing.

## 4.7 Cyclic Shear Wall Test Results

The test matrix of cyclic wall tests was identical to that of the static wall tests, i.e. three tests of each configuration for a total of 12 tests. The hysteresis loops of the AOSB specimens exhibited significantly less pinching and loss of capacity relative to the monotonic response. Overall, the AOSB specimens exhibited less damage due to load cycling, and absorbed an average of 52% more energy than the control specimens with a 6 in. nail spacing and 73% more energy with a 4 in. nail spacing.

The average results of the cyclic wall tests are given for walls with 6 in. and 4 in. perimeter nail spacing in Table 4.6 and Table 4.7 respectively. The last column in the tables labeled "strength loss" is a comparison of the average peak load of the cyclic tests compared to the average peak load observed in the static tests. AOSB specimens were

observed to exhibit less strength and stiffness degradation than the control specimens when subject to cyclic loading. AOSB walls of both perimeter nail spacings exhibited substantial increases in energy dissipation.

**Table 4.6 Cyclic Test Results of Walls with 6 in. Perimeter Nail Spacing.**

| Sheathing Type | Max Load (lbs) | Energy (lb-in) | Strength Loss (%) |
|---|---|---|---|
| Control | 5184 | 89,043 | 12% |
| AOSB | 5676 | 135,815 | 3% |

**Table 4.7 Cyclic Test Results of Walls with 4 in. Perimeter Nail Spacing.**

| Sheathing Type | Max Load (lbs) | Energy (lb-in) | Strength Loss (%) |
|---|---|---|---|
| Control | 7239 | 116,854 | 1% |
| AOSB | 8901 | 202,613 | 2% |

Typical load-displacement plots for walls with 6 in. and 4 in. perimeter nail spacing are shown in Figure 4.13 and Figure 4.14 respectively. Tabulated results and hysteresis plots for each test along with pictures illustrating typical failure modes are provided in Appendix B. The walls were built late in the fall and stored in the

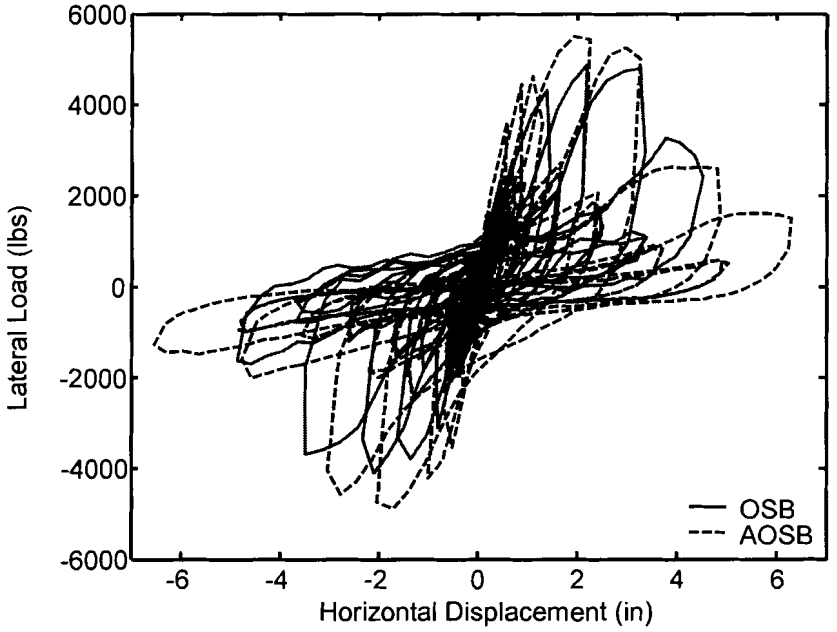


**Figure 4.13 Typical Hysteretic Response of OSB and AOSB walls with 6 in. Perimeter Nail Spacing.**

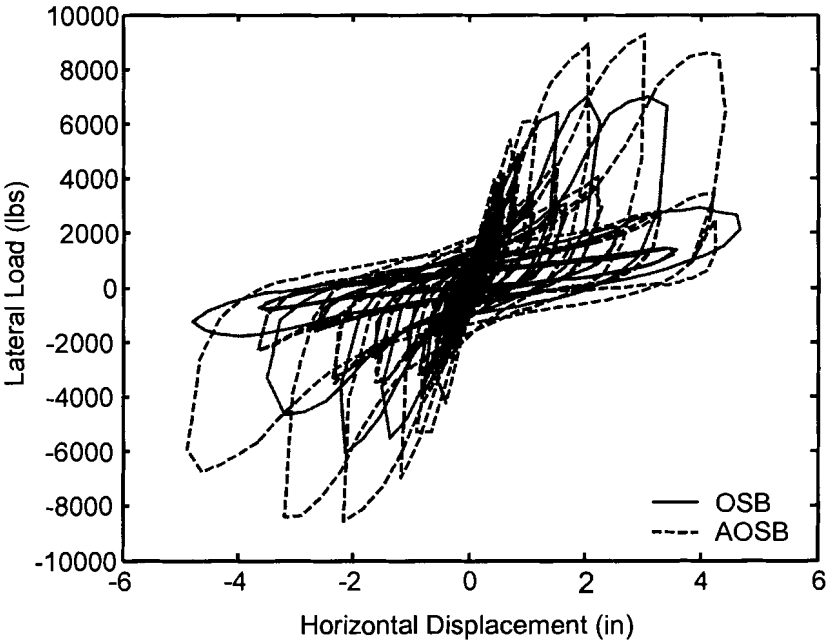


**Figure 4.14 Typical Hysteretic Response of OSB and AOSB walls with 4 in. Perimeter Nail Spacing.**

laboratory until mid winter. Since the lab becomes very dry during the winter months, the moisture contents of the framing members were measured with an electrical resistance moisture meter when the walls were built and again when the walls were tested. These values are also provided in Appendix B.

Note that the positive portion of the curves in Figure 4.13 and Figure 4.14 correspond to the wall being pulled back by the actuator, while the negative portion of the curves is the wall response as it is being pushed forward. The curves are generally quite symmetrical with respect to loading direction, however the highest loads typically occur when the wall is being pulled backward (positive displacement). This is thought to be because this is the initial loading direction. Loading in the opposite direction (pushing forward) occurs after the wall has already undergone the same displacement in the positive direction. Damage incurred from loading in the initial direction is thought to reduce the wall capacity upon load reversal.

The ultimate failure of the AOSB walls with 4 in. perimeter nail spacing was often initiated by the top plate pulling off the double end post as the wall was pushed forward. This indicates that the use of steel angles, straps or similar types of connectors to reinforce stud-to-plate connections at the top corners of the wall may increase the capacity of walls constructed with AOSB.

Similar to the static tests, the predominant nail failure modes of the control walls, were edge tear and nail-head pull-through. In the AOSB walls, nail pullout and nail fatigue were the most common failures. No nail-head pull-through failures were observed. Edge tear failures were observed but were not common. The nails were

substantially withdrawn from the framing when edge tear failures occurred. The frequency of each type of failure mode is listed in Table 4.8 and Table 4.9.

**Table 4.8 Cyclic Nail Failure Modes of Walls with 6 in. Perimeter Nail Spacing.**

| Sheathing Type | %Nails Failed | %Edge Tear | %Pull Through | %Nail Fatigue | %Pull Out |
|---|---|---|---|---|---|
| Control | 43 | 46 | 54 | 0 | 0 |
| AOSB | 65 | 4 | 0 | 77 | 19 |

**Table 4.9 Cyclic Nail Failure Modes of Walls with 4 in. Perimeter Nail Spacing.**

| Sheathing Type | %Nails Failed | %Edge Tear | %Pull Through | %Nail Fatigue | %Pull Out |
|---|---|---|---|---|---|
| Control | 50 | 38 | 62 | 0 | 1 |
| AOSB | 56 | 6 | 0 | 48 | 46 |

While the sheathing panels of the control specimens were extensively damaged under cyclic loading due to edge tear of nails, very little damage of the AOSB panels was observed. This, coupled with the fact that failure of the AOSB walls was driven primarily by nail fatigue and nail pullout, indicates that AOSB sheathing panels provide as much capacity as the framing and the nails will allow. Further investigation of how to improve the AOSB shear wall system as a whole to utilize the full strength of AOSB is one of the primary focuses of current and future research efforts at the University of Maine.

## 4.8 Design Loads for AOSB Shear Walls

An alternative to marketing AOSB as a commodity product sold by the sheet would be to market prefabricated wood-frame shear walls constructed with AOSB sheathing. With this alternative in mind, allowable stress design (ASD) loads were calculated from the first cycle envelope of the cyclic load displacement curves in accordance with the *Acceptance Criteria for Prefabricated Wood Shear Panels* (ICBO ES AC130). For means of comparison, ASD loads were calculated from the data of both AOSB and conventional OSB walls.

The first cycle envelope curves derived from the cyclic wall test data that were used to calculated the design values given in Table 4.10 are plotted in Appendix B. Note that there are two sets of design values listed in Table 4.10, one set for Prefabricated Wood Shear Panels (PWSP) and the other for Wood-shear resisting Frames (WSRF). AC130 defines PWSPs as prefabricated assemblies (with sheathing) designed and constructed to resist in-plane shear in walls. WSRFs are defined as an assembly of one or more PWSPs connected at the top by a horizontal beam of known length and stiffness. (ICBO ES AC130). WSRFs have a minimum safety factor of 2.5, while PWSPs are only subject to a safety factor of 2.0. This in combination with the fact that the allowable loads for PWSP were controlled by drift limits while allowable loads for WSRFs were controlled by ultimate load limits explains the difference in the two design values.

**Table 4.10 ASD Loads Calculated from Cyclic Test Data.**

| Wall Construction Methods | | Prefabricated Wood Shear Panels | | Wood Shear-resisting Frame | |
|---|---|---|---|---|---|
| Wall Type | Nail Spacing at Panel Edges (in) | Allowable Stress Design Load (lb) | Drift at Allowable Load (in) | Allowable Stress Design Load (lb) | Drift at Allowable Load (in) |
| OSB | 4 | 3122 | 0.414 | 2891 | 0.366 |
| AOSB | 4 | 3693 | 0.404 | 3549 | 0.380 |
| OSB | 6 | 2379 | 0.389 | 2049 | 0.303 |
| AOSB | 6 | 2649 | 0.346 | 2258 | 0.276 |

AC130 defines the allowable stress design (ASD) load as the lesser of the two values determined by ultimate load or the load that satisfies drift limits according to UBC 1630.9 (ICBO 1997).

The ASD ultimate load is the mean ultimate load determined by cyclic testing (according to sec 5.1 of AC 130) divided by the appropriate safety factor (2.5 for WSRFs and 2 for PWSPs). The drift limit load is the load corresponding to displacement $\Delta_S$ on the first cycle backbone curve divided by 1.4. $\Delta_S = \Delta_M / 0.7R$ The R factor for bearing wall structures made of wood structural panel walls less than three stories high is 5.5 (ICBO 1997). $\Delta_M$ is the lesser of the following:

a) 2.4 in. = the inelastic drift limit according to UBC 1630.10.2 (ICBO 1997) for an 8 ft. high wall in a typical wood structure ($\Delta_M$ =0.025h, since the fundamental period is less than 0.7 seconds).

b) $\Delta_{SLS}$ = mean displacement at peak load determined from the first cycle envelope curves.

AOSB walls with 4 in. nail spacing at the panel edges showed increases of 18% and 23% in allowable load over the control walls for PWSPs and WSRFs respectively. AOSB walls with 6 in. nail spacing at panel edges showed increases of 11% for PWSPs and 10% for WSRFs.

Consideration of the parameters controlling these design loads reveals some possible focus areas for continued research on AOSB shear wall systems. Design loads are controlled by the lower of the allowable stress level load at the drift limit or the ultimate load divided by the appropriate factor of safety. To increase the design load of AOSB walls, stiffness and ultimate load will need to be increased simultaneously. Increasing either stiffness or ultimate load alone will not increase the design load since it is limited by the lower of these two properties. The peak load of AOSB walls generally occurs at or above the maximum drift limit of 0.025h (2.4 in. for an 8 ft. wall) imposed by the Uniform Building Code (ICBO 1997). This means that any further increase in displacement at peak load without simultaneous increases in stiffness and ultimate load will not translate into a higher design value.

There are many possibilities for increasing both the stiffness and ultimate strength capacity of AOSB shear walls. One is to investigate other sheathing-to-framing connectors, namely screws or deformed shank nails. Using fasteners of this type which have a higher withdrawal capacity than smooth shank nails, may prevent the nails from pulling out of the framing and force an edge tear failure which would utilize the full strength of the AOSB and likely increase the ultimate load of the wall assembly.

Other modifications that are independent of AOSB sheathing panels may also substantially increase the initial stiffness of the walls. Some modifications that have been employed by manufacturers of prefabricated wood shear wall systems currently on the market (i.e. Simpson Strong Tie, Trus Joist, Shear Transfer Systems, etc.) are listed below.

- Have end posts bear directly on the foundation. This prevents excessive deflection from perpendicular to grain crushing of the sole plate under the compression stud.
- Investigate the use of other tension hold downs, namely Simpson HDQ8 or equivalent. Tie downs that attach with screws rather than bolts prevent initial slippage of the tension post due to over-sizing of bolt holes.
- Inset the edges of the sheathing into the framing. This forces the panels to bear on the perimeter framing members as the wall racks providing displacement compatibility and increased racking resistance through bearing.

Preliminary results found during the development of a finite element model of AOSB shear walls with 4 in. nail spacing at panels edges indicate that these modifications may be highly effective ways of increasing both initial stiffness and ultimate load of walls built with AOSB. The development and results of this computer model are discussed in the following chapter.

# Chapter 5

# COMPUTER MODELING OF SHEAR WALLS

The objectives of the finite-element analysis described in this chapter were to gain a better understanding of the response of the shear walls tested in this study, and to form a basis for studies on the further refinement and optimization of wood-framed shear walls. To achieve these objectives, a two-dimensional finite element model of two panel AOSB shear walls with 4 in. perimeter nail spacing was developed using the computer program ANSYS 5.7 (ANSYS 2000). The model has 15,749 degrees of freedom and employs a small displacement nonlinear analysis to model the monotonic load-deflection response of the shear wall test specimens discussed previously in Chapter 4. The development, results, and verification of the model are presented in this chapter.

## 5.1 Overview of Model

The model consists of 1) beam elements for framing, 2) 8 node quadrilateral plane stress elements for sheathing, 3) springs connecting framing members, 4) two uncoupled orthogonal nonlinear springs to represent each sheathing to framing nail, 5) frictional contact elements between sheathing panels, and 6) linear springs to represent tension hold-down connectors and other base restraints.

Each sheathing-to-framing connector was modeled with two independent one-dimensional nonlinear springs oriented orthogonal to each other. The properties of the connector springs were developed from experimental nailed connection test data as discussed in Chapters 3 and 4. The use of perpendicular spring pairs to connect the

sheathing and framing nodes is a very common modeling approach found in the literature (e.g. Easley *et al.* 1982; Itani and Cheung 1984; Dolan and Foschi 1991; White and Dolan 1995; Folz and Filiatrault 2001).

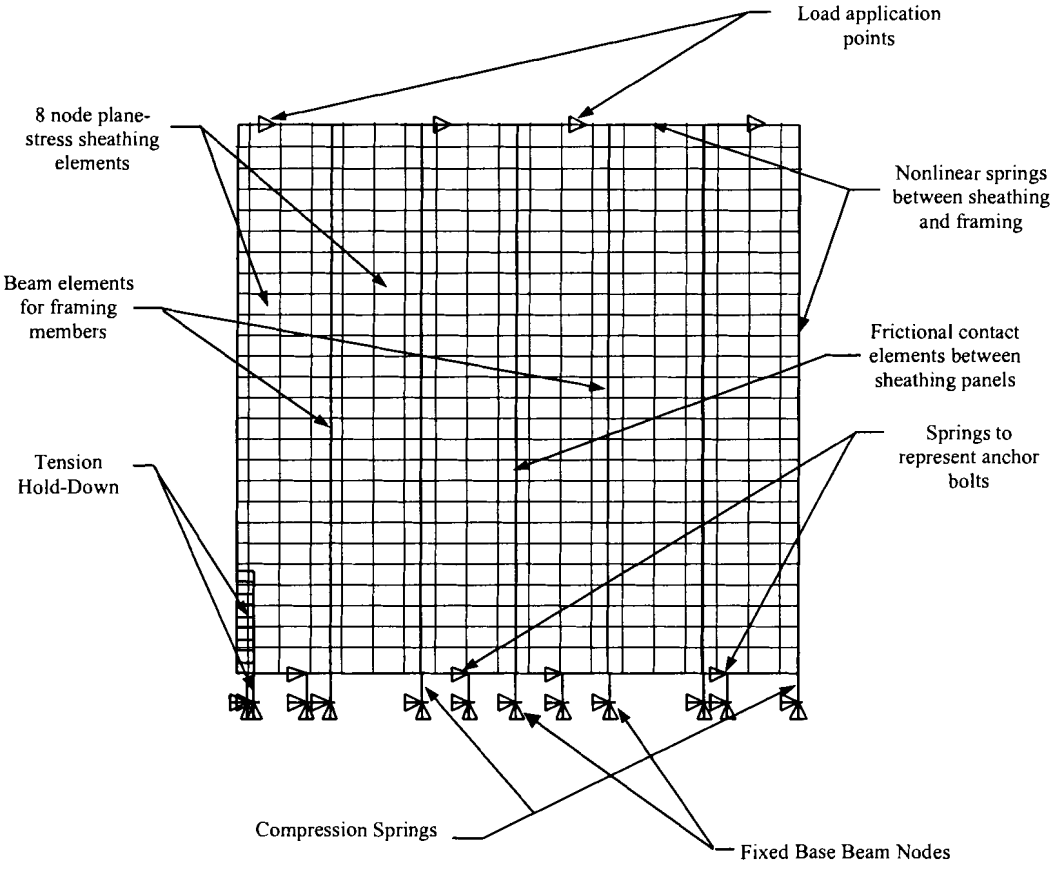


**Figure 5.1 Overview of Model.**

The use of compression only springs to model contact of adjacent sheathing panels is another common feature of many shear wall models. Gutkowski and Castillo (1988) developed a shear wall model that incorporated elements of this type. Similar elements have also been included in more recent computer models developed by Dolan and Foschi (1991) and White and Dolan (1995). These elements are typically used to prevent the nodes of adjacent panels from overlapping and offer no resistance tangential

to the contact surface (panels sliding relative to each other). Frictional sliding resistance was included in the model of AOSB walls for completeness and because it was simple to incorporate with the predefined element, CONTAC12, in ANSYS. A more detailed discussion of this element is provided in section 5.2.

One unique feature of the model is the inclusion of tension hold-down restraints and compressive deflection of the wall bottom plate. Despite the recognized importance of tension hold-downs and other anchorage devices used to resist global overturning, the effect of such restraints has been neglected in past finite element models. However, Simpson Strong-Tie Inc. has recently developed models for their proprietary "strong walls" which do include the effect of tension hold-downs. (Pryor & Murphy 2002).

A detailed discussion of the model and its development is provided in the sections that follow.

## 5.2 Basic Model Components

A brief description of each element type used in the model is provided in this section. For more details about these elements see the ANSYS Element Reference which is provided with the ANSYS software (ANSYS 1999).

The beam elements used to model the framing are predefined as BEAM3 in ANSYS. BEAM3 is a common two dimensional line element with three degrees of freedom at each node, a linear displacement field in the axial direction and a cubic displacement field for deflections perpendicular to the beam. Input values required for this element include nominal material and section properties. The material properties required were modulus of elasticity, shear modulus and Poisson's ratios for the three

principal directions. These values were obtained from Chapter 4 of the Wood Handbook (Forest Products Laboratory 1999). Although the framing material used in the experimental wall tests was Southern Yellow Pine, which encompasses several different species of pine, Loblolly pine at 12% moisture content was used as the reference species for the purposes of defining the model parameters. The section properties (area and moment of inertia) of the framing members were input into the model as well. For simplicity the double 2x4 end posts and double top plate were modeled as solid sawn sections.

The sheathing elements were modeled with the ANSYS element PLANE82. PLANE82 is a two-dimensional 8-node structural solid with two translational degrees of freedom at each node. The material properties of the sheathing panels were defined as the minimum values required of conventional OSB by the Structural Board Association (http://www.sba-osb.com). The Structural Board Association's standard requires that panels have a modulus of elasticity (MOE) of 800,000 psi in the direction of the strong axis and a weak axis MOE of 225,000 psi (Schwentker 2001).

Contact between the adjacent vertical surfaces of the two sheathing panels was simulated by using point-to-point frictional contact elements called CONTAC12, which allow two surfaces to maintain or break physical contact and slide relative to each other. CONTAC12 is a compression-only element in the direction normal to the surfaces and provides Coulomb frictional resistance in the tangential direction. Theoretically the contact stiffness is infinite and the panels deform at the interface due to their own inherent stiffness. A contact stiffness of 900 k/in was found to be effective at preventing

the two panels from overlapping without causing numerical difficulties. Since both of the two surfaces in contact are dry smooth wood, a static friction coefficient of 0.6 was used (Ritter 1990). Rolling friction was not considered.

Each sheathing-to-framing nail was represented by two uncoupled nonlinear springs. Each of the two springs had only a single degree of freedom. One spring was only allowed to translate in the x-direction and the other only in the y-direction. The two springs were orthogonal to each other so that the resultant of the two spring forces acts along the axis of the nail. The nonlinear spring element used to model the orthogonal springs is referred to as COMBIN39 in ANSYS. The average load-displacement response, found in the monotonic connection tests, was used as constitutive input for the nonlinear spring connector elements as discussed in the section 5.4.1.

## 5.3 Convergence Study

Initially a simplified linear model was developed to study the effects of mesh refinement. This simplified model consisted of pin connected framing members with pinned restraints along the sole plate at the bolt locations of the shear wall test rig. Linear springs with a stiffness of 4000 lb/in. were used to model the sheathing-to-framing nails. This stiffness value is identical to the lower limit found by Salenikovich (2000) for OSB nailed connections. Comparable initial stiffness values have also been used by Dolan and Foschi (1991) and White and Dolan (1995) to model shear walls sheathed with plywood or waferboard.

Four different mesh sizes were considered: 16, 8, 4, and 2 inch element edge lengths. In all four cases the framing and sheathing elements were meshed with elements

of equal edge length. This was done so that the perimeter nodes of the sheathing panels would be in the same location as the framing nodes, allowing for proper definition of the sheathing-to-framing spring connectors.

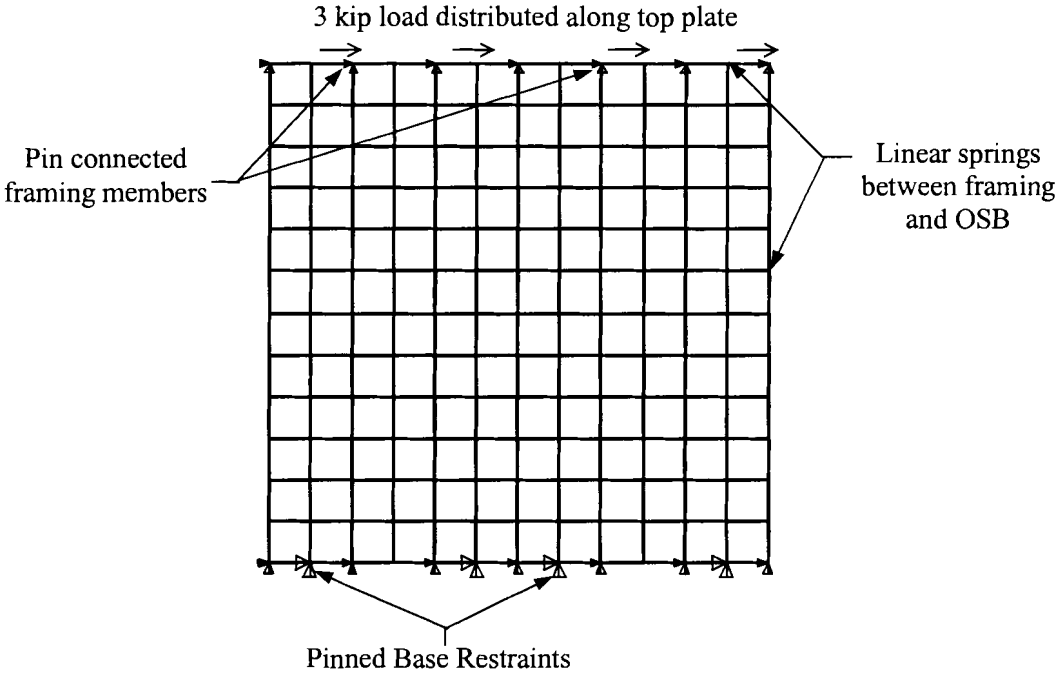


**Figure 5.2 Simplified Linear Model.**

For the models with 2 in. and 4 in. element edge lengths, the springs representing the sheathing-to-framing nails were defined at the proper locations, i.e. every 4 in. around the perimeter of the panels and every 12 in. in the field. In the case of the models with 8 in. and 16 in. element edge lengths, where there are not enough nodes to define nail springs in their proper locations, the nails were grouped at the available nodes. As shown in Figure 5.3, the solution converges with a 4 in. element edge length. However, in an effort to make the model more versatile, the 2 in. edge length was chosen for further

development. With a 2 in. edge length the model can be easily modified to model walls with 6 in. perimeter nail spacing, without having to group the nails at the nodes. The cost of using this more refined mesh is increased computational time, but that was deemed of secondary importance for the development of this model. The primary goal was to capture the complex load sharing behavior of the AOSB shear wall system to aid in future design improvements of AOSB shear wall systems.

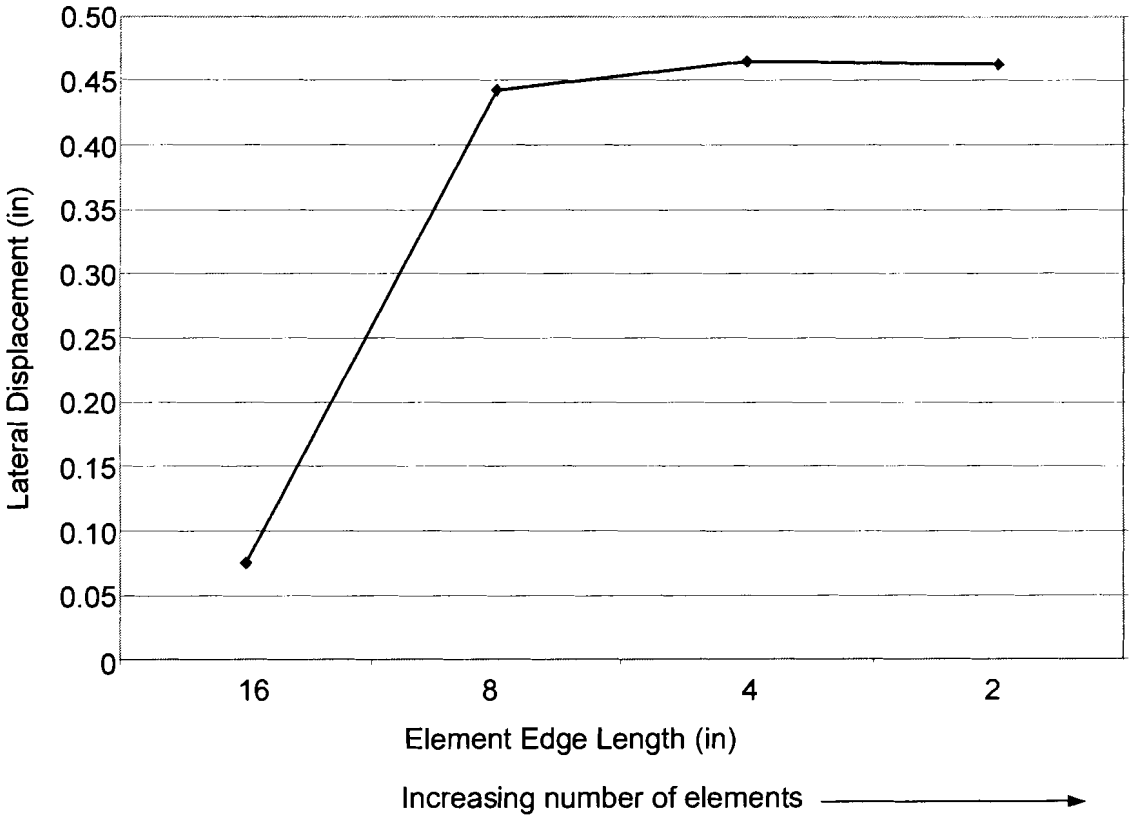


**Figure 5.3 Wall Displacement vs. Mesh Size.**

## 5.4 Modeling Parameters

A discussion of the modeling approach for individual components of the model along with a justification of the parameters used is provided in this section. The model parameters/components discussed in this section include: sheathing-to-framing connectors, tension hold-downs, anchor bolts, compressive deflection of the sole plate and stud-to-plate connections.

### 5.4.1 Sheathing-to-Framing Connectors

The average load-displacement curve was used as input for the nonlinear sheathing-to-framing springs in the model. A detailed discussion of the procedure used to develop the average curve is provided in Chapter 3.

The initial stiffness of the average load-displacement curve for AOSB single nail connections was found to be approximately 5,169 lbs/in. in the monotonic connection tests. As described in Chapter 4, these tests were performed according to ASTM D1761, which states that the specimens shall be tested as quickly as possible after assembly (ASTM 1998b). However, the static wall specimens were allowed to condition in the laboratory for a minimum of two weeks prior to testing. Nailed connections exhibit reduced stiffness over time due to shrinkage and relaxation of wood fibers around the nail. This was accounted for in the model by adjusting the initial stiffness of the connectors to a value that produced results which were in good agreement with the experimental wall test data in the linear range. The linear range was considered to end at approximately 3,000 lb, which corresponds to the peak load in the first half load cycle of the static shear wall tests. An initial stiffness of 4,000 lb/in was found to provide results

that agreed reasonably well with experimental data in the linear range. To reduce the initial stiffness without changing subsequent stiffness values along the curve, a constant was added to the displacements defining the load-displacement curve. As illustrated in Figure 5.4 this simply shifts the load-displacement curve to the right. Since the origin of the curve remains at zero displacement, the initial stiffness is reduced however, all other tangential stiffness values remain unchanged since all other points defining the curve have been shifted to the right by the same amount.

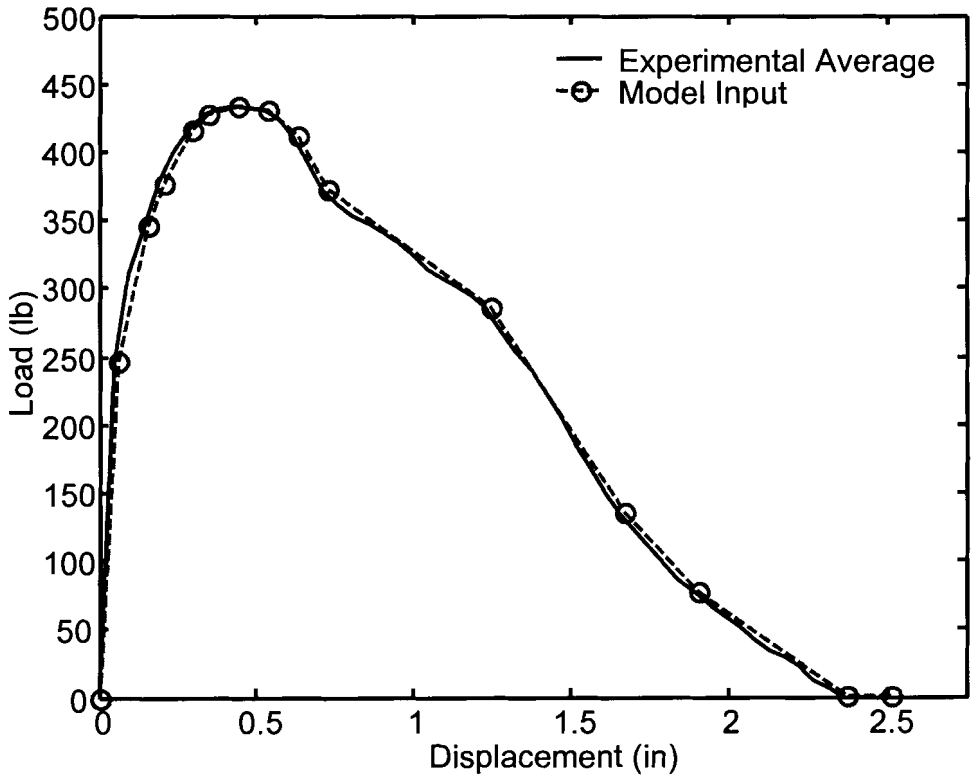


**Figure 5.4 Nonlinear Sheathing-to-Framing Connector Properties.**

### 5.4.2 Tension Hold-Downs

As described in Chapter 4, Simpson HD10A hold-down anchors were used at the bottom corners of all wall specimens. Pictures of the hold-downs are provided in Figure 5.5 courtesy of Simpson Strong-Tie (http://www.strongtie.com). Simpson provides data relating to the allowable and ultimate tensile loads of the hold-downs. This data is available online as well as in Simpson's Wood Construction Connectors Catalog (Simpson Strong Tie 2002). A copy of the hold-down data table provided on the Simpson Strong Tie web site is provided in Figure 5.5. This table lists the hold-down dimensions along with allowable tension loads.

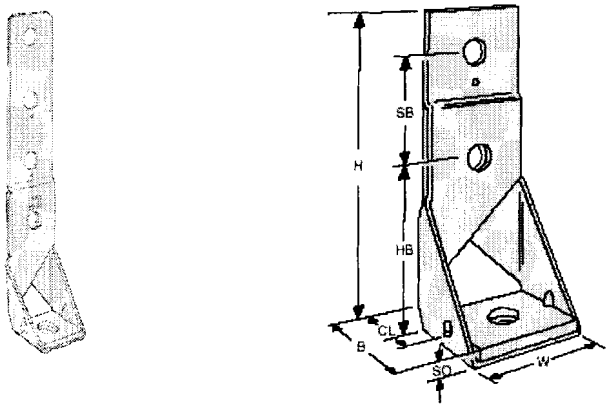


| Model No. | Material | | Dimensions | | | | | | | Fasteners | | | Avg Ult | Allowable Tension Loads[1,7,8,10] (133) | | | | | | Holdown[11] Deflection at Highest Allowable Design Load |
|---|---|---|---|---|---|---|---|---|---|---|---|---|---|---|---|---|---|---|---|---|
| | Base Ga | Body Ga | HB[4] | SB | W | H | B | SQ | CL | Anchor Dia[5,6] | Stud Bolts Qty | Stud Bolts Dia | | Length of Bolt[2,9] in Vertical Wood Member (DF/SP) 1½ | 2 | 2½ | 3 | 3½ | 5½ | |
| HD2A | 7 | 12 | 4⅝ | 2½ | 2½ | 8 | 2⅝ | ⅛ | 1⅞ | ⅝ | 2 | ⅝ | 12150 | 1555 | 2055 | 2565 | 2775 | 2775 | 2760 | 0.058 |
| HD5A | 3 | 10 | 5¼ | 3 | 3⅛ | 9⅞ | 3⅝ | ½ | 2⅜ | ⅝ or ¾ | 2 | ¾ | 20767 | 1870 | 2485 | 3095 | 3705 | 4010 | 3980 | 0.067 |
| HD6A | ⅜ | 7 | 6⅝ | 3½ | 3¼ | 11⅛ | 3⅞ | ⅜ | 2⅛ | ⅞ | 2 | ⅞ | 27333 | 2275 | 2980 | 3685 | 4405 | 5105 | 5510 | 0.041 |
| HD8A | ⅜ | 7 | 6⅝ | 3½ | 3¼ | 14⅛ | 3⅞ | ⅜ | 2⅛ | ⅞ | 3 | ⅞ | 28667 | 3220 | 4350 | 5415 | 6465 | 7460 | 7910 | 0.111 |
| HD10A | ⅜ | 7 | 6⅝ | 3½ | 3¼ | 18⅛ | 3⅞ | ⅜ | 2⅛ | ⅞ | 4 | ⅞ | 28667 | 3945 | 5540 | 6935 | 8310 | 9540 | 9900 | 0.269 |
| HD14A | ½ | 3 | 7 | 4 | 3½ | 20⅝ | 3½ | ½ | 2⅜ | 1 | 4 | 1 | 38167 | — | — | — | — | 11080 | 13380 | 0.215 |
| HD20A | ½ | 3 | 7 | 4 | 4¼ | 20¾ | 4⅛ | ⅛ | 2⅜ | 1¼ | 4 | 1 | 51333 | — | — | — | — | 11080 | 13380 | 0.250 |
| HD15 | ⅝ | 3 | 7 | 4 | 3½ | 24½ | 4⅞ | 3⅝ | 2⅛ | 1¼ | 5 | 1 | 55333 | — | — | — | — | — | 15305 | 0.082 |

**Figure 5.5 Simpson HD10A Hold-Down Connectors (Simpson Strong Tie 2002).**

Figure 5.5 lists an allowable tension load of 8,310 lbs. for a HD10A when the length of the bolts in the vertical stud is 3 in. The corresponding deflection at the design allowable load is 0.269 in.. Dividing 8310 lbs by 0.269 in. produces a linear spring stiffness of 30,892 lb/in., which is the value that was used in the model. Although the hold-down is a tension only restraint, it was necessary to model them as linear springs with equal resistance in both tension and compression to reach convergence at high loads, since modeling the hold-down as a tension only element produced oscillation in the residual force vector preventing convergence near peak load. However, due to the geometry and loading direction of the model, the hold-down spring never goes into compression.

The approach used to model the hold-down is illustrated in Figure 5.6. Given the geometry of the hold-down anchor, the tension force in the vertical end post is transmitted to the base beam eccentrically. This eccentricity was included in the model by defining a series of rigid links that extend horizontally from the nodes of the tension stud to the actual eccentricity as measured from the centerline of the tension stud to the centerline of the bolt hole in the base of the hold-down (See Figure 5.6). The small frame created by the series of rigid links was connected to a fixed slave node representing the base beam of the shear wall test rig with a linear spring with a stiffness of 30,892 lb/in as discussed previously. To allow for differential movement between the sole plate and the tension stud, the hold-down spring was not connected to the sole plate of the wall. A separate spring was used to represent the lifting restraint imposed on the sole plate by the hold-down base bolt . The stiffness of this spring is discussed separately in section 5.4.3.

To avoid large stress concentrations at the nodes of the tension stud, rigid links were created at every node along the 18 in. height of the hold-down. In this way the hold-down tension force is distributed to the tension stud at a total of eight nodes (see Figure 5.6.)

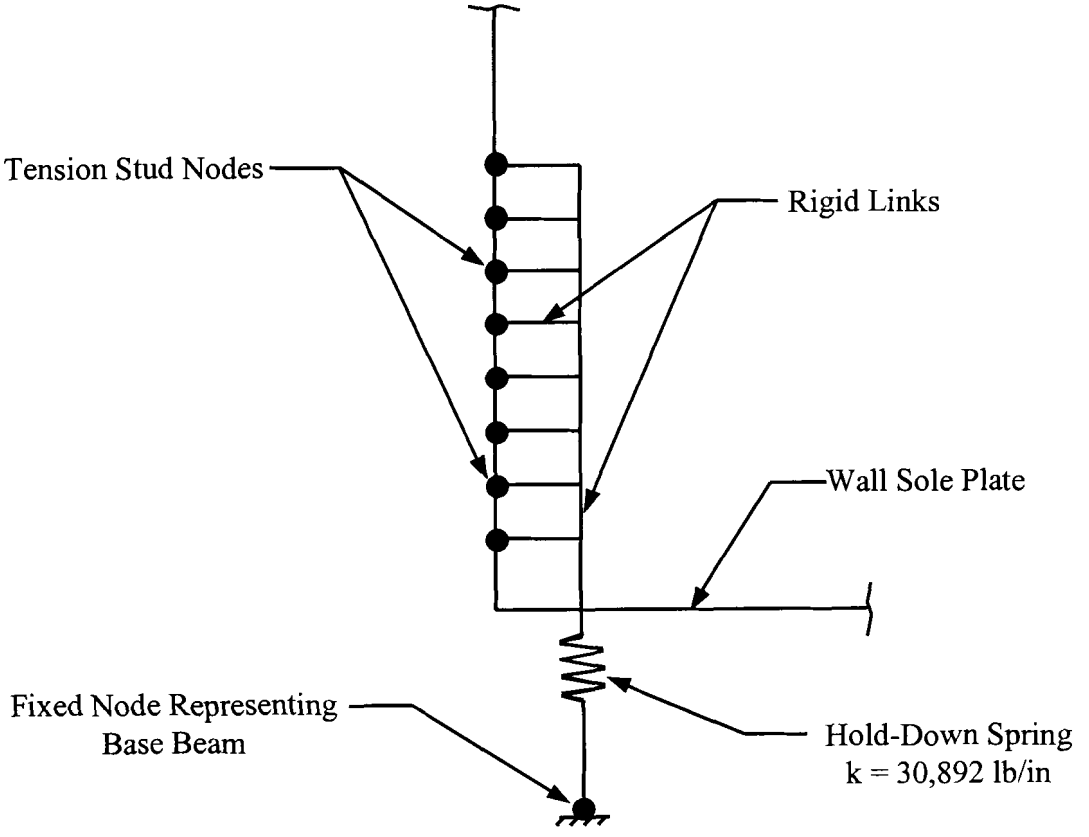


**Figure 5.6 Modeling of Tension Hold-Down Anchor.**

### 5.4.3 Anchor Bolts

The steel base beam was anchored to the 30 in. thick concrete reaction floor with 1 in. diameter steel rod at four locations. Given the high stiffness of this connection relative to all other connections in the shear wall system, the base beam was considered fixed and modeled as a series of fixed nodes below the sole plate. In addition to the

tension hold-down bolts in the wall corners, the sole plates of the wall specimens were bolted to the top of the base beam in four locations for a total of six anchor bolts. Each anchor bolt was modeled as a spring with its initial node being a fixed based beam node and its terminal node being the sole plate node directly above. The bolts provide tension resistance only, however to avoid convergence difficulties, a compressive stiffness of approximately 2% of the tensile stiffness was used. The model results were checked to verify that the springs had not gone into compression. The bolt springs were found to remain in tension at all times. Furthermore, the results show that the two bolts nearest the tension corner of the wall carry the bulk of the uplift reaction, while the tensile load in the other bolts was found to be negligible.

The tensile stiffness of the anchor bolt springs was taken as the stiffness of the wall sole plate under compressive loading perpendicular to grain. As shown in Figure 5.7, a 3 in. square steel plate was used to distribute the bolt force to the sole plate. Since the sole plate was modeled with two dimensional line elements, the effective area of the sole plate in compression was approximated by projecting the area of the steel plate onto the mid-plane of the sole plate. This was done by assuming a $45^{\circ}$ load transmission angle (pyramid approximation). The elastic modulus perpendicular to grain was taken as 11.3% of the adjusted allowable modulus parallel to grain of No. 2 Southern Pine given in the NDS (AF&PA 1997), or 180,800 psi. The 11.3% proportion was based on modular ratios given for Loblolly pine in Chapter 4 of the Wood Handbook (Forest Products Laboratory 1999).

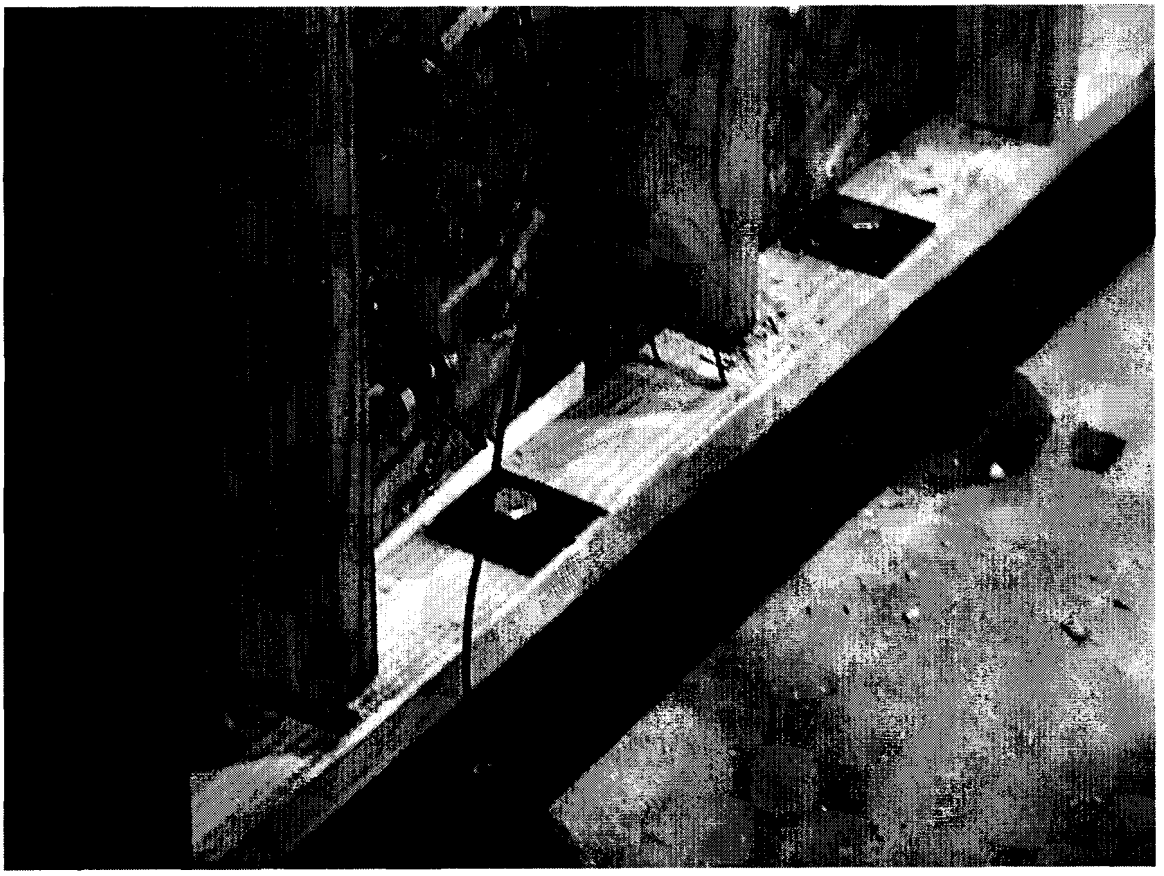

**Figure 5.7 Shear Wall Base Bolts.**

The spring stiffness ($k$) was then calculated as:

$$k = \frac{E_{\perp} \times A_{proj}}{L} = \frac{180{,}800\text{psi} \times (4.5" \times 3.5")}{1.5"} = 1{,}898{,}400\text{psi} \qquad 6.1$$

where $A_{proj}$ is the projected area of the steel plate on the mid-plane of the sole plate based on the pyramid approximation and L is the thickness of the sole plate.

Experimental measurements of horizontal slip of the sole plate showed an average slip of 0.044 in. at ultimate load. Based on this finding the slip was considered negligible and the horizontal DOF of the sole plate was fixed at the nodal locations of the four interior anchor bolts. The horizontal DOF of the sole plate was not constrained at the

location of the tension hold-down bolts. This was done to allow for localized axial deflection of the sole plate, since the bolt holes for the tension hold-downs were oversized by $\frac{1}{8}$ in. for ease of fabrication.

### 5.4.4 Compressive Deflection of Sole Plate

During the development of the model, the sole plate node directly under the extreme compression stud was fixed in the vertical direction. This result was that the model predicted a much stiffer response than was observed in the experimental tests. Upon review of the experimental data, it was noted that the maximum deflection of the sole plate under the compression stud ranged from 0.141 in. to 0.38 in.. This deflection was accounted for in the model by defining a linear spring from the sole plate to a fixed node representing the base beam. Similarly to the tension hold-down spring it was necessary to give this spring equal stiffness in both compression and tension to avoid convergence difficulties. In reality it is a compression-only restraint, but due to the geometry and loading direction of the model, this compression spring never goes into tension.

Given the variability in the experimental measurements of sole plate deflection under the compression stud, a secant stiffness was fitted to the data rather than trying to model the actual nonlinear load-deflection response at this point. Note that since the wall aspect ratio is 1:1, the lateral load is nearly equal to the compressive load in the end stud. Since the compressive deflection appeared consistent for both the control and reinforced walls, experimental data from both was used to develop this parameter. The secant

stiffness from zero load to peak load varied from 21,820 to 104,244 lbs/in for the six walls tested with 4 in. perimeter nail spacing. The average stiffness value was approximately 55,900 lb/in. A spring stiffness of 41,000 lbs/in was found to provide a reasonable fit to the experimental data and produce an overall load-displacement response of the wall that was within range of the experimental tests results. A plot comparing the secant stiffness used for the model to a typical experimental measurement is provided in Figure 5.8.

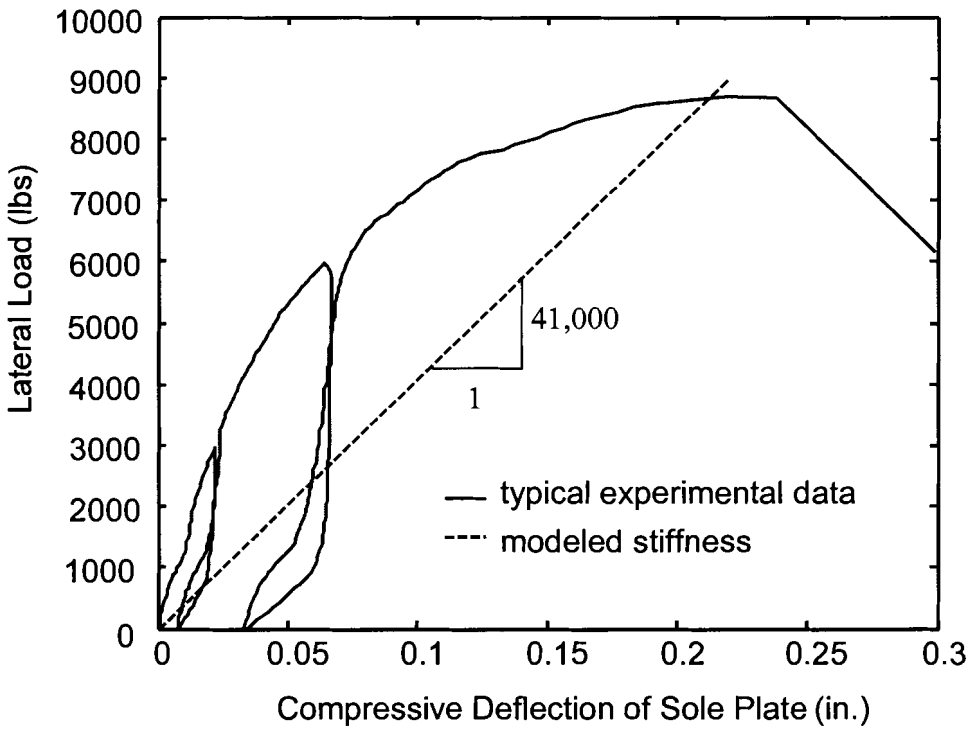


**Figure 5.8 Compressive Deflection of Sole Plate Under Compression Stud.**

Since the sole plate of the wall rests on the base beam, the base beam provides compressive restraint all along the base of the wall. However, the only locations where significant compression forces are applied to the sole plate is at the stud locations. For

this reason, springs with the same properties as discussed above were defined under all interior studs.

### 5.4.5 Stud-to-Plate Connections

The studs were connected to the top and bottom plates with two single DOF springs: one with only a horizontal ($U_x$) DOF, and one allowed to translate only in the vertical direction ($U_y$). The horizontal springs were given a stiffness 12,000 lb/in, which corresponds to results published by Dolan *et al.* (1995) for 2x4/2x4 connections made with 16d common nails. This parameter was found to have very little effect on the overall load-displacement response of the wall. It was included for completeness and to provide a better approximation of the complex load sharing behavior of the shear wall system.

The vertical stud-to-plate connections were modeled with a bilinear spring having different stiffness in compression and tension. In tension the spring is very weak to represent nail withdrawal from end grain. The author is not aware of any published data on the stiffness for nail withdrawal from end grain. This is a very variable and weak connection which is not allowed for use in design (AF&PA, 1997). A stiffness of 100 lb/in was used to model the withdrawal resistance. This value was chosen as it was the lowest value that did not cause premature instability of the model. The model results indicate that this is a very important parameter. Modeling this connection with a stiff spring or with pin connections was found to increase the amount of force transferred between the studs and plates. This increases the sheathing-to-framing connector forces and produces a much stiffer load-displacement response of the wall.

In compression the stud-to-plate connections are controlled by compression perpendicular to grain of the plate. The stiffness value of 41,000 lb/in developed to model compressive crushing of the sole plate was also used as the vertical compression stiffness for the stud-to-plate connections (See Figure 5.9).

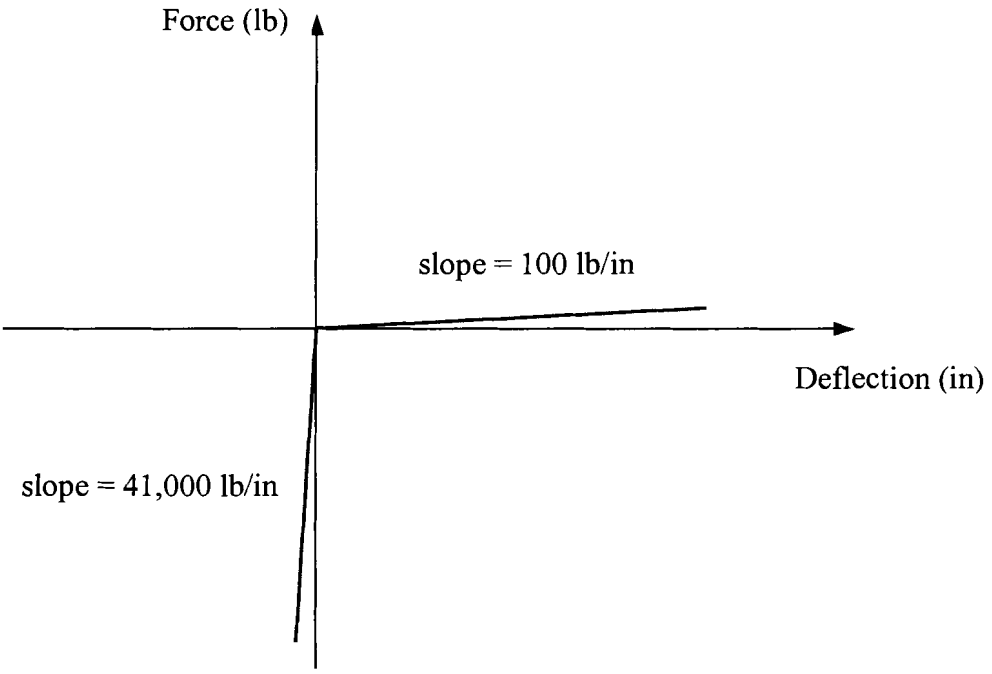


**Figure 5.9 Force-Deflection Relationship for Vertical Stud-to-Plate Connectors.**

## 5.5 Loading and Boundary Conditions

The application of both gravity loads and lateral loads is discussed in this section. A detailed discussion of the development and application of the boundary conditions was provided in the previous section of this Chapter. For clarity a sketch showing loads and boundary conditions applied to the model in its final form has been provided in this section.

### 5.5.1 Gravity Load

The nominal self-weights of the studs and sheathing panels were included in the model. The southern pine studs were assumed have a density of 50 pcf and a corresponding weight of 1.823 lb/ft. The weight of the reinforced sheathing panels was approximated with a uniform density of 50 pcf and a panel thickness of $\frac{9}{16}$ in.

The superimposed dead load applied to the wall specimens included the weight of the loading beam and half of the weight of the actuator. Although the intent of using a heavy loading beam was to distribute this dead weight evenly along the top plate of the wall, this was not the case. The corner of the wall nearest the actuator (tension corner) appears to carry most of the weight since it supports half of the weight of the actuator in addition to the distributed weight of the loading beam.

The idea that most of the weight is supported on this side is supported by the failure modes observed in the cyclic wall tests. The top plate pulled off the stud on the side opposite the actuator in nearly every test, but pull off of the top plate in the corner near the actuator was not observed in any of the tests (static or cyclic). Having more dead weight near the tension corner of the wall increases resistance to overturning and increases the initial stiffness of the wall. To quantify this effect, a structural analysis of the load beam/actuator assembly was performed to find the reaction loads developed in the top plate of the shear wall specimen (see Figure 5.10). The reaction loads shown in the figure were reversed in sign and applied to the top plate of the wall at the appropriate framing nodes.

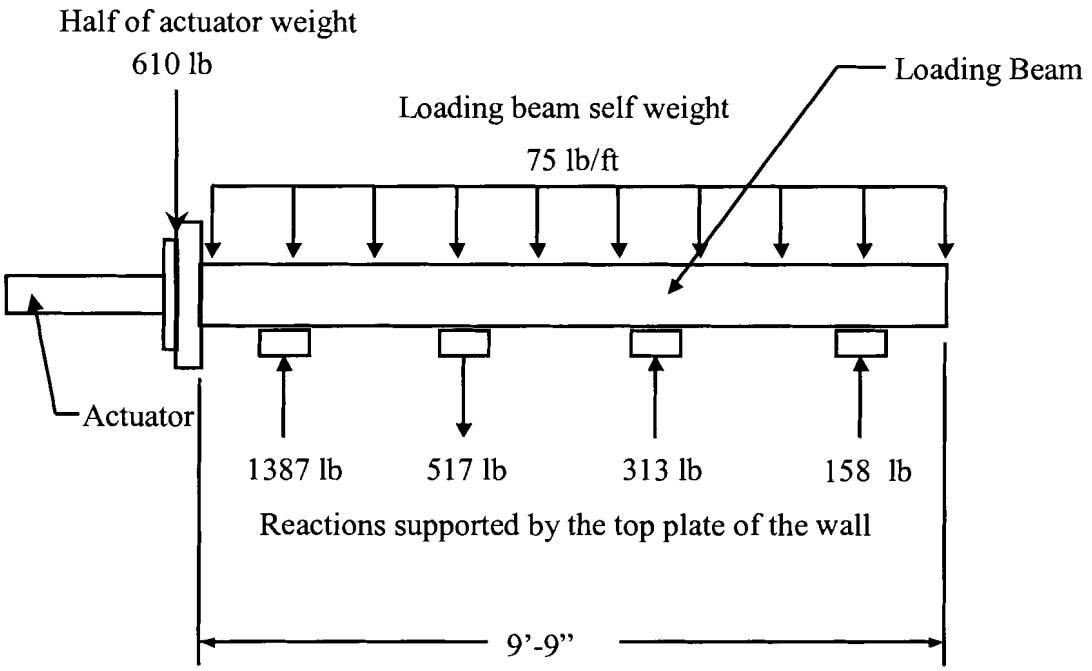


**Figure 5.10 Structural Analysis of Loading Beam / Actuator Assembly.**

### 5.5.2 Lateral Loading

Initially, lateral forces were applied to the model to be consistent with the experimental testing which was conducted under load control. Running the model in load control above the peak load capacity of the wall causes the stiffness matrix to become ill-conditioned, resulting in numerical singularities. Since one of the most notable benefits of using FRP reinforced OSB for shear wall construction is increased ductility, modeling the load-deflection of the wall beyond peak load was of interest. It found that more of the load-displacement curve could be modeled by running the model in displacement control. Displacements were enforced at the four top plate nodes corresponding to the points where the loading beam is bolted to the top plate of the wall. The corresponding lateral load was found from the computer results as the sum of the reactions at these four nodes.

The entire load displacement curve could not be modeled by applying displacements to the wall rather than loads, but it was possible to capture more points beyond peak load. Computational time increased significantly for points beyond peak load. Very small displacement increments were required to solve for these points. If the displacement increment was too large, the computer results produced either an unrealistic load increment for a given displacement increment or small equation pivot terms developed and the solution would not converge. This is consistent the findings of Dolan and Foschi (1991) in the development of their program SHWALL. A sketch of the model in its final form is provided in Figure 5.11. All of the applied loads and boundary conditions are labeled on the figure.

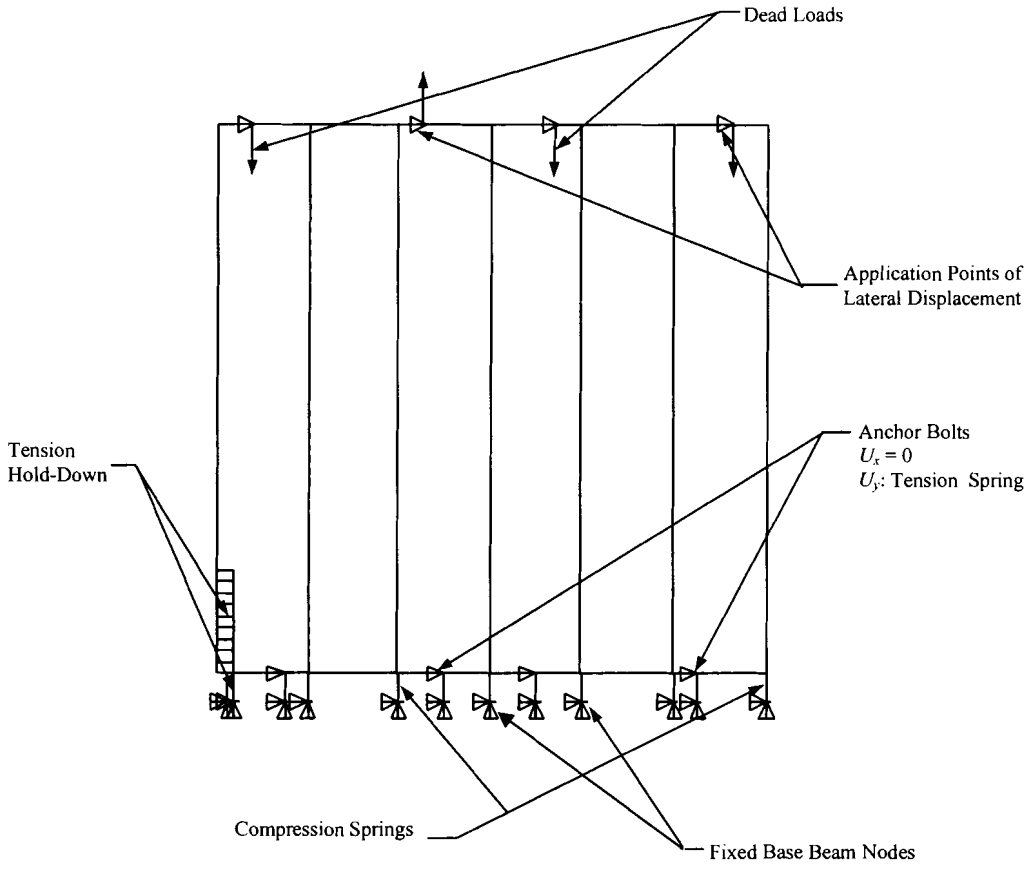


Note: Sheathing elements not shown for clarity.

**Figure 5.11 Loading and Boundary Conditions.**

## 5.6 Results and Modifications

A discussion of the computer model results along with subsequent corrections and modifications is provided in this section. The method of using two orthogonal springs to model sheathing-to-framing connectors is a very common approach found in the literature (see for example Dolan and Foschi (1991); Folz and Filiatrault (2001)). There are however some inherent problems with this approach. A discussion of these problems and the method employed to account for them is also provided here.

### 5.6.1 Initial Results

A comparison of the model results to the experimental test results for AOSB walls with 4 in. perimeter nail spacing is shown in Figure 5.12. The monotonic load-displacement response predicted by the model agrees reasonably well with the experimental data in the linear range, however as the load-displacement response of the wall becomes increasingly nonlinear, the model results become less accurate. The general shape of the load-displacement response in the non-linear range is comparable to the experimental results, however the model over predicts the ultimate load and stiffness.

The primary reason for this over prediction is most likely due to the fact that the sheathing-to-framing nails have been modeled with two uncoupled orthogonal springs, while each nail should be represented by a single spring aligned in the direction of the nail force. Since the sheathing and framing nodes are coincident in the undeformed position of the wall, it is not possible to define a single two-dimensional nonlinear spring without making some kinematic assumption of the initial direction of the spring force. Note that two orthogonal springs are only structurally equivalent to one aligned spring when the springs are linearly elastic. (Folz & Filiatrault, 2001). In the nonlinear range two orthogonal springs will absorb more energy than a single spring aligned in the proper direction.

Folz and Filiatrault (2001) accounted for this energy over-prediction by increasing the spacing of the sheathing-to-framing connectors. This reasonable and simple approach is a convenient solution when one is writing his own code or has access to the source code of a program written by someone else. However, it is not easily accomplished with

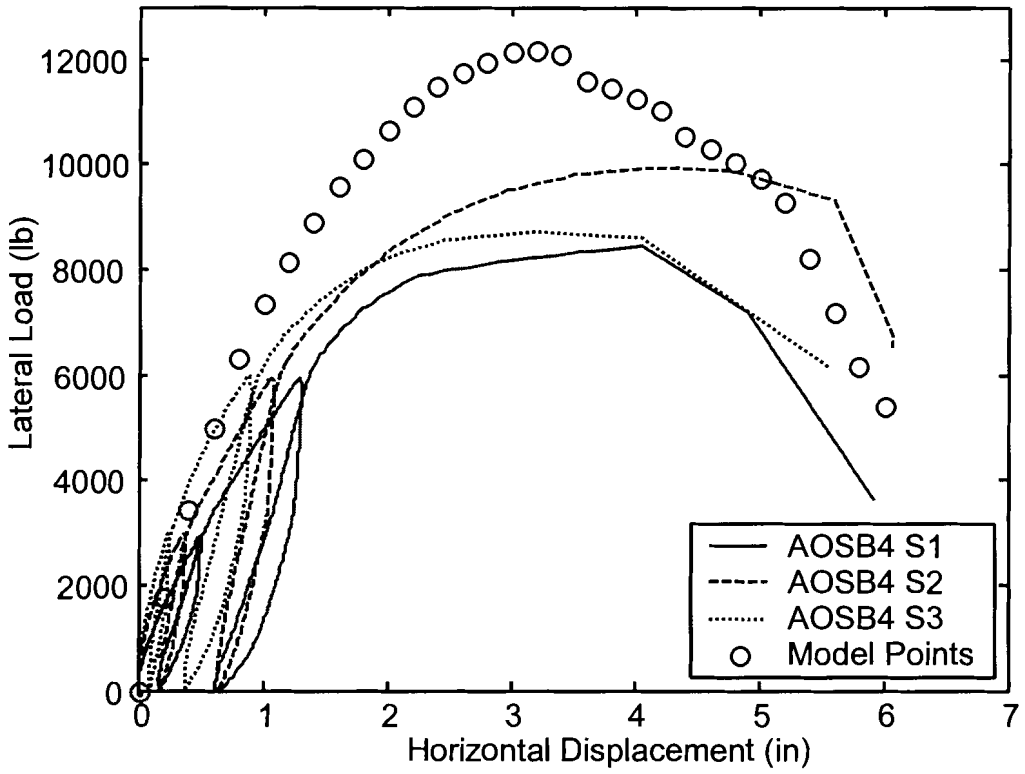


**Figure 5.12 Comparison of Initial Model Results to Experimental Data.**

commercial finite element code. To the best of the author's knowledge the only way to increase the connector spacing in ANSYS would be to redefine the nodes of both the framing and sheathing so that connectors could be placed at the desired locations. This is a time consuming process and was not considered a feasible alternative. Another alternative would be the approach used by Pryor and Murphy (2002). This modeling approach uses a single aligned spring to represent each sheathing-to-framing nail. This approach eliminates the need for two orthogonal springs, providing a more accurate and theoretically correct representation of the actual wall response. The author learned of the modeling approach from telephone conversations and e-mail correspondence with Steve

Pryor, P.E., S.E. and Tim Murphy, P.E. from Simpson Strong-Tie Co. Inc.(Pryor & Murphy 2002) Pryor and Murphy have developed a finite element model for Simpson's high aspect ratio strong walls using a computer program called MSC Nastran for Windows. The model uses pin connected framing members with the following exceptions. The $U_y$ degree of freedom was released for the stud-to-top plate connections at the top of the wall to capture the top plate lifting off the studs. Similarly, the $U_y$ degree of freedom was released at the bottom tension corner.

The use of two orthogonal springs to represent the sheathing to framing nails was discussed over the phone. They have moved away from the two orthogonal spring approach and seem convinced that the wall response cannot be modeled accurately this way. Their solution was to use one two-dimensional spring to represent each sheathing-to-framing nail. Springs of this type cannot be created at coincident nodes because there is no initial length or orientation of the spring. To overcome this problem, rigid cantilever beam elements were created from the framing nodes to nodes that were slightly offset. The nodes were offset in the direction of the initial nail force. For example if the lateral load on the wall is applied from left to right then along the left most vertical stud (tension stud) a node would be created just above the framing node of interest. Then a rigid cantilever beam would be created from the actual framing node to the new offset node. A single spring with two degrees of freedom ($U_x$, $U_y$) at each node can then be defined from the sheathing node to the offset node. By running a large deformation analysis the local axis geometry of the springs is updated within each iteration. With every iteration the spring will realign itself as the sheathing rotates away from the

framing and the actual orientation of the spring will be captured assuming that the initial directional of the nail forces is defined correctly.

Given more time an approach similar to that used by Pryor and Murphy (2002) would have been implemented. However, by the time the author learned of this approach the model was nearly complete and an alternative method of accounting for the energy over-prediction of two springs had already been developed. The method used, was to develop a connector load reduction factor based on energy considerations. Development of the connector load reduction factor is discussed in the following section.

### 5.6.2 Energy Correction

Quantification of the excess energy absorbed by two one-dimensional orthogonal springs is dependent on the true orientation of the nail force. This makes it a difficult parameter to quantify since the nail forces act in many different directions in the wall, and these orientations change with increasing racking deflection of the wall. Rather than try to quantify the energy reduction for each individual nail, a single energy reduction factor was calculated and used for all sheathing-to-framing connectors. Two energy reduction factors were considered. Using these two factors, two separate load-displacement curves were produced with the model. One represents a reasonable prediction of wall performance and the other provides a lower-bound solution.

The energy over-prediction was quantified by defining a parameter, $\alpha$, which varies for different orientations of a single nonlinear spring. $\alpha$ is computed as the energy

absorbed by the nonlinear spring under a given displacement divided by the energy absorbed by two identical nonlinear springs subjected to $\Delta_x$ and $\Delta_y$, where

$$\Delta = \sqrt{\Delta_x^{\,2} - \Delta_y^{\,2}} \qquad 6.2$$

Note that $\alpha$ is dependent on the shape of the load-displacement curve, and for any value of $\Delta$ there are an infinite number of values of $\alpha$ that correspond to different combinations of $\Delta_x$ and $\Delta_y$. A plot of the variation in alpha for AOSB nailed connections is shown in Figure 5.13. The eleven curves correspond to total displacements (displacement of a single aligned spring) of 0.3", 0.5", 0.7" ... 2.3". The horizontal axis was taken as $\Delta_x$; $\Delta_y$ can be computed from the total displacement and $\Delta_x$ as:

$$\Delta_y = \sqrt{\Delta^2 - \Delta_x^{\,2}} \qquad 6.3$$

where $\Delta$ is the total displacement. Note that when $\Delta = \Delta_x$, $\Delta_y = 0$ and $\alpha = 1$. Further, for all values of $\Delta$, there is a minimum value of $\alpha$ corresponding to a unique combination of $\Delta_x$ and $\Delta_y$.

The plot shows that the energy over prediction grows as the total displacement, $\Delta$, increases, which is expected since the load-displacement curve becomes increasingly nonlinear with increasing displacement. Another interesting result of Figure 5.13 is that for any given displacement, $\alpha$ appears to reach a minimum at a spring orientation of approximately $45^\circ$. Both the model results and the static wall test results indicate that the nails in the corners of the sheathing panels are the most highly loaded nails. These are also the nails that will be oriented most closely to an angle of $45^\circ$. This leads to the

logical conclusion that the most critical nails are also the ones that are subject to the most error when modeled with two uncoupled orthogonal springs.

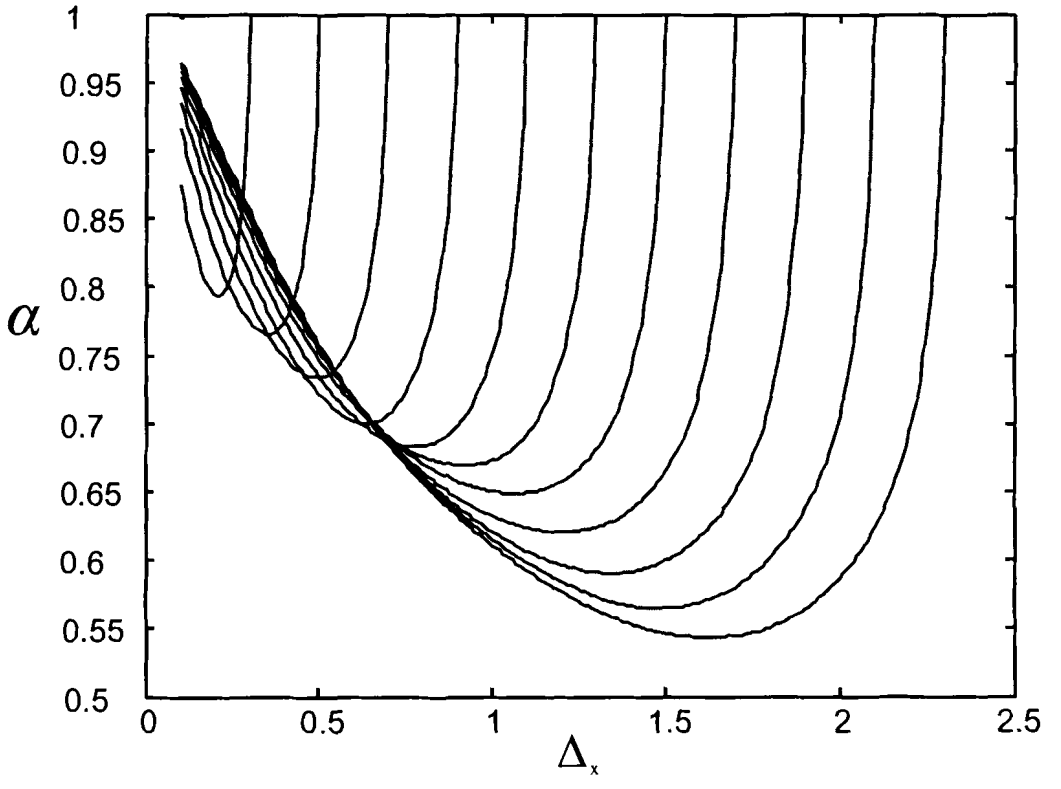


**Figure 5.13 Variation in Energy Reduction Factor for AOSB Nailed Connections.**

The minimum value for $\alpha$ was found to be about 0.55 when computed with $\Delta$ equal to the maximum displacement of the connector. If $\alpha$ is based on $\Delta$ at peak load the minimum value of $\alpha$ is 0.76. These two values were used as reduction factors for the sheathing-to-framing connector load-displacement input. The displacements were unchanged and all of the input loads were multiplied by $\alpha$. A comparison of the

modified connector load-displacement curve to the original ANSYS input is provided in Figure 5.14.

Adjusting the connector load displacement curve in this way reduces the tangent stiffness modulus along the nail load-displacement curve. The result is a softening of the wall response in both the linear range and nonlinear range. This is theoretically inaccurate, since two orthogonal springs are equivalent to one two dimensional spring as long as all the springs are linearly elastic. In theory the wall response should be unchanged as long as all of the sheathing-to-framing connector springs are in the linear elastic range. However, since the difference in the model results is small within the linear range and the results with the energy adjustment factors agree better with the experimental data in the nonlinear range, this error was considered to be acceptable. As illustrated in Figure 5.15 the model results with the peak load $\alpha$ value of 76% provide a reasonable prediction of the experimental results, while the results with the minimum $\alpha$ value of 55% provide a lower bound on the experimental data.

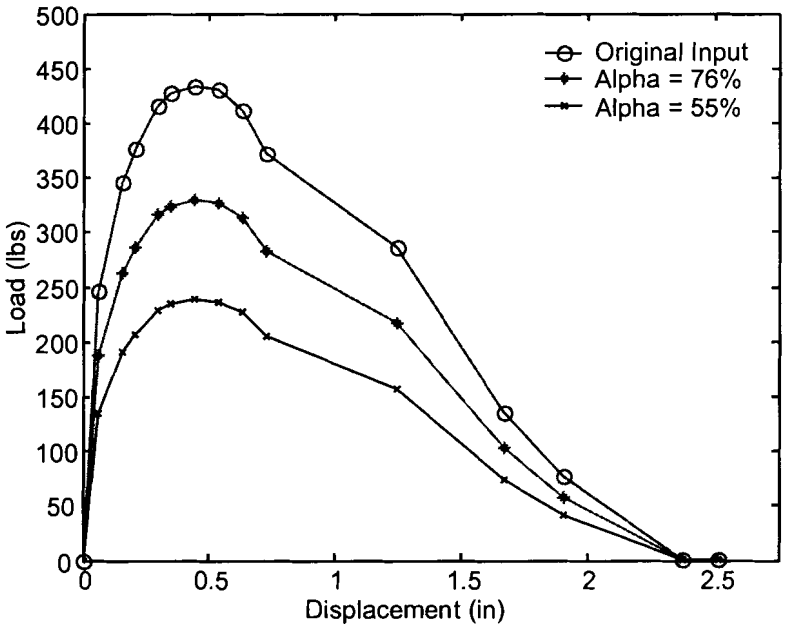


**Figure 5.14 Modified Nonlinear Sheathing-to-Framing Connector Properties.**

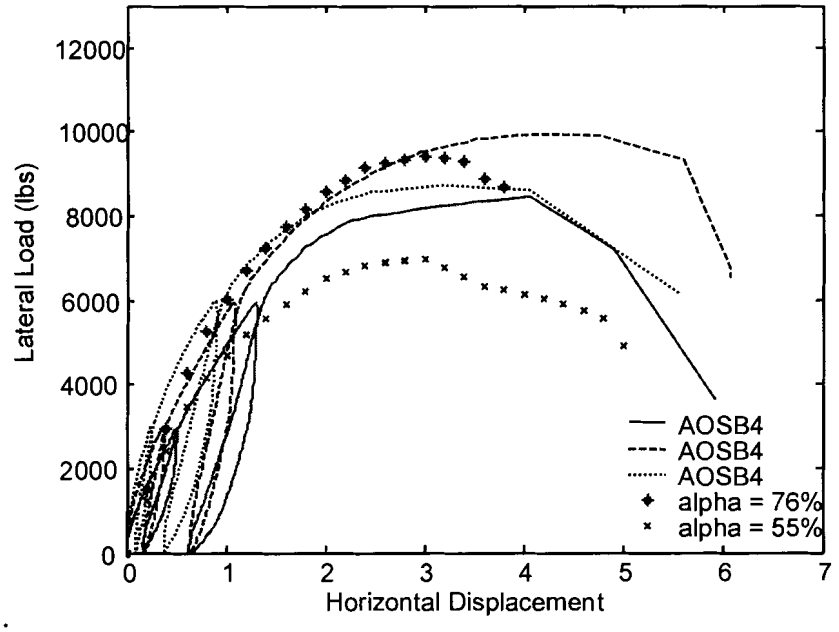


**Figure 5.15 Model Results with Energy Correction Factor.**

## 5.7 Verification

As a form of independent verification, the average monotonic load-displacement curve for conventional OSB nailed connection specimens was input into the model and the computer results were compared to the static wall tests of conventional OSB walls with 4 in. perimeter nail spacing. The minimum energy correction factor ($\alpha$) was found to be 0.53, and $\alpha$ at peak load was approximately 0.78 for conventional OSB nailed connections (See Figure 5.16). Similarly to the AOSB model, three load-displacement curves were produced for conventional OSB shear walls. First the model was run without including the energy correction factor, and then model results were calculated after multiplying the input connector loads by the appropriate energy correction factor. The results of all three modeling runs are shown in comparison to the experimental data in Figure 5.17.

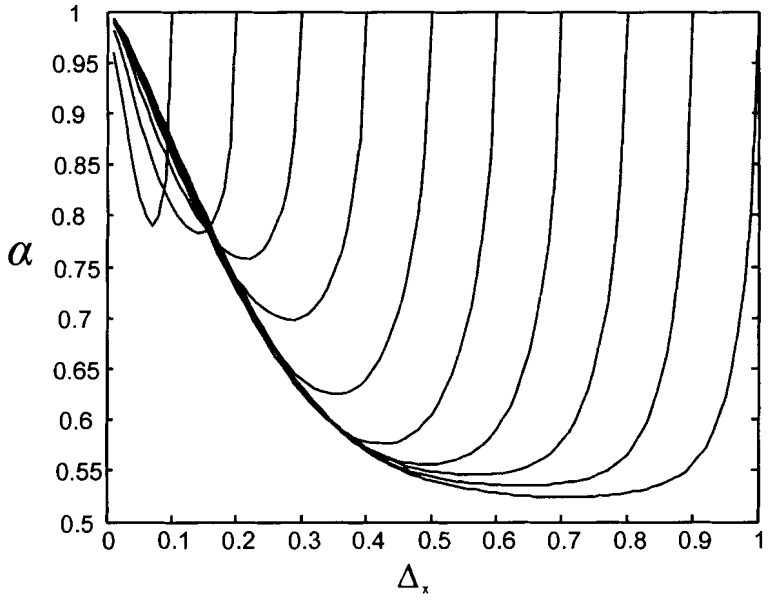


**Figure 5.16 Variation in Energy Reduction Factor for Conventional OSB Nailed Connections.**

Conversely to the AOSB modeling results, the conventional OSB results show that the peak load of the wall is better predicted by the unmodified sheathing-to-framing connector properties. Although the ultimate load is under predicted with the model when modified connector properties are used, the modified results follow the experimental load-displacement curves more closely. It was not possible to model the post peak response for conventional OSB. This is thought to be due to the sharp descent of the connector load-displacement response following peak load, which can cause solution instability.

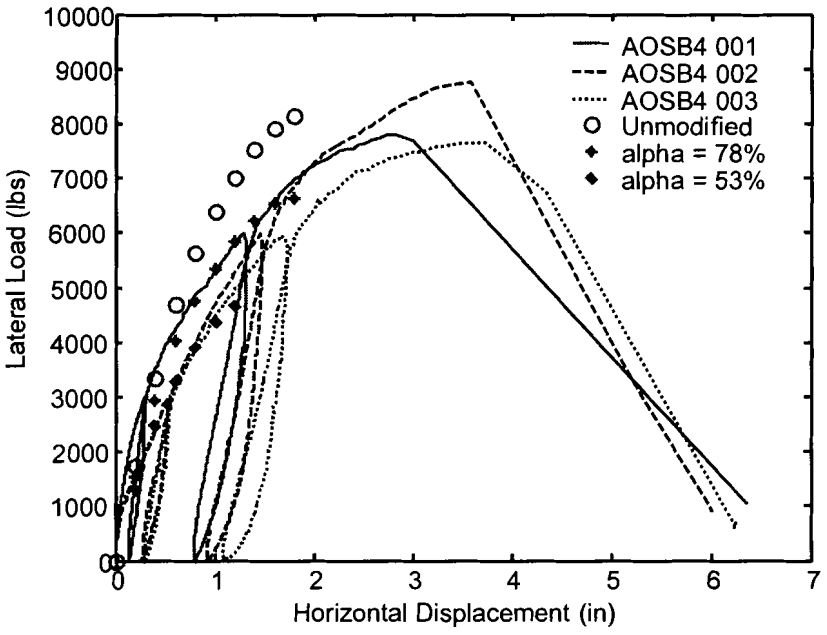


**Figure 5.17 Model Results for Conventional OSB Shear Walls.**

The point at which the model results will no longer converge should not be considered as the failure point of the wall. It is expected that the model would provide a reasonable fit to the experimental data, as was seen with the AOSB walls, if the solver

were capable of handling the numerical difficulties associated with the sharp descending branch of the load-displacement curve. To illustrate this and to show that the early failure prediction is solely a function of the connector load-displacement curve, a model run was performed where the connector load-displacement curve was assumed to be perfectly plastic after reaching peak load. The peak load $\alpha$ value of 78% was used for this model run as it provides the best fit to the experimental data. The results are shown in Figure 5.18. Although the individual sheathing-to-framing connectors are

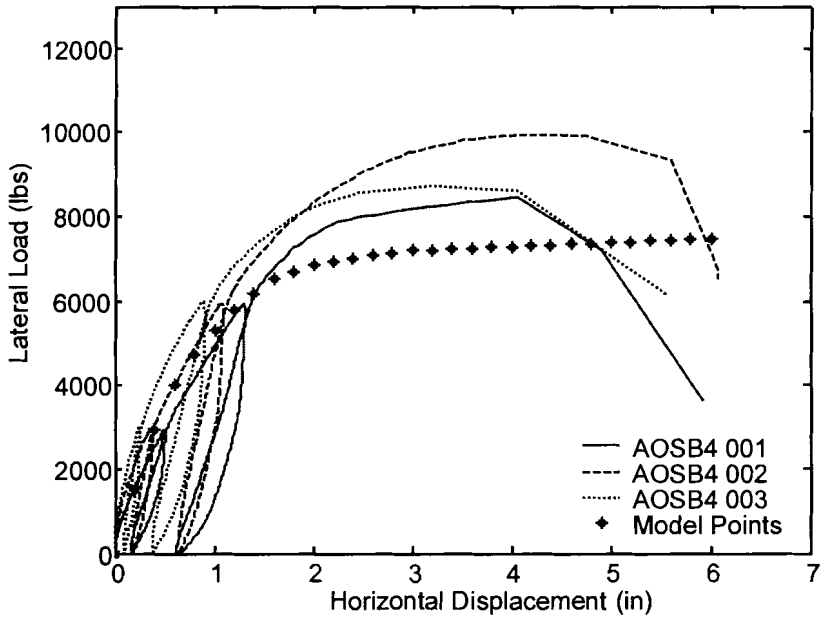


**Figure 5.18 Model Results with Perfectly-Plastic Sheathing-to-Framing Connectors.**

perfectly-plastic (no strain hardening), the predicted load-displacement response of the wall does exhibit strain hardening, indicating the wall still has capacity remaining beyond

the point at which numerical difficulties with the stiffness matrix develop and the solution will no longer converge.

In its current form, the model is capable of providing a reasonable comparison of shear wall systems with different connector properties and is expected to be a very useful design aid for further development of AOSB shear wall systems, which was the primary goal of this study. There are recognized problems with the approach of using two uncoupled springs to model each sheathing-to-framing connector. Other parameters may also require adjustment, however given that all parameters are justifiable, it is recommended that an approach similar the method used by Pryor and Murphy (2002) (see section 5.6.1) be implemented if further refinements of the model are considered. The use of two uncoupled orthogonal springs to model the sheathing-to-framing nails is thought to be the most significant deficiency in the model. If this issue were resolved then it would become much easier to isolate any other parameters that may require adjustment.

# Chapter 6

# CONCLUSIONS AND RECOMMENDATIONS

A brief summary of the results of this research is provided in this Chapter. Conclusions drawn from these results and recommendations for future research are also discussed.

## 6.1 Reinforcing Materials and Panel Fabrication

A variety of fiber/resin combinations were studied with varying degrees of success. Final selection was based on structural performance, economic considerations, and ease of fabrication (see Cassidy *et al.* 2002). The final FRP reinforcing system selected for AOSB was bonded to the ¼" thick OSB cover sheets with a thermosetting resin.

A thermosetting adhesive resin, which is typically slow cured under ambient conditions, was used for the fabrication of AOSB. However, the curing reaction was accelerated with heat to reduce fabrication time. After testing several sets of process parameters, the fabrication procedure that produced the highest quality product with the shortest fabrication time was selected (refer to Cassidy *et al.* 2002).

## 6.2 Connection Tests

The monotonic and cyclic behavior of AOSB nail connections with southern pine framing, 8d nails and the minimum recommended edge distance of 3/8 in. was quantified. The average monotonic load-deflection curve was incorporated into a finite

element model of an AOSB shear wall. These connection tests results along with the results of the nail-head-pull-through tests indicate that timber shear walls constructed with AOSB may be better able to survive disastrous events such as earthquakes and hurricanes, through increased strength and energy dissipation of the sheathing-to-framing connectors.

It has been demonstrated that nailed connections made with AOSB exhibit improved performance over conventional OSB connections. The presence of the mid-plane reinforcing changes the primary failure mode from a shear out type failure where the nail tears through the edge of OSB to a more a ductile failure mode where the nails exhibit double curvature and are withdrawn from the framing. The monotonic tests show an average increase of 39% in ultimate load and an average energy dissipation capacity approximately 4 ½ times that of conventional OSB connections. The displacement at maximum load increased from an average value of 0.28 in. for conventional OSB to 0.50 in. for the AOSB specimens. Initial stiffness appears to be unchanged.

Comparison of the hysteresis curves of conventional and AOSB single nail connections shows that the reinforcing is less beneficial when loaded in the compressive direction, where the edge distance is essentially unlimited. Under tensile loading however, where the edge distance is minimal (3/8 in.), AOSB provides a marked improvement in both strength and displacement capacity as well as improved resistance to damage accumulation when compared to conventional OSB connections. After being subjected to the same cyclic deformation history that caused failure in all of the conventional OSB connection specimens, the AOSB specimens maintained 40% of their

monotonic load capacity and 60% of their monotonic energy dissipation capacity (see Figure 3.15).

The ultimate load required to pull the head of the nail through the AOSB specimens was more than twice that of the conventional OSB specimens. The initial stiffness when loaded in this manner was also increased significantly. Also, important to note is that the nail-head-pull-through specimens made of AOSB and soaked in water for 24 hours exhibited more strength and stiffness than the conventional OSB specimens that were tested dry (see Table 3.3). This may prove to be a valuable property when considering the resistance of wood-frame buildings to hurricanes, where high wind pressures localized near the corners or eaves of the building can result in the loss of roofing and roof sheathing. Maintaining structural integrity after being exposed to water is another important property of this product, since water damage from heavy rains accounts for much of the damage observed after hurricanes.

### 6.3 Shear Wall Tests

The overall load-displacement response of the AOSB shear walls tested according to ASTM E564 (ASTM 1998a) was characterized by a substantial increase in ductility over the control specimens. On average, walls built AOSB panels were able to maintain at least 80% of their peak load up to a drift of approximately 5.5 in. compared to approximately 4.0 in. for the control walls. The AOSB walls with 4 in. perimeter nail spacing exhibited a 24% strength increase over the controls on average. No statistically significant difference was found in the strength of AOSB and control walls with a 6 in. perimeter nail spacing.

The predominant nail failure modes for all of the control walls were edge tear and nail-head pull-through. In the AOSB walls, nail pullout was the most common failure mode, and no nail-head pull-through failures were observed. A small percentage of edge tear failures were noted, however the nails were substantially withdrawn from the framing before tearing through the edge of the sheathing.

When tested cyclically, AOSB walls exhibited less strength and stiffness degradation than the control walls. AOSB walls of both perimeter nail spacings (4 and 6 inch) exhibited substantial increases in ductility and energy dissipation. Similar to the static tests, the predominant nail failure modes of the control walls were edge tear and nail-head pull-through. In the AOSB walls, nail pull-out and nail fatigue were the most common failures. No nail-head pull-through failures were observed. A very small percentage of edge tear failures were observed.

While the sheathing panels of the control specimens were extensively damaged under cyclic loading due to edge tear of nails, very little damage of the AOSB panels was observed. This coupled with the fact that failure of the AOSB walls was driven primarily by nail fatigue and nail pullout indicates that AOSB sheathing panels provide as much capacity as the framing and the nails will allow.

An alternative to marketing AOSB as a commodity product sold by the sheet would be to market prefabricated wood-frame shear walls constructed with AOSB sheathing. With this alternative in mind, allowable stress design loads were calculated from the first cycle envelopes of the cyclic load displacement data in accordance with the *Acceptance Criteria for Prefabricated Wood Shear Panels* (ICBO ES AC130). The

allowable stress design loads depend on whether the walls are used as Prefabricated Wood Shear Panels (PWSP) or Wood-shear resisting Frames (WSRF) as defined in AC130 (ICBO ES AC130). AOSB walls with 4 in. nail spacing at the panel edges showed increases of 18% and 23% in allowable load over the control walls for PWSPs and WSRFs respectively. AOSB walls with 6 in. nail spacing at panel edges showed increases of 11% for PWSPs and 10% for WSRFs.

## 6.4 Computer Modeling

A finite element model of two panel AOSB shear walls with 4 in. perimeter nail spacing has been developed using the computer program ANSYS. The model consists of 1) beam elements for framing, 2) 8 node quadrilateral plane stress elements for sheathing, 3) springs connecting framing members, 4) two orthogonal nonlinear springs to represent the sheathing to framing nails, 5) compression only elements to capture contact between sheathing panels, and 6) linear springs to represent tension hold-down connectors and other base restraints.

The use of two nonlinear springs to represent each sheathing-to-framing connector is known to over-predict the ultimate load and stiffness. Each nail should be represented by a single spring. However, since the sheathing and framing nodes are coincident in the undeformed position of the wall, it is not possible to define a single nonlinear spring without making some kinematic assumption of the initial direction of the spring force. Two orthogonal springs are only energy equivalent to one aligned spring within the linear elastic range. (Folz and Filiatrault, 2001). To account for this over

prediction, a correction factor was developed using energy methods. The model results with the correction factor are in good agreement with the experimental test results.

## 6.5 Recommendations

Based on the results of this study, AOSB panels appear to have great potential for increasing the energy dissipation capacity and lateral load resistance of wood-framed structures subjected to extreme wind and seismic events. Research beyond that described here is ongoing at the University of Maine Advanced Engineered Wood Composites Center. This research will help further refine and optimize AOSB and AOSB shear wall systems.

It is recommended that further research be focused in two areas. One area, which is very important to the marketability and future success of this product, is the development of a faster, more efficient and less expensive fabrication process. Fast drying adhesives mixed with chopped fibers that can be applied with a sprayer are one possibility. The other recommended focus area, which is perhaps more important, at least from a structural engineering standpoint, is to increase the allowable design loads for prefabricated AOSB shear walls. As discussed in Chapter 4, both stiffness and ultimate strength will need to be increased to increase the allowable stress design load. The use of screws or deformed (ring or spiral) shank nails may prevent the nails from pulling out of the framing, forcing edge tear failures which would utilize the full strength of the AOSB and is likely to increase the ultimate load of the wall assembly.

In its current form, the finite element model is capable of providing a reasonable comparison of shear wall systems with different connector properties and is expected to

be a very useful design aid for further development of AOSB shear wall systems. There are recognized problems with the approach of using two uncoupled springs to model each sheathing-to-framing connector. It is recommended that an approach similar to the method used by Pryor and Murphy (2002) (see section 5.6) be used to resolve this issue if further refinement of the model is considered.

## REFERENCES


Adams, N.R. (1987). Plywood shear walls: Research Report 105 . Tacoma, WA. American Plywood Association. Technical Services Division.

AF&PA (1997). National Design Specification for Wood Construction. Washington, D.C. American Forest & Paper Association

AF&PA. (1995). Wood Frame Construction Manual for One- and Two-Family Dwellings – SBC High Wind Edition. Washington, D.C. American Forest & Paper Association.

American Wood Council. (1999). General dowel equations for calculating lateral connection values. Technical Report No. 12. Washington, D.C. American Forest & Paper Association.

ANSYS (1999). ANSYS online help. [CD-ROM] SAS IP, Inc. Available: ANSYS, Inc.

ANSYS (2000). ANSYS 5.7 University high option. [CD-ROM] SAS IP, Inc. Available: ANSYS, Inc.

APA (1972). Basic panel properties of plywood overlaid with fiberglass-reinforced plastic: Research Report 119, Part 1. Tacoma, WA. American Plywood Association.

APA (1992). PS2-92 Performance Standard for Wood-Based Structural-Use Panels. Tacoma, WA. APA-The Engineered Wood Association.

APA (1998). FRP Plywood: Form No. G215E. Tacoma, WA. APA-The Engineered Wood Association.

ASTM (1998a). Standard Practice for Static Load Test for Shear Resistance of Framed Walls for Buildings, ASTM E 564-95, Annual Book of Standards Vol. 4.11, ASTM, West Conshohocken, PA.

ASTM (1998b). Standard Test Methods for Mechanical Fasteners in Wood, ASTM D1761-88, Annual Book of Standards Vol. 4.10, ASTM, West Conshohocken, PA.

ASTM (1998c). Standard Test Methods of Conducting Strength Tests of Panels for Building Construction, ASTM E72-98, Annual Book of Standards Vol. 4.11, ASTM, West Conshohocken, PA.

ASTM (1998d). Standard Test Methods for Evaluating Properties of Wood-Base Fiber and Particle Panel Materials, ASTM D1037-96a, Annual Book of Standards Vol. 4.10, ASTM, West Conshohocken, PA.

BSSC (1998). NEHRP Recommended Provisions for Seismic Regulations for New Buildings and Other Structures. 1997 Edition. Washington, D.C. Building Seismic Safety Council.

Cassidy, E., Davids, W., Dagher, H. & Gardner, D. (2002). Report No. AEWC 02-29 Screening and Selection of Reinforcing Materials for AOSB Sheathing Panels. Advanced Engineered Wood Composites Center, University of Maine, Orono, Maine.

Chou, C. & Polensek, A. (1987). Damping and stiffness of nailed joints response to drying. Wood and Fiber Science. Vol.19, No. 1. pp. 45-58.

Chui, Y.H. & Ni, C. (1997). Load Embedment Response of Timber to Reversed Cyclic Load. Wood and Fiber Science. Vol. 29, No. 2. pp. 148-160.

Chui,Y.H., Ni, C. & Jaing, L. (1998). Finite-element model for nailed wood joints under reversed cyclic load. Journal of Structural Engineering. Vol.124, No. 1. pp. 96-103.

Dinehart, D.W. & Shenton III, H.W. (1998). Comparison of the Static and Dynamic Response of Timber Shear Walls. Journal of Structural Engineering.Vol. 124, No. 6. pp. 686-695.

Dolan, J.D. & Foschi, R.O. (1991). Structural Analysis Model for Static Loads on Timber Shear Walls. Journal of Structural Engineering. Vol.117, No. 3. pp. 851-861.

Dolan, J.D. & Madsen, B. (1992a). Monotonic and Cyclic Tests of Timber Shear Walls. Canadian Journal of Civil Engineering. Vol. 19, No. 1. pp. 97-104.

Dolan, J.D. & Madsen, B. (1992b). Monotonic and Cyclic Nail Connection Tests. Canadian Journal of Civil Engineering. Vol. 19, No. 1. pp. 415-422.

Dolan, J.D. (1989). The Dynamic Response of Timber Shear Walls. PhD Dissertation. Vancouver, BC, Canada. Dept. of Civil Engineering, University of British Columbia.

Dolan, J.D., Gutshall, S.T. & McLain, T.E. (1995). Monotonic and Cyclic Tests to Determine Short-Term Load Duration Performance of Nail and Bolt Connections Vol1: Summary Report. Timber Engineering Report No. TE-1994-001.Virginia Polytechnic Institute and State University. 31p.

Douglas Fir Plywood Association. (1948). The Lateral Bearing Strength of Nailed Plywood Joints:Technical Data on Douglas Fir Plywood for Engineers and Architects. Tacoma, WA. Douglas Fir Plywood Association.

Dugan, K. (1995). Nail slip curves. Unpublished Report. Urbana, IL. Dept. of Civil Engineering, University of Illinois at Urbana-Champaign.

Easley, J.T., Foomani, M. & Dodds, R.H. (1982). Formulas for Wood Shear Walls. Journal of the Structural Division. Vol.19, No. 11. pp. 2460-2478.

Energy Degradation of Wood Frame Shear Walls. Canadian Journal of Civil Engineering. Vol. 25, No.3. pp. 412-423.

EXTREN Design Manual. (1998). Strongwell, Inc., Bristol, VA.

Falk, R.H. & Itani, R.Y. (1989). Finite Element Modeling of Wood Diaphragms. Journal of Structural Engineering. Vol.115, No.3. pp. 543-559.

Foliente, G.C. (1995). Hysteresis Modeling of Wood Joints and Structural Systems. Journal of Structural Engineering. Vol.121, No. 6. pp. 1013-1021.

Foliente, G.C. (1997). Earthquake Performance of Light-frame Wood and Wood-based Buildings: State-of-the-art and Research Needs. Proceedings of the Pacific Conference on Earthquake Engineering. Vol.2. Melbourne, Australia. Australian Earthquake Engineering Society. Parkville, Victoria, Australia. pp. 333-342.

Folz, B. & Filliatrault, A. (2000). CASHEW—Version 1.0: A computer program for cyclic analysis of wood shear walls. Report No. SSRP-2000/10. Struct. Sys. Res. Proj. Dept. of Structural Engineering, University of California-San Diego, La Jolla, CA.

Folz, B. & Filliatrault, A. (2001). Cyclic Analysis of Wood Shear Walls. Journal of Structural Engineering. Vol.127, No.4. pp. 433-441.

Fonseca, F.S. (1997). Cyclic loading response of reinforced concrete tilt-up structures with plywood diaphragms. PhD Dissertation, Urbana, Illinois. University of Illinois at Urbana-Champaign.

Fonseca, F.S., Pratt, T.R. & Fielding, M.B. (2001). Behavior of Plywood Shear Walls with Fiberglass Edge Reinforcement. Proceedings of the Second International Conference on Advanced Engineered Wood Composites. Bethel, Maine. Deparment of Civil and Environmental Engineering, University of Maine, Orono, ME.

Forest Products Laboratory. (1999). Wood Handbook: Wood as an Engineering Material. Gen Tech. Rep. FPL-GTR-113. Madison, WI. 463p.

Foschi, R.O. (1974). Load-Slip Characteristics of Nails. Wood Science, Vol.7, No.1. pp. 69-76.

Foschi, R.O. (1977). Analysis of Wood Diaphragms and Trusses: Part I Diaphragms. Canadian Journal of Civil Engineering. Vol.4, No.3. pp. 345-352.

Foschi, R.O. (2000). Modeling of the hysteretic response of mechanical connections for wood structures. Proceedings of the World Conference on Timber Engineering. Department. of Civil. Engineering, Department of Wood Science and School of Architecture, University of British Columbia, Vancouver, Canada.

Griffiths, D.R. (1984). Determining the racking resistance of timber framed walls. Proceedings of the Pacific Timber Engineering Conference Vol.1: Timber Construction Auckland, New Zealand. Wellington, New Zealand. Institute of Professional Engineers. pp. 504-512.

Gutkowski, R.M. & Castillo, A.L. (1988). Single- and Double-Sheathed Wood Shear Wall Study. Journal of Structural Engineering. Vol.114, No.6. pp. 1268-1284.

He, B., Magnusson, H., Lam, F. & Prion, H.G.L. (1999). Cyclic Performance of Perforated Wood Shear Walls with Oversize OSB Panels. Journal of Structural Engineering. Vol. 125, No.1. pp.10-18.

ICBO. (1997). 1997 Uniform Building Code. Whittier, CA. International Conference of Building Officials.

ICBO ES (n.d.). Acceptance Criteria for Prefabricated Wood Shear Panels (AC130). Whittier, CA. International Conference of Building Officials Evaluation Service.

ISO (1983). Timber structures—joints made with mechanical fasteners—general principles for the determination of strength and deformation characteristics, ISO 6891-1983. Switzerland. International Organization for Standardization.

ISO. (1997). Timber structures—joints made with mechanical fasteners—quasi-static reversed-cyclic test method. WG7 Draft, ISO TC Secretariat Standards Council of Canada.

Itani, R.Y. & Cheung, C.K. (1984). Nonlinear Analysis of Sheathed Wood Diaphragms. Journal of Structural Engineering. Vol. 110, No.9. pp. 2137-2147.

Itani, R.Y. & Robledo, F.M. (1984). Finite Element Modeling of Light-Frame Wood Walls. Civil Engineering for Practicing and Design Engineers. Vol. 3, No.10. pp. 1029-1045.

Judd, P.J. & Fonseca, F.S. (2002). Strength and Behavior of Hybrid Diaphragms. Journal of Composites for Construction, ASCE, in press.

Kasal, B. (1992). A Nonlinear Three-Dimensional Finite Element Model of a Light-Frame Wood Structure. PhD Dissertation. Corvallis, Oregon. Oregon State University.

Kasal, B. & Leichti, R.J. (1992). Nonlinear Finite-Element Model for Light-Frame Stud Walls. Journal of Structural Engineering. Vol.118, No. 11. pp. 3122-3135.

Krawinkler, H., Parisi, F., Ibarra, L., Ayoub, A. & Medina, R. (2000). Development of a Testing Protocol for Wood-Frame Structures:CUREE Publication No. W-02, Consortium of Universities for Research in Earthquake Engineering, Richmond, CA.

Lhuede, E.P. (1988). Nail loads for plywood/solid wood connections. Proceedings of the 1988 International Conference on Timber Engineering. Seattle, WA. Vol.I, Forest Products Research Society. pp. 3-10.

Matlab (2000). Matlab 6.0.0.42a Release 12 Student Version. [CD-ROM]. The Mathworks. Available: The Mathworks.

Menogotto, M. & Pinto, P.E. (1973). Method of analysis for cyclically loaded reinforced concrete plane frames including changes in geometry and bending. Proceedings of the IABSE Symposium on the Resistance and Ultimate Deformability of Structures Acted on by Well-Defined Loads. Lisbon, Portugal, pp.15-22.

NES. (1997). Power-driven Staples and Nails for Use in all Types of Building Construction. Nation Evaluation Report: NER-272. Falls Church, VA. National Evaluation Service.

Peterson, J. (1983). Bibliography on lumber and wood panel diaphragms. Journal of Structural Engineering. Vol.109, No.12. pp. 2838-2852.

Polensek, A. (1976). Finite Element Analysis of Wood-Stud Walls. Journal of the Structural Division. Vol. 102, No. ST7. pp. 1317-1335.

Pryor, S. & Murphy, T. (2002). Personal Telephone and E-mail Correspondence May 2, 2002 to May 8, 2002.

Pryor, S.E., Taylor, G.W. & Ventura, C.V. (2000). Seismic Testing and Analysis Program on High Aspect Ratio Wood Shear Walls. Proceedings of the 2000 World Conference on Timber Engineering.Whistler, Canada. pp. 1-13

Ritter, M.A. (1990). Timber Bridges: Design, Construction, Inspection, and Maintenance. Washington, D.C. 944p.

Salenikovich, A.J. (2000). The racking performance of light-frame shear walls. PhD Dissertation, Blacksburg,VA. Virginia Polytechnic Institute and State University.

Schwentker, F. (2001). Oriented Strand Board. Technical Source Guide no. 30, University of Texas at Austin. Austin, TX.

Shenton, H.W. III, Dinehart, D.W. & Elliot, T.E. (1997). Stiffness and
Simpson Strong-Tie Co., Inc (2002). Wood Construction Connectors, Catalog C-2002. p.18.

Stanton, J.F. & McNiven, H.D. (1979). The development of a mathematical model to predict the flexural response of reinforced concrete beams to cyclic loads, using system identification. Report No. UCB/EERC-79/02, Berkeley, CA. Earthquake Engineering. Res. Center, University of California.

Tissel, J.R. (1993). Structural panel shear wall: Research Report 154. Tacoma, WA. American Plywood Association, Technical Services Division.

Tissel, J.R. & Elliot, J.R. (1986). Plywood diaphragms: Research Report 138. Tacoma, WA. American Plywood Association, Technical Services Division.

White, M.W. & Dolan, J.D. (1995). Nonlinear Shear-Wall Analysis. Journal of Structural Engineering. Vol.121, No.11. pp. 1629-1635.

Yancey, C.W., Cheok, G.S., Sadek, F. & Mohraz, B. (1998). A Summary of the Structural Performance of Single-Family, Wood-Frame Housing: NISTIR 6224. Gaithersburg, MD. National Institute of Standards and Technology.

# APPENDICIES

## Appendix A

## CONNECTION TEST RESULTS

**Table A.1 Monotonic Nail Connection Test Results of Control Specimens (7/16" OSB)**

Note: ET = edge tear; NPO = nail pullout

| Specimen ID | Max Load (lb.) | Displ@ Max Load (in.) | Total Displ. (in.) | Energy Absorbed (lb-in) | Failure Mode |
|---|---|---|---|---|---|
| 01ng_control | 347.8 | 0.283 | 0.615 | 125.1 | IIIS ET |
| 02ng_control | 235.3 | 0.270 | 0.532 | 74.5 | IIIS ET |
| 03ng_control | 386.9 | 0.227 | 0.576 | 125 | IIIS ET |
| 04ng_control | 297.8 | 0.160 | 0.522 | 70 | IIIS ET |
| 05ng_control | 314.2 | 0.217 | 0.623 | 106.6 | IIIS ET |
| 06ng_control | 314.9 | 0.263 | 0.312 | 74.8 | IIIS ET |
| 07ng_control | 356.8 | 0.461 | 1.037 | 280.1 | IIIS ET |
| 08ng_control | 390.4 | 0.276 | 0.633 | 136.9 | IIIS ET |
| 09ng_control | 367 | 0.183 | 0.566 | 121.4 | IIIS ET |
| 10ng_control | 380.1 | 0.261 | 0.533 | 138.6 | IIIS ET |
| 11ng_control | 314.9 | 0.621 | 0.898 | 191.2 | IIIS ET |
| 12ng_control | 311.5 | 0.195 | 0.610 | 138 | IIIS ET |
| 13ng_control | 297.8 | 0.221 | 0.608 | 127.1 | IIIS ET |
| 14ng_control | 334.1 | 0.269 | 0.566 | 122 | IIIS ET |
| 15ng_control | 258.6 | 0.274 | 0.665 | 94.5 | IIIS ET |
| **Average** | **327.2** | **0.279** | **0.619** | **128** | |
| **St. Dev.** | **45.4** | **0.1** | **0.2** | **52.2** | |
| **COV (%)** | **14%** | **42%** | **27%** | **41%** | |

**Table A.2 Monotonic Nail Connection Test Results of AOSB Specimens**

Note: ET = edge tear; NPO = nail pullout

| Specimen ID | Max Load (lb.) | Displ@ Max Load (in.) | Total Displ. (in.) | Energy Absorbed (lb-in) | Failure Mode |
|---|---|---|---|---|---|
| StaticET 001 | 450.1 | 0.420 | 2.056 | 626.8 | IV NPO |
| StaticET 002 | 489.2 | 0.587 | 2.362 | 816.8 | IV NPO |
| StaticET 003 | 386.9 | 0.452 | 2.052 | 530 | IV NPO |
| StaticET 004 | 430.2 | 0.528 | 1.975 | 594.1 | IV NPO |
| StaticET 005 | 502.9 | 0.317 | 1.600 | 610.7 | IV NPO |
| StaticET 006 | 532.1 | 0.808 | 2.089 | 744.9 | IV NPO |
| StaticET 007 | 364.0 | 0.218 | 1.783 | 414.9 | IV NPO |
| StaticET 008 | 335.2 | 0.210 | 1.722 | 360.3 | IV NPO |
| StaticET 009 | 476.5 | 0.972 | 2.222 | 770.2 | IV NPO |
| StaticET 010 | 581.1 | 0.539 | 1.151 | 331.3 | IV ET |
| **Average** | **454.8** | **0.505** | **1.90** | **580.0** | |
| **St. Dev.** | **77.2** | **0.2** | **0.4** | **170.8** | |
| **COV (%)** | **17%** | **48%** | **18%** | **29%** | |

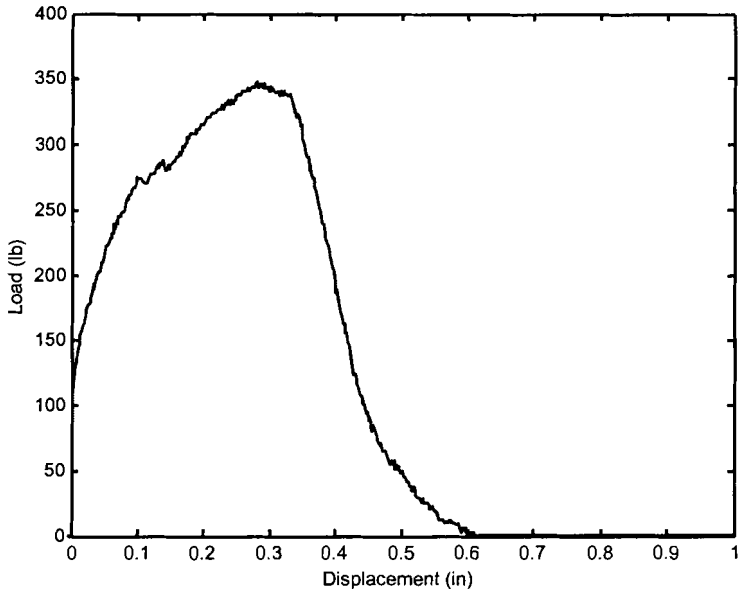


**Figure A.1 Load-Displacement Curve; Specimen ID: 01_ng_control**

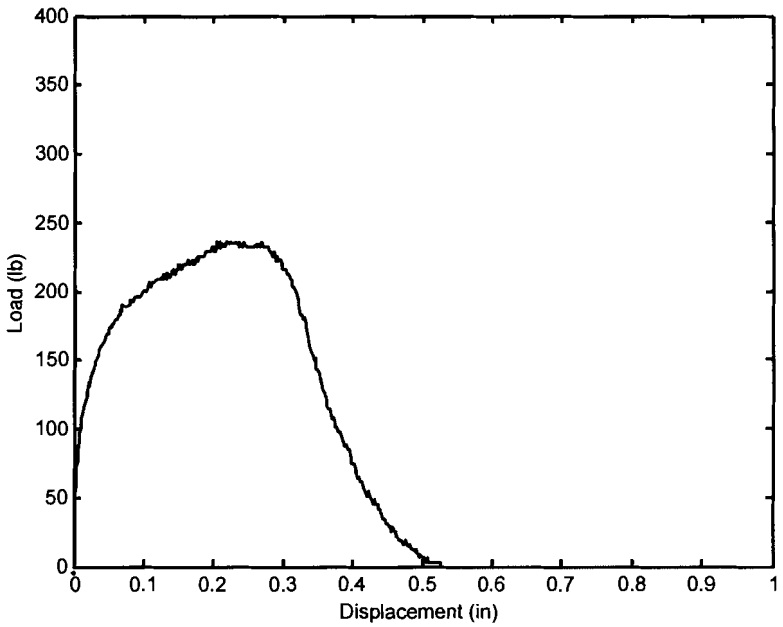


**Figure A.2 Load-Displacement Curve; Specimen ID: 02_ng_control**

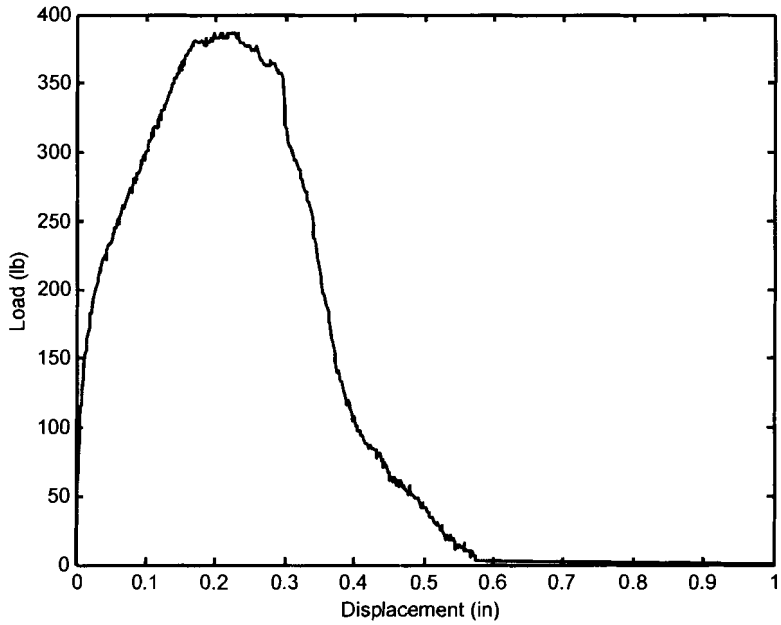


**Figure A.3 Load-Displacement Curve; Specimen ID: 03_ng_control**

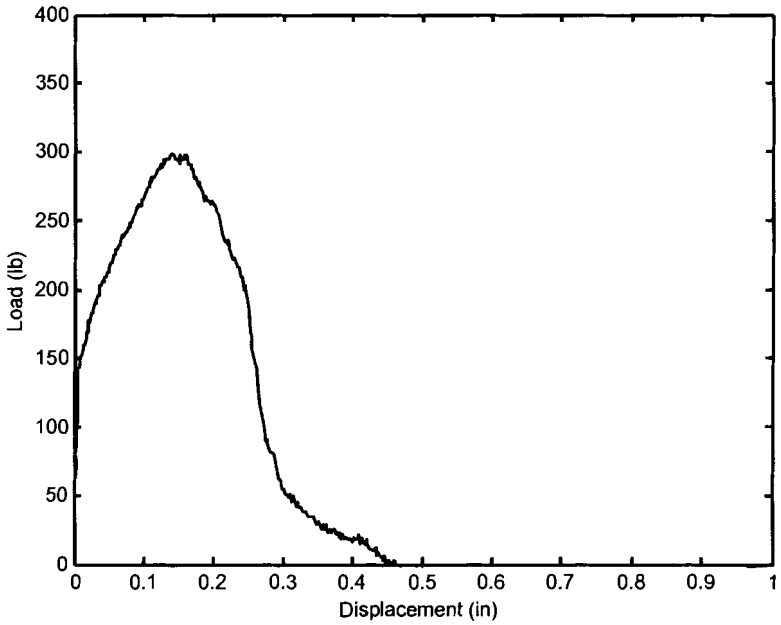


**Figure A.4 Load-Displacement Curve; Specimen ID: 04_ng_control**

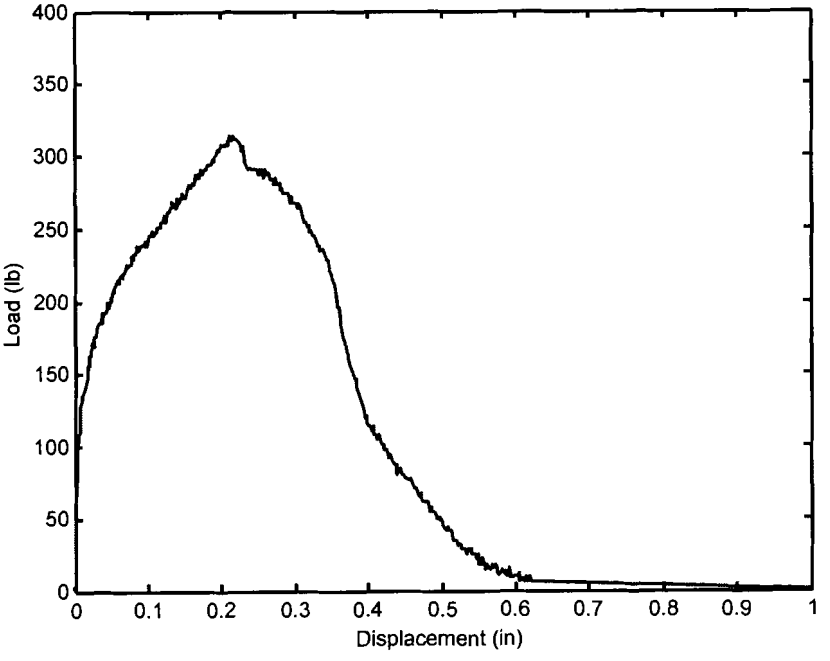


**Figure A.5 Load-Displacement Curve; Specimen ID: 05_ng_control**

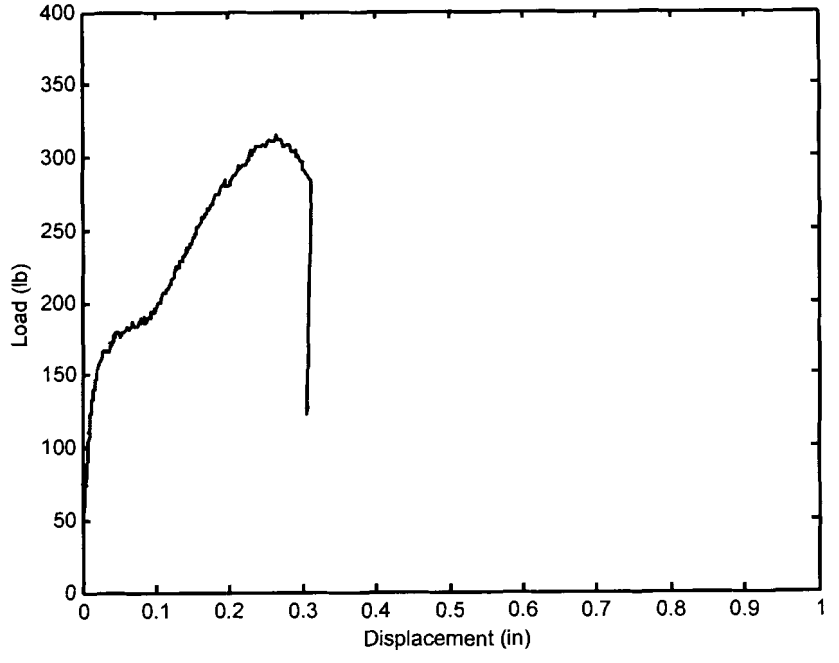


**Figure A.6 Load-Displacement Curve; Specimen ID: 06_ng_control**

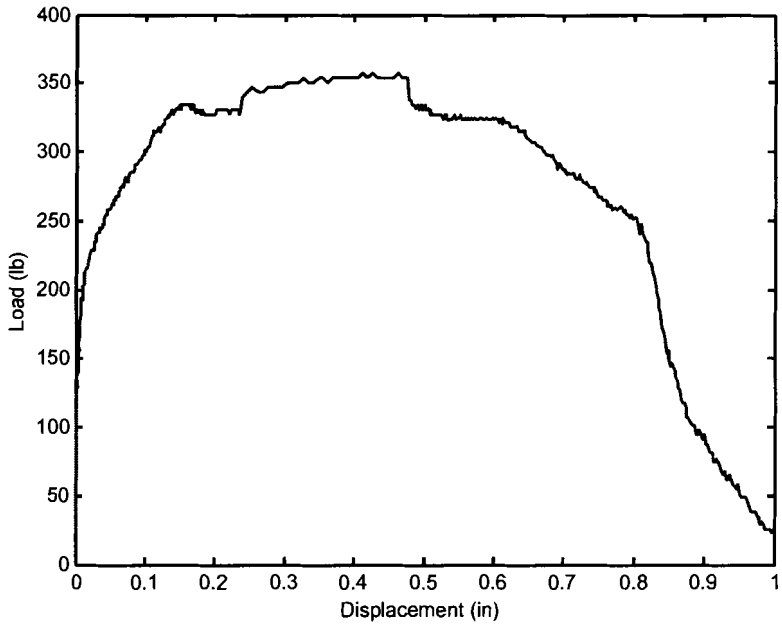


**Figure A.7 Load-Displacement Curve; Specimen ID: 07_ng_control**

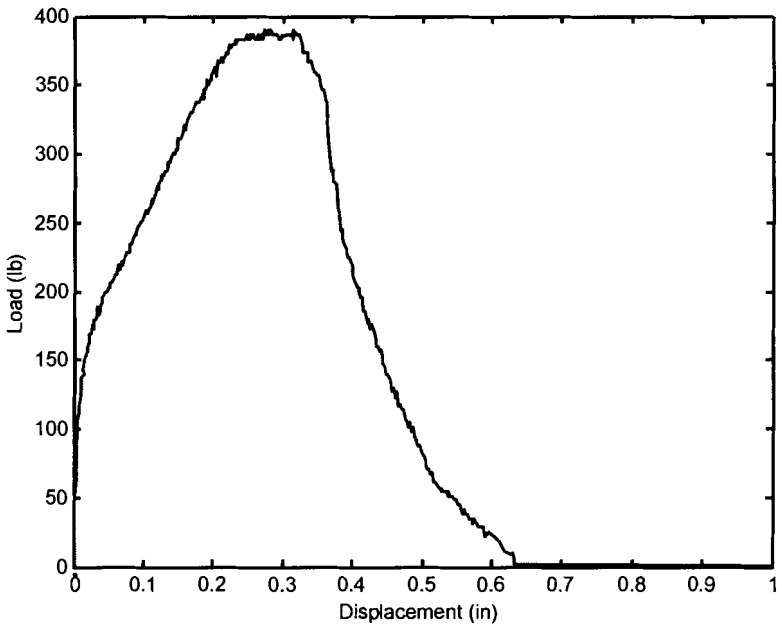


**Figure A.8 Load-Displacement Curve; Specimen ID: 08_ng_control**

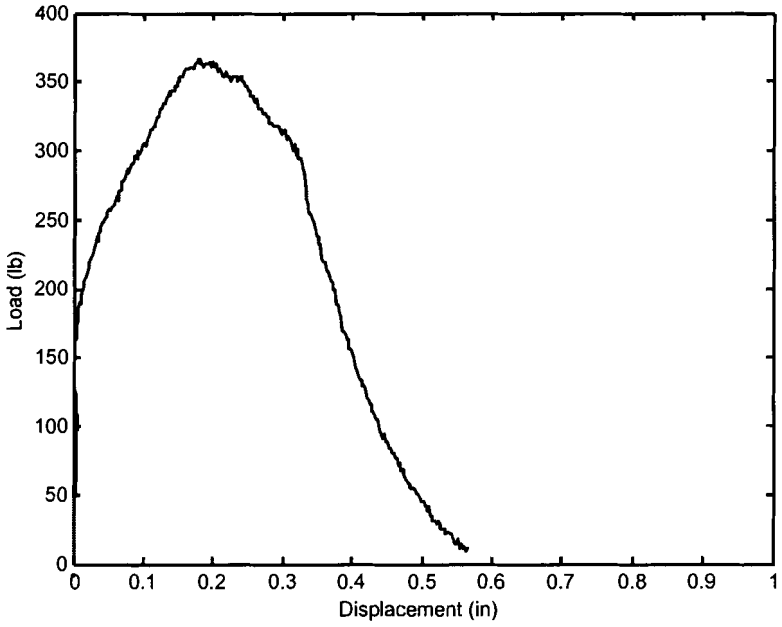


**Figure A.9 Load-Displacement Curve; Specimen ID: 09_ng_control**

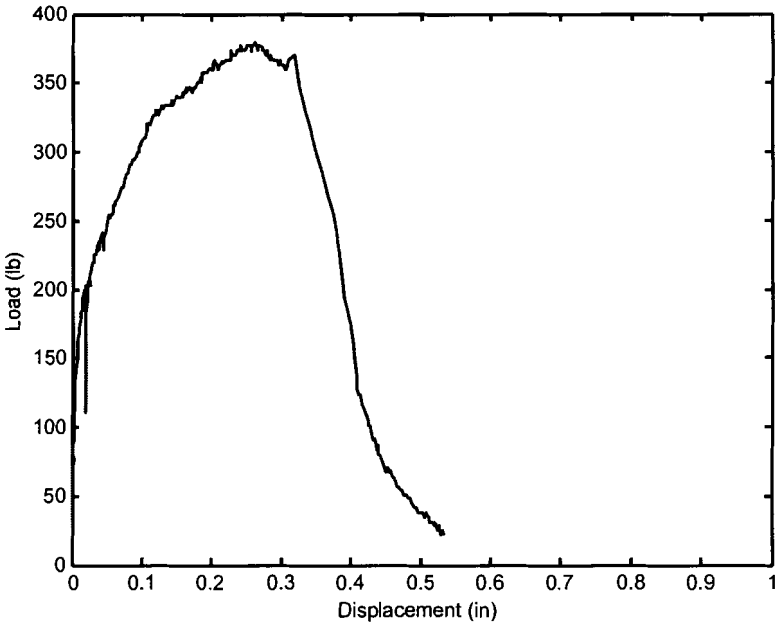


**Figure A.10 Load-Displacement Curve; Specimen ID: 10_ng_control**

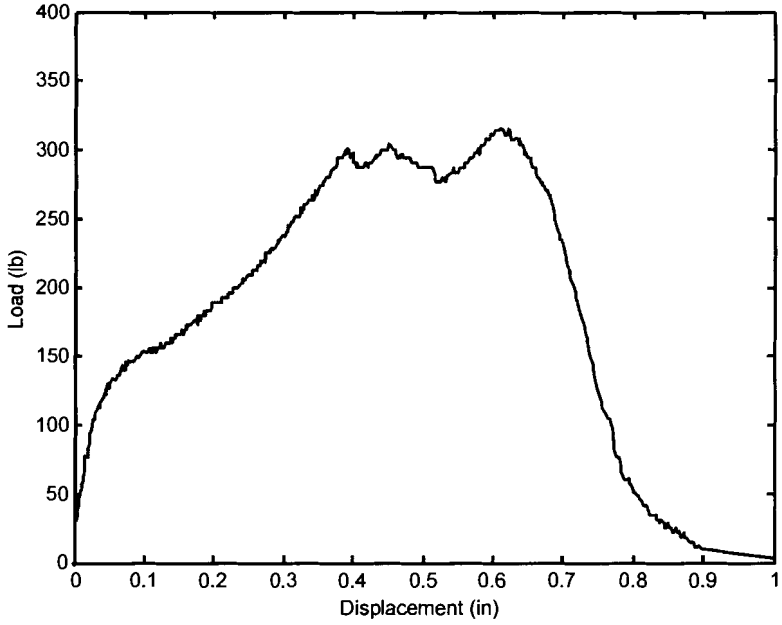


**Figure A.11 Load-Displacement Curve; Specimen ID: 11_ng_control**

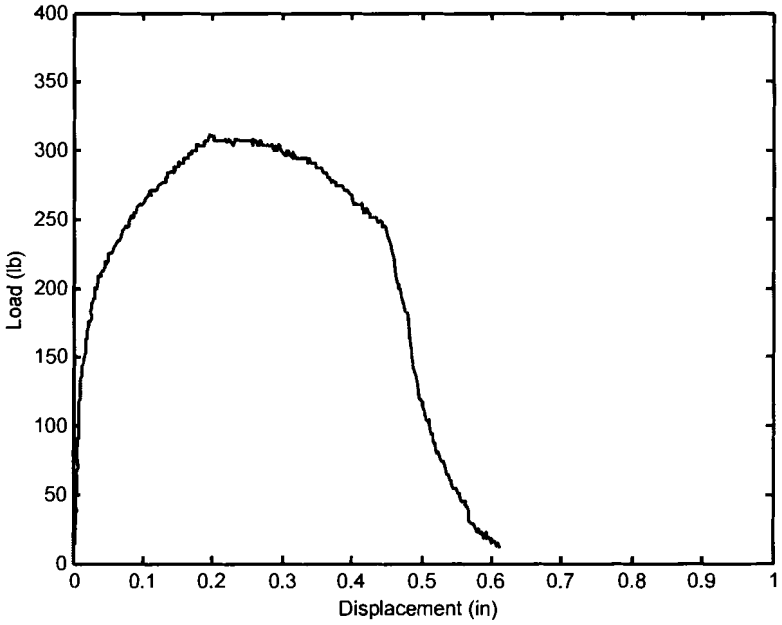


**Figure A.12 Load-Displacement Curve; Specimen ID: 12_ng_control**

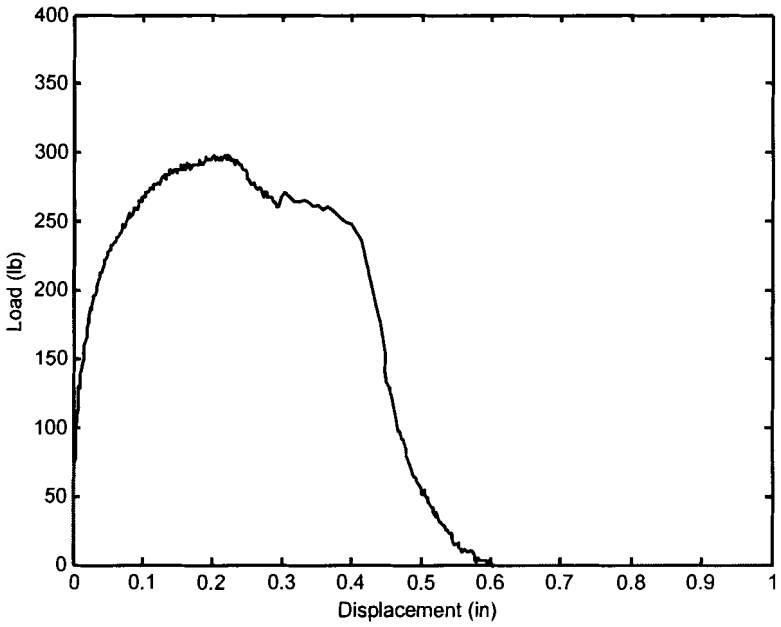


**Figure A.13 Load-Displacement Curve; Specimen ID: 13_ng_control**

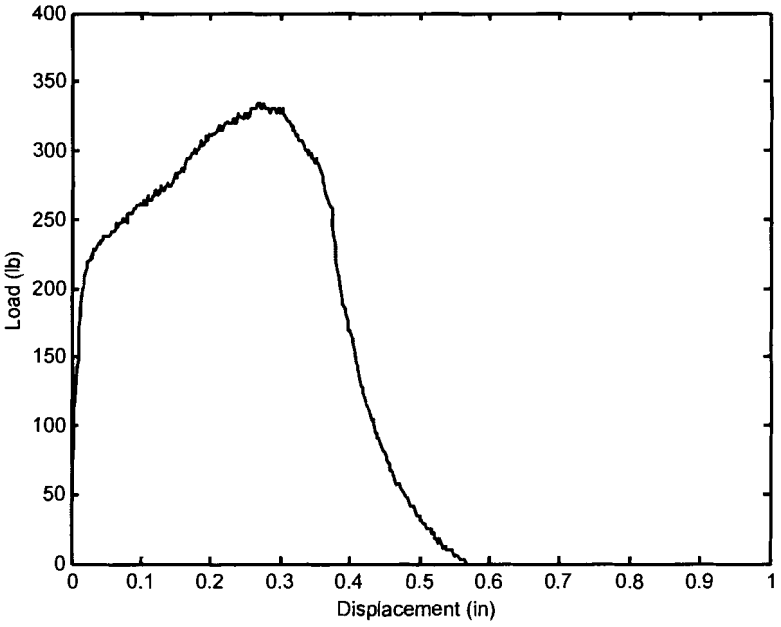


**Figure A.14 Load-Displacement Curve; Specimen ID: 14_ng_control**

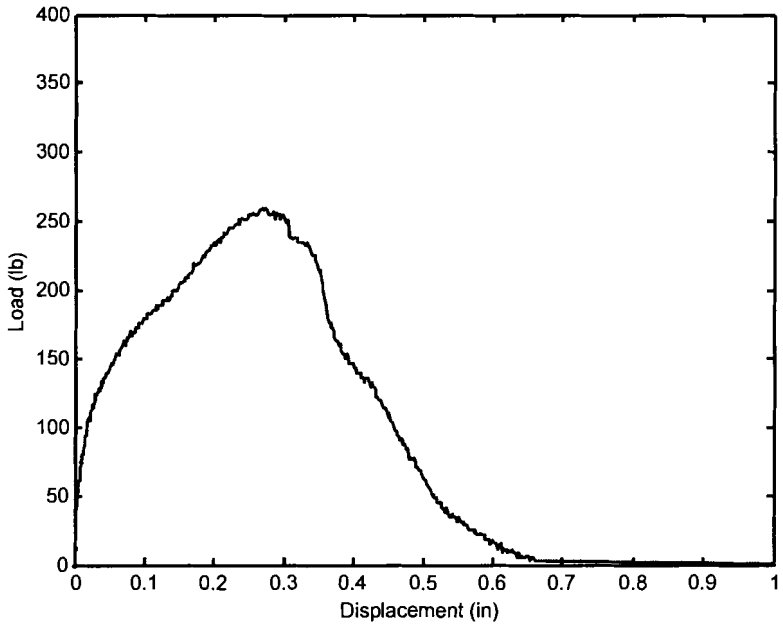


**Figure A.15 Load-Displacement Curve; Specimen ID: 15_ng_control**

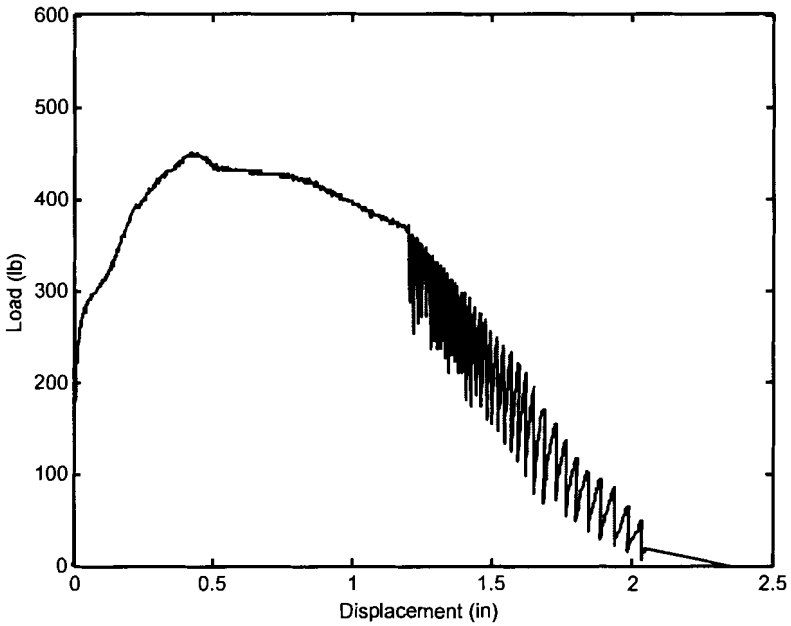


**Figure A.16 Load-Displacement Curve; Specimen ID: StaticET_001**

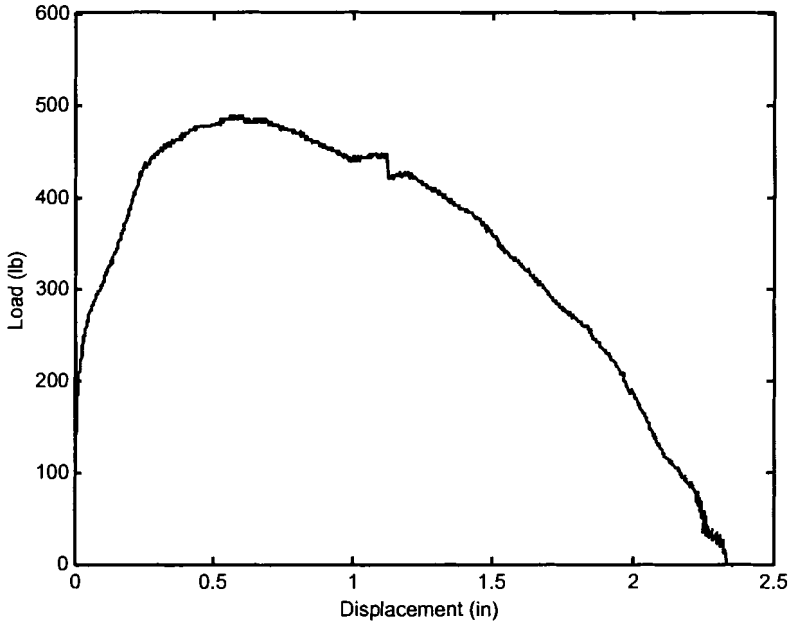


**Figure A.17 Load-Displacement Curve; Specimen ID: StaticET_002**

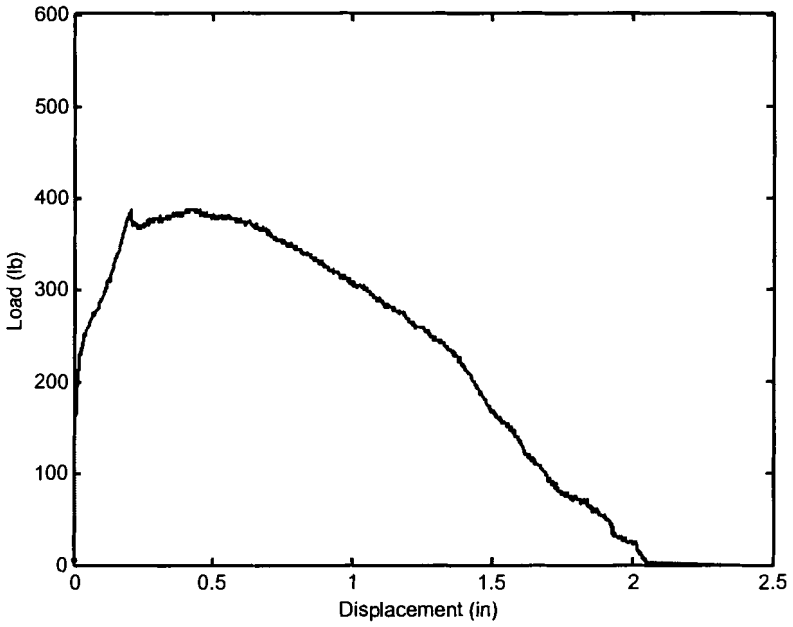


**Figure A.18 Load-Displacement Curve; Specimen ID: StaticET_003**

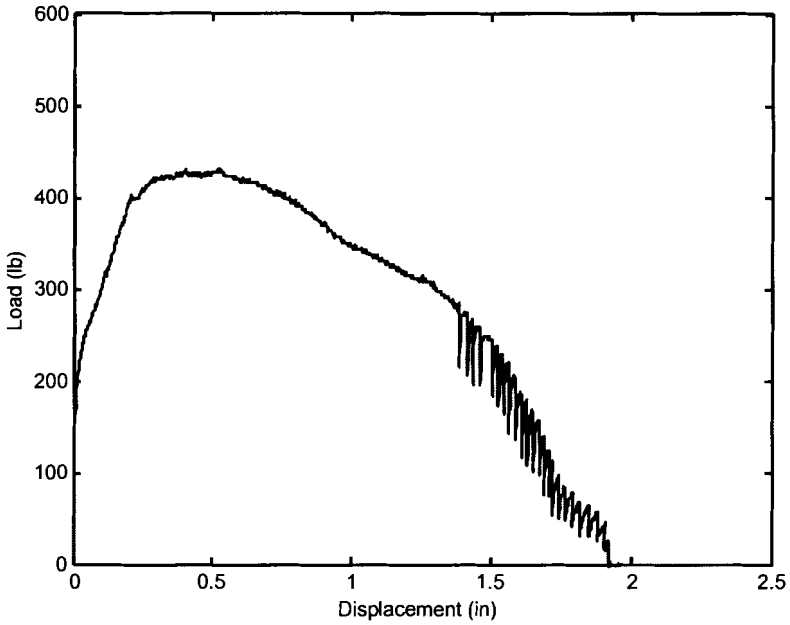


**Figure A.19 Load-Displacement Curve; Specimen ID: StaticET_004**

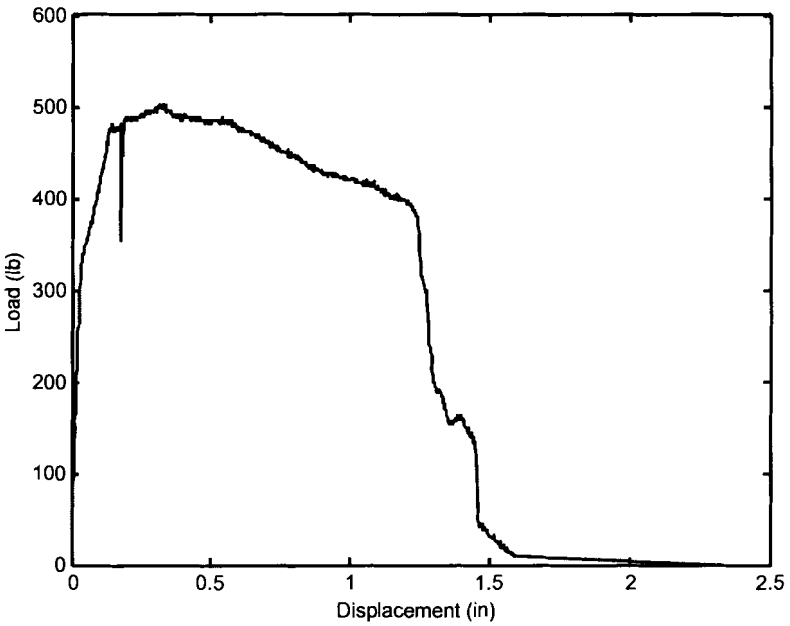


**Figure A.20 Load-Displacement Curve; Specimen ID: StaticET_005**

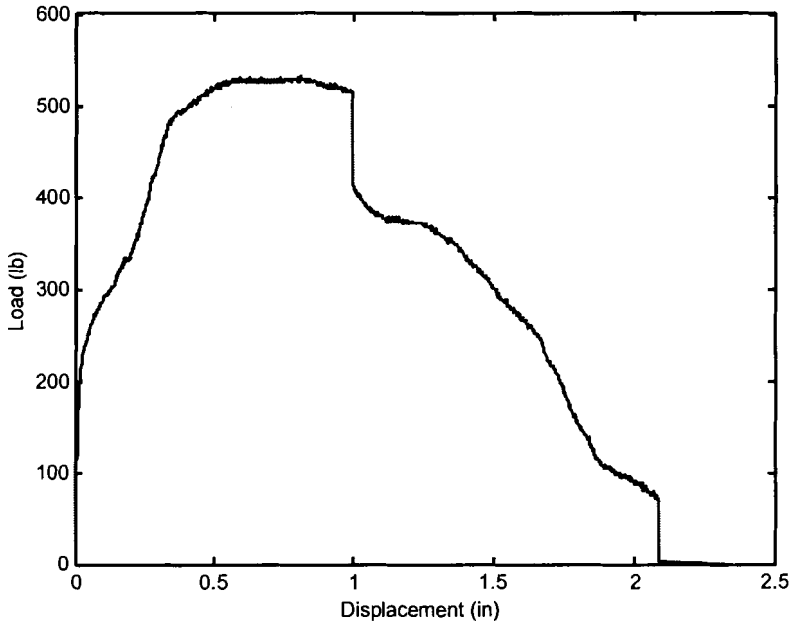


**Figure A.21 Load-Displacement Curve; Specimen ID: StaticET_006**

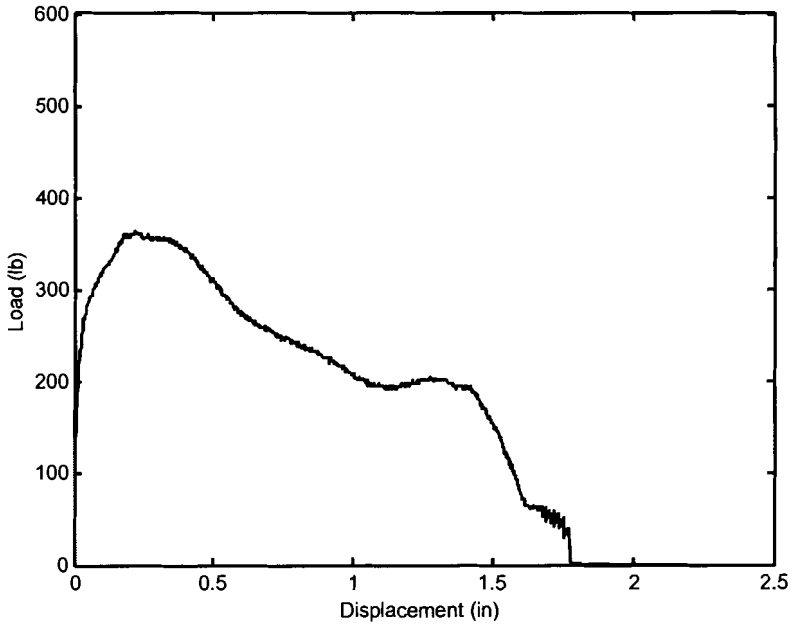


**Figure A.22 Load-Displacement Curve; Specimen ID: StaticET_007**

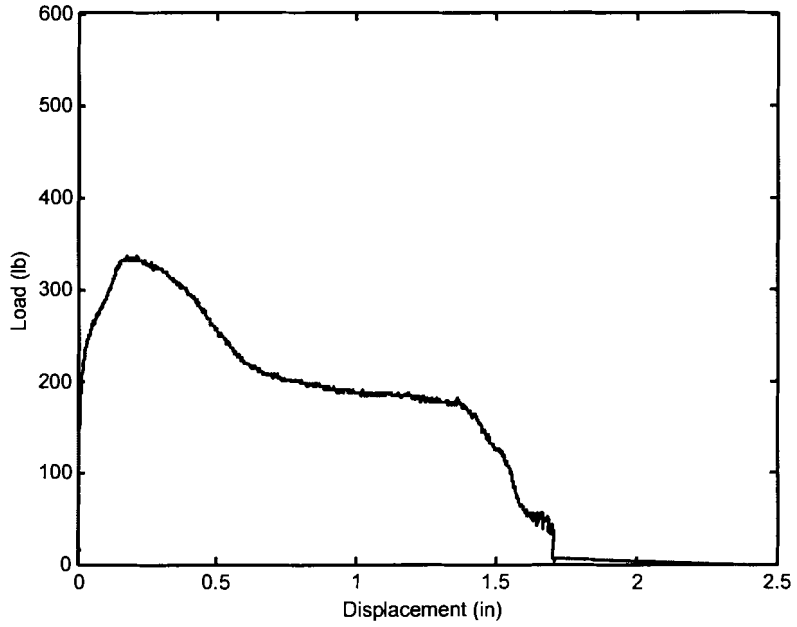


**Figure A.23 Load-Displacement Curve; Specimen ID: StaticET_008**

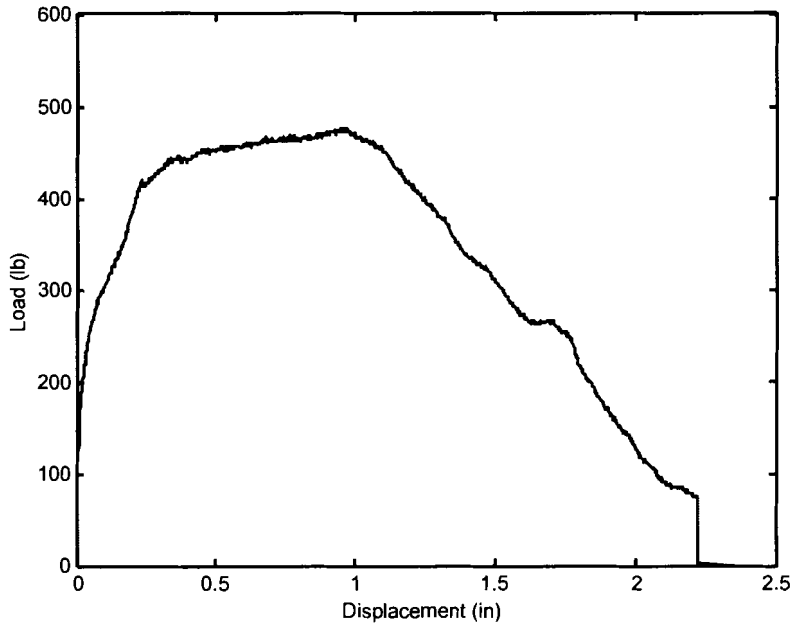


**Figure A.24 Load-Displacement Curve; Specimen ID: StaticET_009**

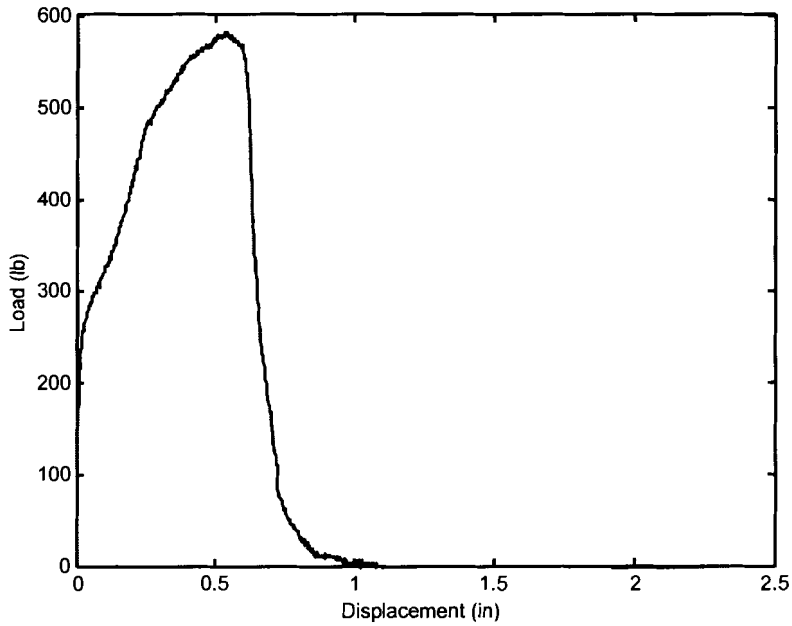


**Figure A.25 Load-Displacement Curve; Specimen ID: StaticET_010**

**Table A.3 Cyclic Nail Connection Test Results of Control Specimens (7/16" OSB)**

Note: ET = edge tear

| Specimen ID | Min Load lb | Disp @ Min Load in | Max Load lb | Disp @ Max Load in | CUREE Toughness lb-in | Failure Mode |
|---|---|---|---|---|---|---|
| Control_1 | 351.9 | 0.261 | 355.4 | 0.232 | 734.1 | IIIS (ET) |
| Control_2 | 308.7 | 0.264 | 260.7 | 0.182 | 621.7 | IIIS (ET) |
| Control_3 | 397.2 | 0.163 | 349.2 | 0.184 | 674.5 | IIIS (ET) |
| Control_4 | 328.6 | 0.189 | 198.3 | 0.109 | 421.1 | IIIS (ET) |
| Control_5 | 295.0 | 0.141 | 227.1 | 0.183 | 692.1 | IIIS (ET) |
| Control_6 | 345.1 | 0.387 | 310.1 | 0.382 | 795.7 | IIIS (ET) |
| Control_7 | 345.7 | 0.253 | 220.9 | 0.183 | 571.5 | IIIS (ET) |
| Control_8 | 305.3 | 0.159 | 214.8 | 0.178 | 413 | IIIS (ET) |
| Control_9 | 341.6 | 0.169 | 233.3 | 0.189 | 453.9 | IIIS (ET) |
| Control_10 | 292.2 | 0.179 | 249.1 | 0.101 | 465.7 | IIIS (ET) |
| **Average** | **331.1** | **0.216** | **261.9** | **0.192** | **584.3** | |
| **St. Dev.** | **32.2** | **0.075** | **56.6** | **0.077** | **139.6** | |
| **COV (%)** | **10%** | **35%** | **22%** | **40%** | **24%** | |

**Table A.4 Cyclic Nail Connection Test Results of AOSB Specimens (CUREE Loading)**

Note: ET = edge tear; NF = nail fatigue; NPO = nail pull-out; SF = split framing

| Specimen ID | Min Load lb | Disp @ Min Load in | Max Load lb | Disp @ Max Load in | CUREE Toughness lb-in | Failure Mode |
|---|---|---|---|---|---|---|
| AOSB_1 | 368.4 | 0.3915 | 348.6 | 0.3905 | 1196.77 | IV, NF |
| AOSB_2 | 441.1 | 0.177 | 450.8 | 0.17 | 1428.5 | IV, NF |
| AOSB_3 | 365.6 | 0.1805 | 299.2 | 0.3995 | 1130.1 | IV (NPO) |
| AOSB_4 | 395.1 | 0.181 | 322.5 | 1.0335 | 1271.1 | IV (ET) |
| AOSB_5 | 332 | 0.1795 | 292.3 | 0.254 | 1117.6 | IV (NPO) |
| AOSB_6 | 345.7 | 0.186 | 275.8 | 0.394 | 1126.1 | IV (NPO) |
| AOSB_7 | 240.1 | 0.1785 | 194.9 | 0.1785 | 763.7 | IV (NPO) SF |
| AOSB_8 | 388.3 | 0.255 | 325.9 | 0.1765 | 1308.3 | IV (NPO) |
| AOSB_9 | 408.2 | 0.166 | 319.1 | 0.1755 | 1300.9 | IV (NPO) |
| AOSB_10 | 335.5 | 0.1655 | 299.8 | 0.1645 | 1130.2 | IV (NPO) |
| **Average** | **362.0** | **0.206** | **312.9** | **0.334** | **1177.3** | |
| **St. Dev.** | **54.7** | **0.070** | **63.8** | **0.266** | **178.4** | |
| **COV (%)** | **15%** | **34%** | **20%** | **80%** | **15%** | |

**Table A.5 Residual Capacity of AOSB Connections After Cyclic Loading**

| Specimen ID | Residual Toughness lb-in | Total Toughness lb-in | Residual Max Load lb |
|---|---|---|---|
| AOSB_1 | 314.1 | 1510.9 | 339 |
| AOSB_2 | 23.2 | 1451.7 | 46.7 |
| AOSB_3 | 362.1 | 1492.2 | 282.7 |
| AOSB_4 | 355 | 1626.1 | 322.5 |
| AOSB_5 | 276.6 | 1394.2 | 234 |
| AOSB_6 | 301.3 | 1427.4 | 223.7 |
| AOSB_7 | 159 | 922.7 | 135.2 |
| AOSB_8 | 401.5 | 1709.8 | 301.9 |
| AOSB_9 | 230.7 | 1531.6 | 229.9 |
| AOSB_10 | 219.9 | 1350.1 | 184.6 |
| **Average** | **264.3** | **1441.7** | **230.0** |
| **St. Dev.** | **112.0** | **211.2** | **90.1** |
| **COV (%)** | **42%** | **15%** | **39%** |

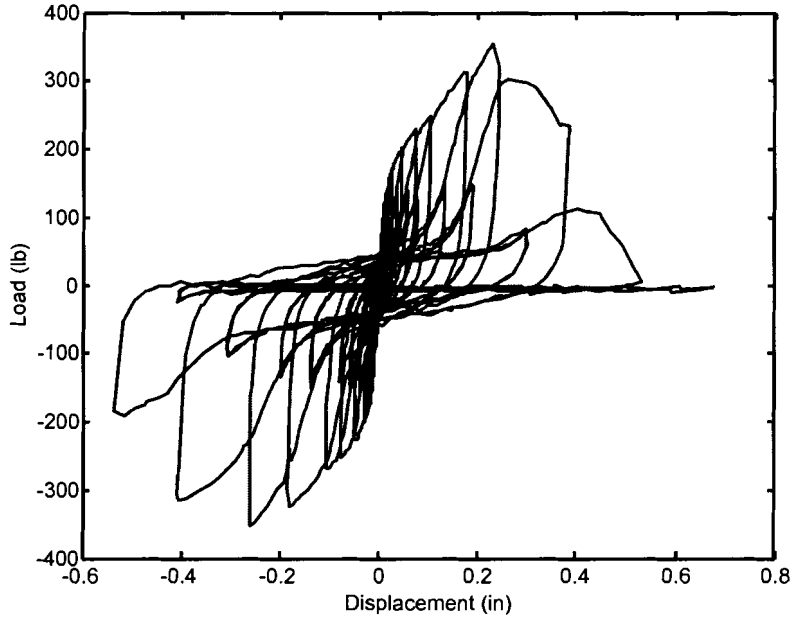


**Figure A.26 Cyclic Load-Displacement Curve; Specimen ID: Control_1**

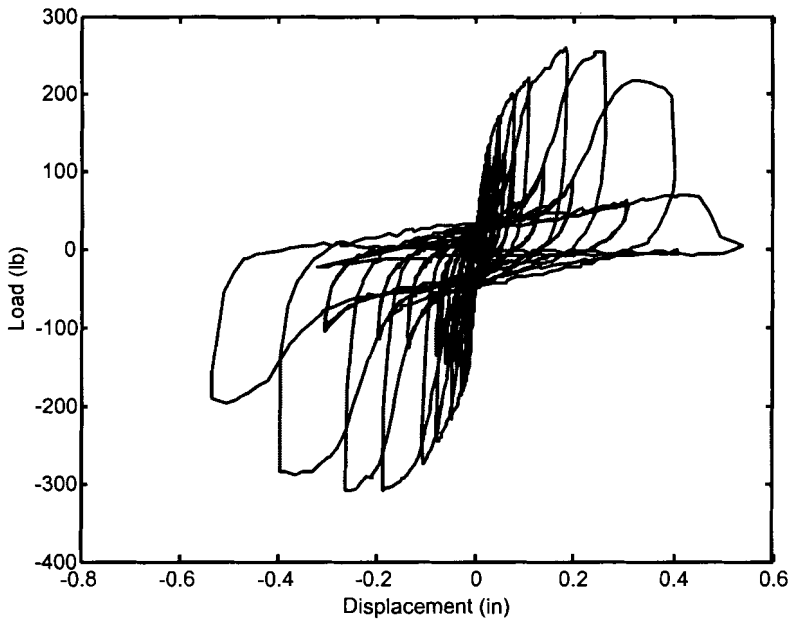


**Figure A.27 Cyclic Load-Displacement Curve; Specimen ID: Control_2**

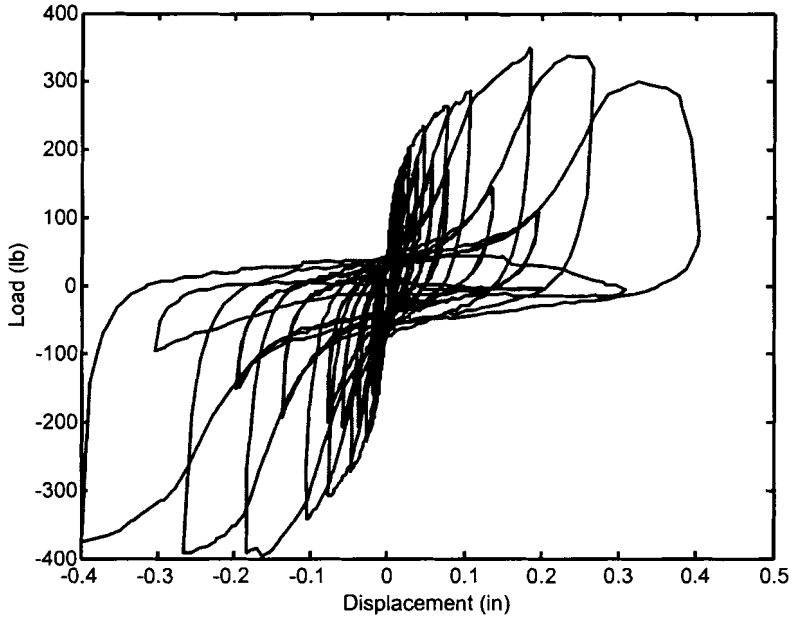


**Figure A.28 Cyclic Load-Displacement Curve; Specimen ID: Control_3**

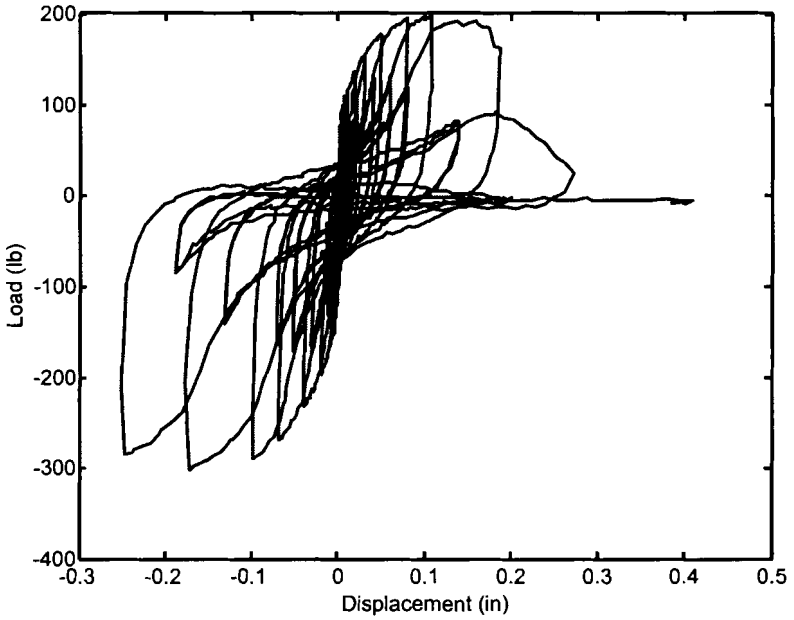


**Figure A.29 Cyclic Load-Displacement Curve; Specimen ID: Control_4**

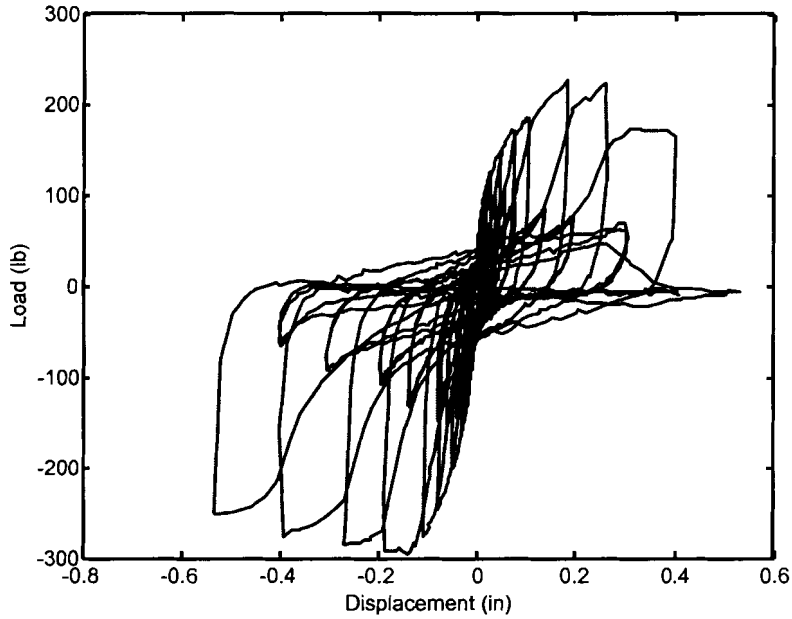


**Figure A.30 Cyclic Load-Displacement Curve; Specimen ID: Control_5**

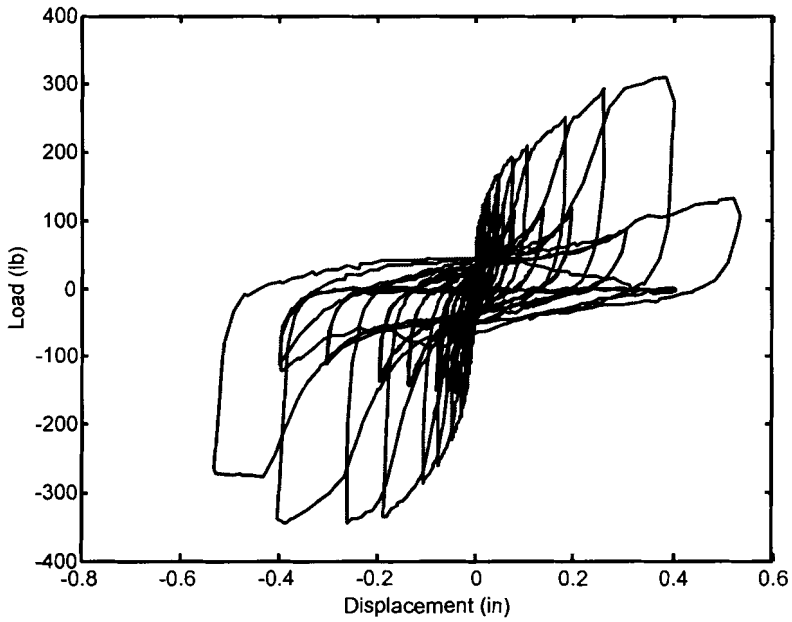


**Figure A.31 Cyclic Load-Displacement Curve; Specimen ID: Control_6**

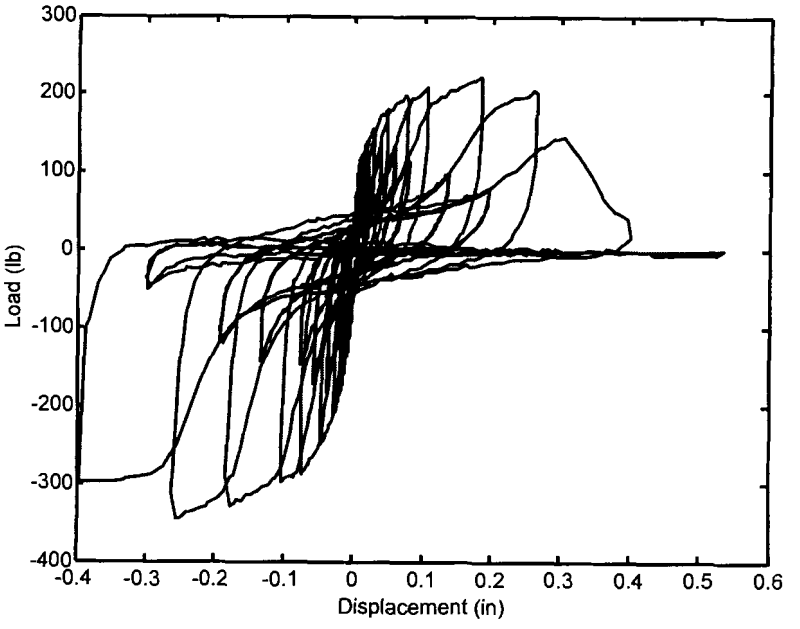


**Figure A.32 Cyclic Load-Displacement Curve; Specimen ID: Control_7**

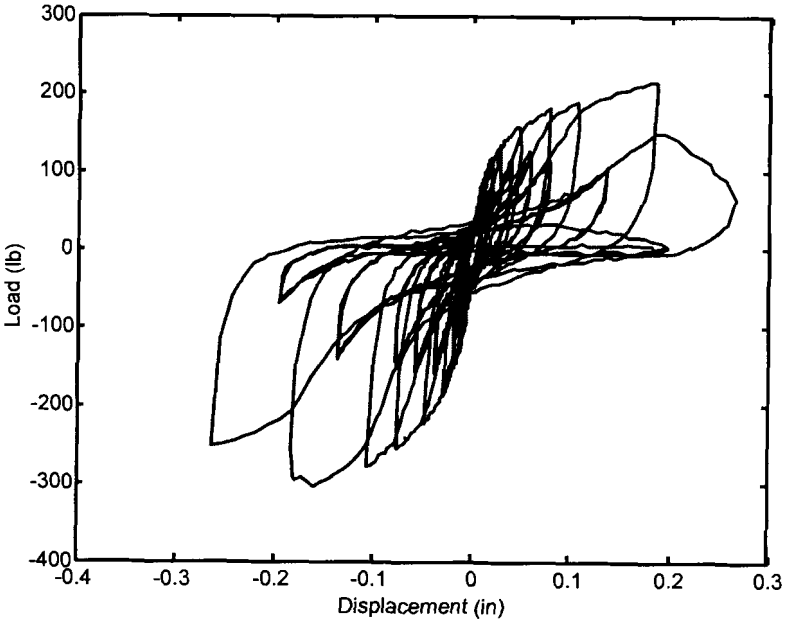


**Figure A.33 Cyclic Load-Displacement Curve; Specimen ID: Control_8**

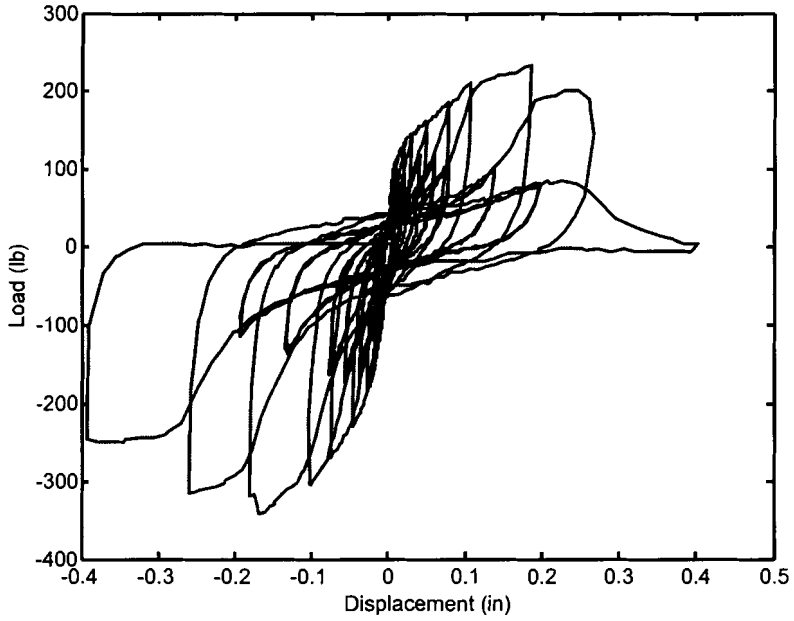


**Figure A.34 Cyclic Load-Displacement Curve; Specimen ID: Control_9**

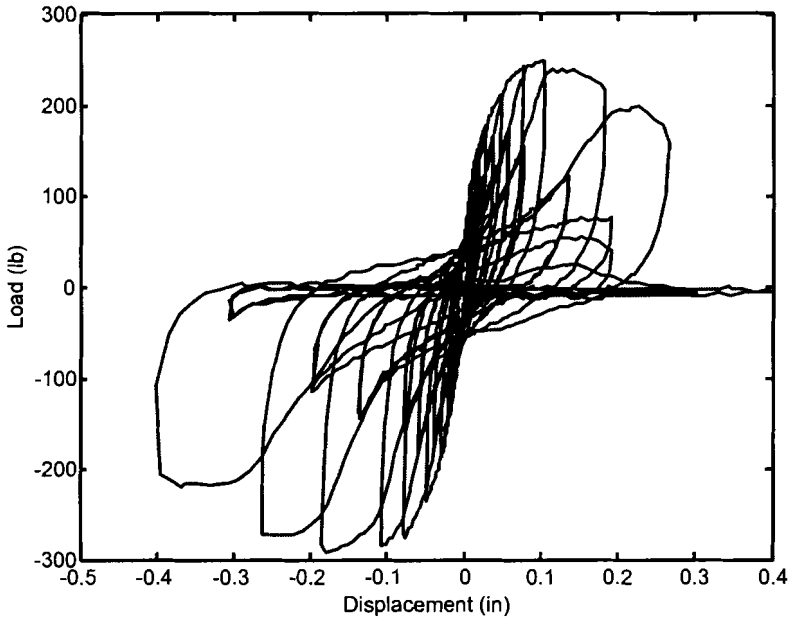


**Figure A.35 Cyclic Load-Displacement Curve; Specimen ID: Control_10**

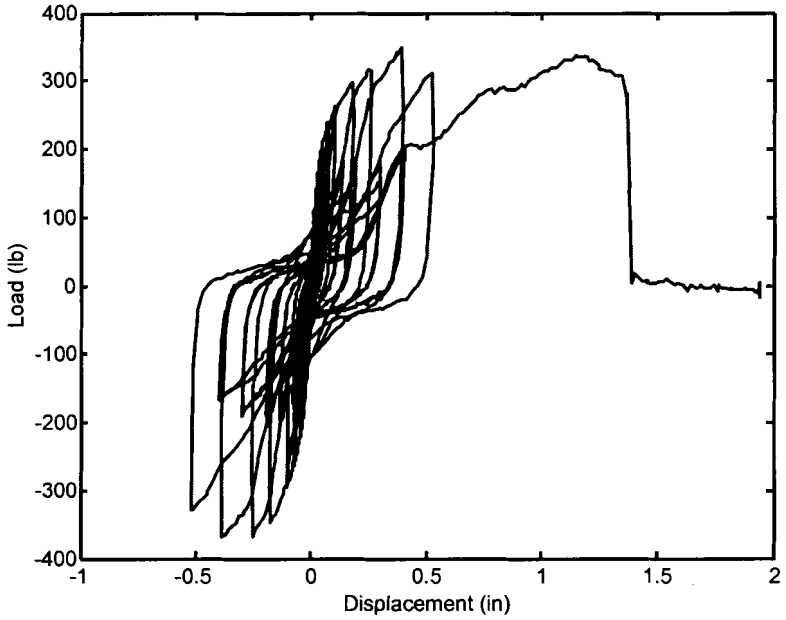


**Figure A.36 Cyclic Load-Displacement Curve; Specimen ID: AOSB_1**

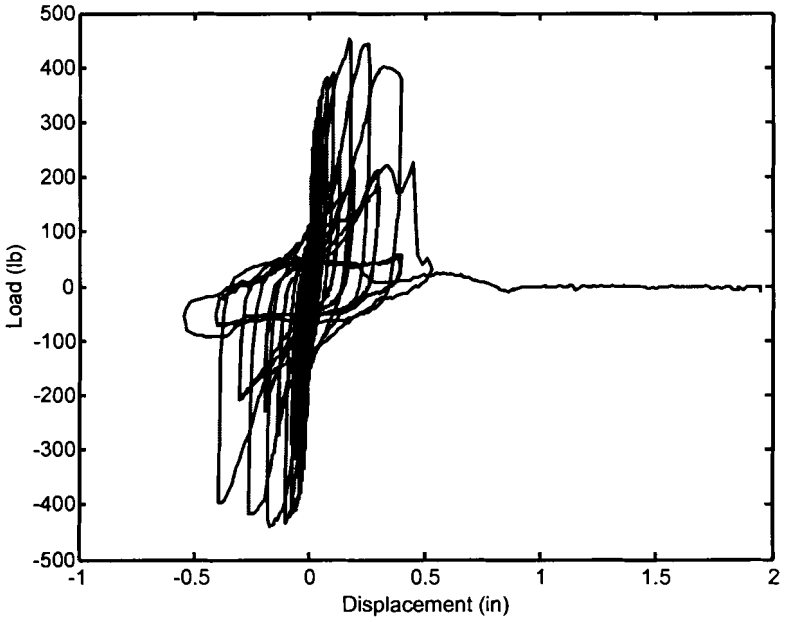


**Figure A.37 Cyclic Load-Displacement Curve; Specimen ID: AOSB_2**

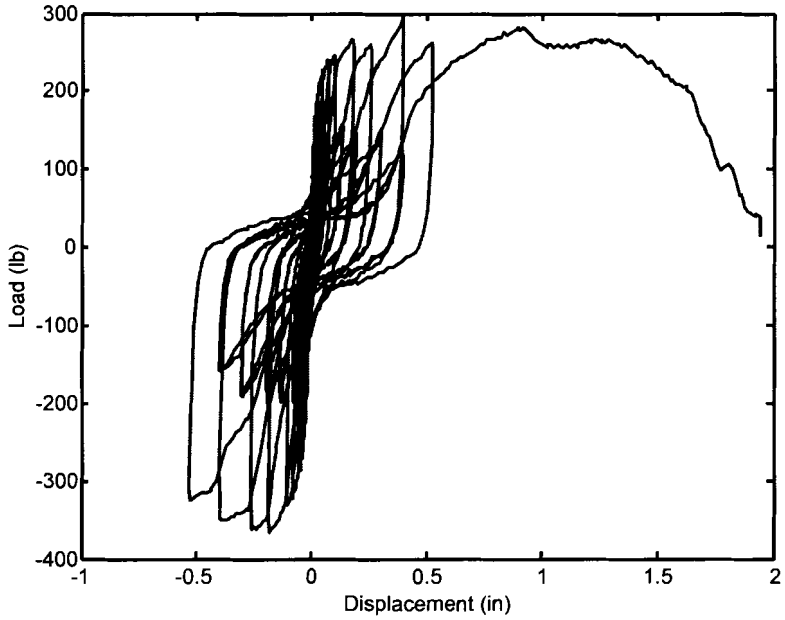


**Figure A.38 Cyclic Load-Displacement Curve; Specimen ID: AOSB_3**

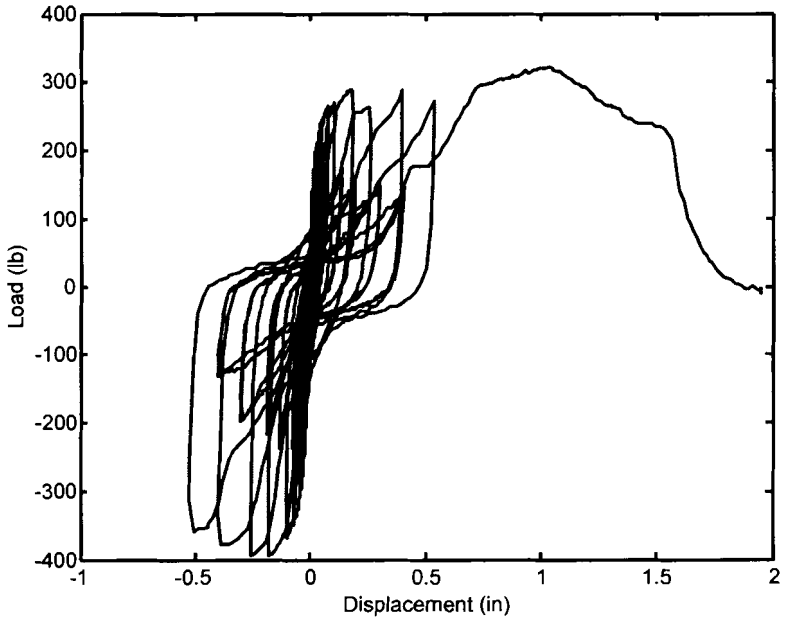


**Figure A.39 Cyclic Load-Displacement Curve; Specimen ID: AOSB_4**

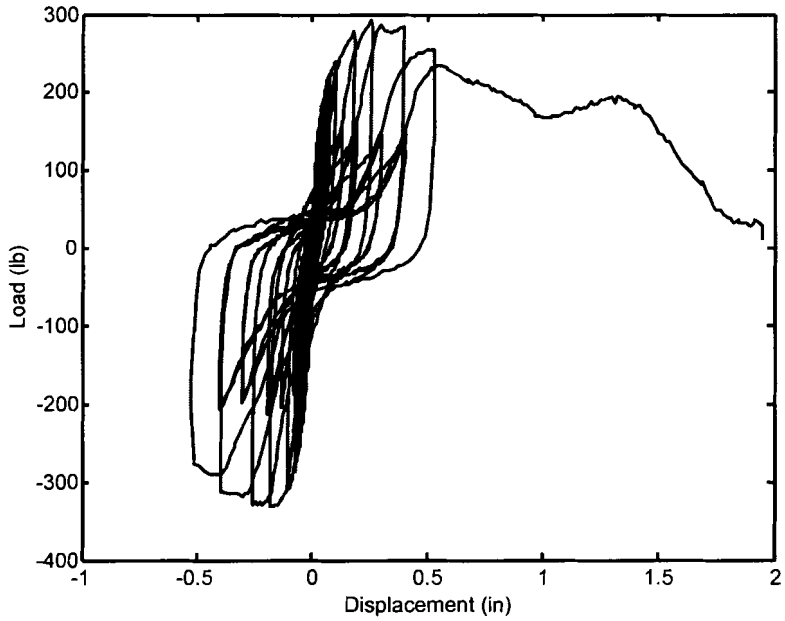


**Figure A.40 Cyclic Load-Displacement Curve; Specimen ID: AOSB_5**

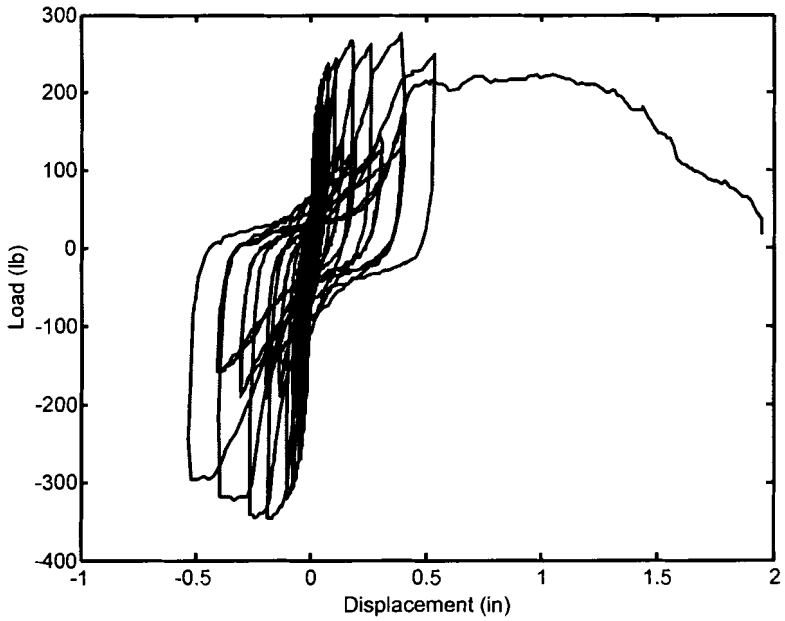


**Figure A.41 Cyclic Load-Displacement Curve; Specimen ID: AOSB_6**

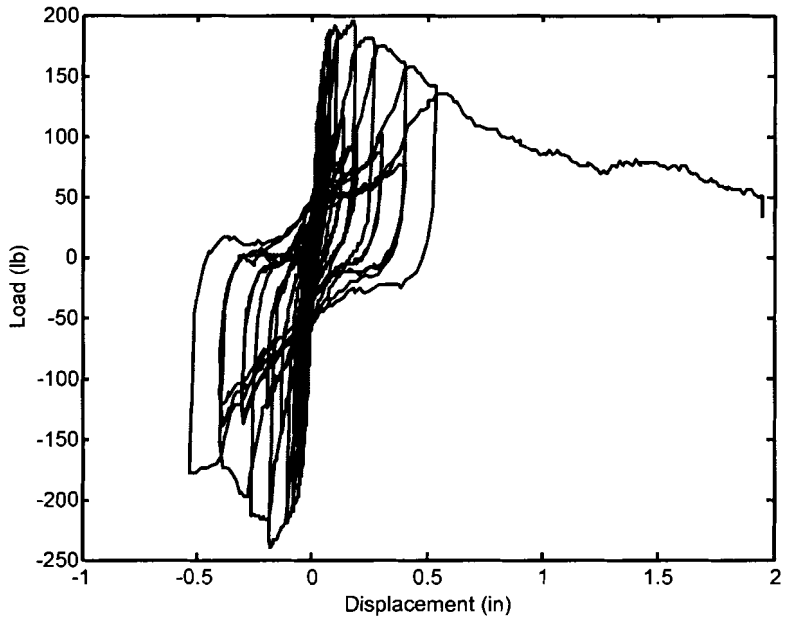


**Figure A.42 Cyclic Load-Displacement Curve; Specimen ID: AOSB_7**

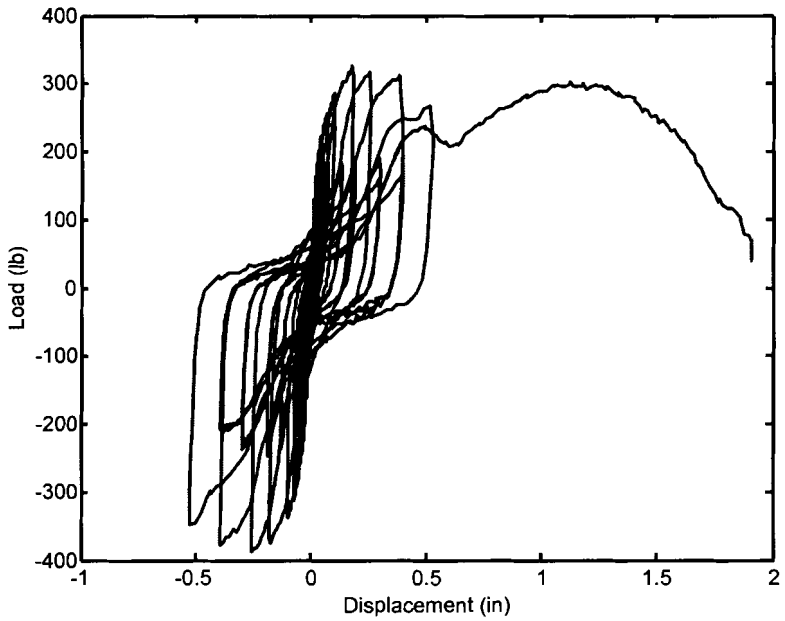


**Figure A.43 Cyclic Load-Displacement Curve; Specimen ID: AOSB_8**

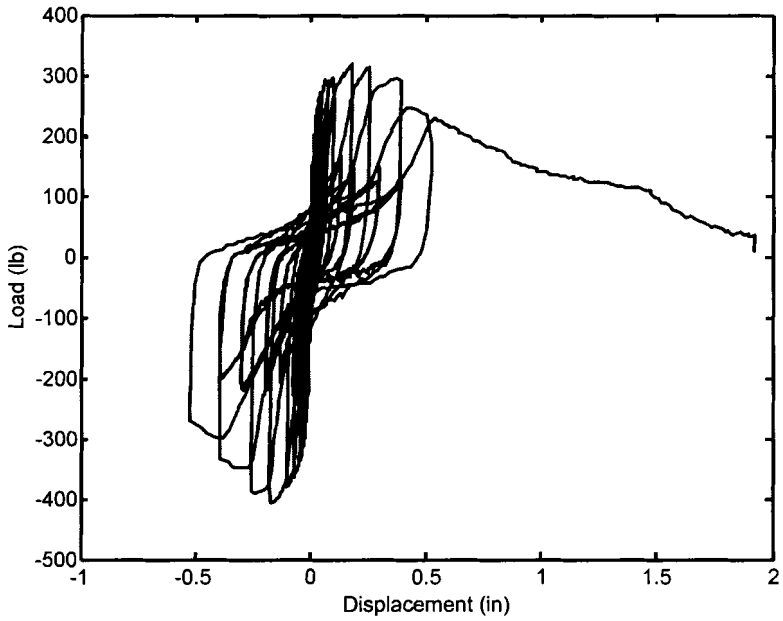


**Figure A.44 Cyclic Load-Displacement Curve; Specimen ID: AOSB_9**

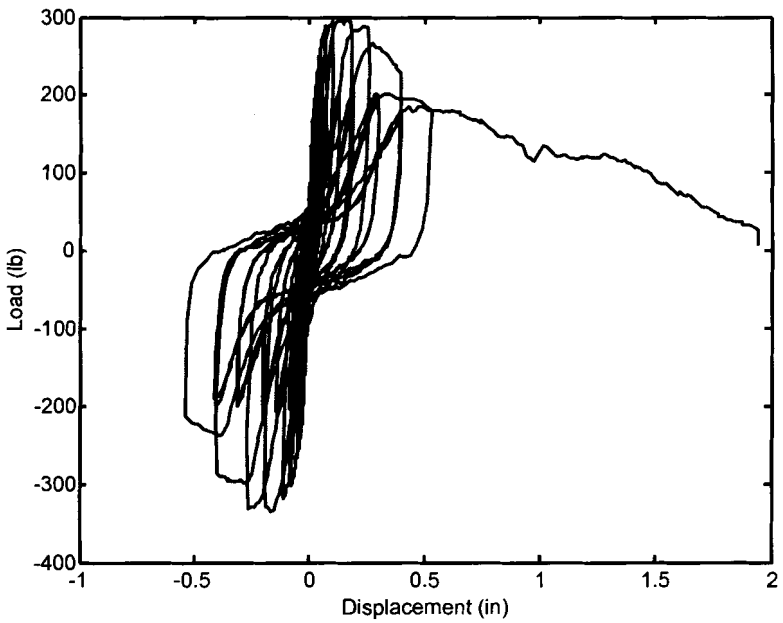


**Figure A.45 Cyclic Load-Displacement Curve; Specimen ID: AOSB_10**

**Table A.6 Nail Head Pull-Through Test Results of Control Specimens (7/16" OSB)**

| Dry | | | Wet | | |
|---|---|---|---|---|---|
| **Specimen ID** | **Peak Load lb** | **Initial Stiffness lb/in** | **Specimen ID** | **Peak Load lb** | **Initial Stiffness lb/in** |
| Control_dry_1 | 278.6 | 1891.6 | Control_wet_1 | 193.2 | 962.7 |
| Control_dry_2 | 208.0 | 1271.0 | Control_wet_2 | 315.0 | 1576.9 |
| Control_dry_3 | 260.5 | 2273.0 | Control_wet_3 | 238.2 | 997.6 |
| Control_dry_4 | 297.3 | 2276.0 | Control_wet_4 | 209.8 | 956.3 |
| Control_dry_5 | 273.7 | 2257.6 | Control_wet_5 | 165.5 | 690.4 |
| Control_dry_6 | 279.0 | 2095.0 | Control_wet_6 | 93.9 | 405.5 |
| Control_dry_7 | 363.4 | 1941.6 | Control_wet_7 | 314.7 | 1289.3 |
| Control_dry_8 | 341.6 | 2338.1 | Control_wet_8 | 230.9 | 1046.7 |
| Control_dry_9 | 355.0 | 2930.9 | Control_wet_9 | 133.5 | 640.4 |
| Control_dry_10 | 277.6 | 1599.1 | Control_wet_10 | 189.7 | 810.6 |
| **Average** | **295.1** | **2109.1** | **Average** | **208.5** | **937.6** |
| **St. Dev.** | **50.3** | **473.7** | **St. Dev.** | **70.9** | **332.9** |
| **COV (%)** | **17%** | **22%** | **COV (%)** | **34%** | **36%** |

**Table A.7 Nail Head Pull-Through Test Results of AOSB Specimens**

| Dry | | | Wet | | |
|---|---|---|---|---|---|
| **Specimen ID** | **Peak Load lb** | **Initial Stiffness lb/in** | **Specimen ID** | **Peak Load lb** | **Initial Stiffness lb/in** |
| AOSB_dry_001 | 527.5 | 3955.3 | AOSB_wet_001 | 553.1 | 2161.2 |
| AOSB_dry_002 | 737.2 | 4478.0 | AOSB_wet_002 | 563.7 | 1932.2 |
| AOSB_dry_003 | 695.0 | 5042.3 | AOSB_wet_003 | 478.2 | 2101.3 |
| AOSB_dry_004 | 745.0 | 5386.5 | AOSB_wet_004 | 485.5 | 1969.3 |
| AOSB_dry_005 | 607.3 | 4852.8 | AOSB_wet_005 | 634.9 | 2778.5 |
| AOSB_dry_006 | 786.7 | 5416.2 | AOSB_wet_006 | 495.4 | 2478.8 |
| AOSB_dry_007 | 646.1 | 4437.4 | AOSB_wet_007 | 565.2 | 2517.9 |
| AOSB_dry_008 | 697.7 | 5816.3 | AOSB_wet_008 | 609.5 | 2587.8 |
| AOSB_dry_009 | 674.4 | 3959.2 | AOSB_wet_009 | 528.6 | 2528.8 |
| AOSB_dry_0010 | 612.1 | 3312.8 | AOSB_wet_0010 | 499.9 | 2685.8 |
| **Average** | **689.1** | **4744.6** | **Average** | **541.4** | **2374.2** |
| **St. Dev.** | **61.0** | **786.2** | **St. Dev.** | **53.4** | **305.7** |
| **COV (%)** | **9%** | **17%** | **COV (%)** | **10%** | **13%** |

# Appendix B

## SHEAR WALL TEST RESULTS

**Table B.1 Static Test Results for Conventional OSB Shear Walls with 4 in. Nail Spacing at the Panel Edges**

| Specimen | Pult (lb) | Δ @ Pult (in) | 1st Cycle Pmax (lb) | 1st Cycle Δ @ Pmax (in) | 1st Cycle Ke lb/in | 2nd Cycle Pmax (lb) | 2nd Cycle Δ @ Pmax (in) | 2nd Cycle Ke (lb/in) | 3rd Cycle Pmax (lb) | 3rd Cycle Δ @ Pmax (in) | 3rd Cycle Ke (lb/in) | Total Energy Absorbed (lb-in) |
|---|---|---|---|---|---|---|---|---|---|---|---|---|
| 1 | 2 | 3 | 4 | 5 | 6 | 7 | 8 | 9 | 10 | 11 | 12 | 13 |
| Static_4C_1 | 7893 | 2.93 | 3000 | 0.30 | 9.97 | 6000 | 1.31 | 5.15 | 7893.1 | 2.93 | 3.71 | 27416 |
| Static_4C_2 | 6305 | 3.46 | 3000 | 0.503 | 5.96 | 6000 | 1.884 | 3.80 | 6304.9 | 3.46 | 4.16 | 30077 |
| Static_4C_3 | 7752 | 3.52 | 3000 | 0.45 | 6.70 | 6000 | 1.58 | 4.36 | 7752.5 | 3.52 | 3.25 | 35135 |
| **Average** | 7317 | 3.30 | 3000 | 0.42 | 7.54 | 6000 | 1.59 | 4.4 | 7316.8 | 3.30 | 3.71 | 30876 |
| **St. Dev.** | 879.18 | 0.32 | 0.00 | 0.10 | 2.13 | 0.00 | 0.29 | 0.67 | 879.2 | 0.32 | 0.46 | 3921 |
| **COV (%)** | 12% | 10% | 0% | 25% | 28% | 0% | 18% | 15% | 12% | 10% | 12% | 13% |

**Table B.2 Static Test Results for AOSB Shear Wallswith 4 in. Nail Spacing at the Panel Edges**

| Specimen | Pult (lb) | Δ @ Pult (in) | 1st Cycle Pmax (lb) | 1st Cycle Δ @ Pmax (in) | 1st Cycle Ke lb/in | 2nd Cycle Pmax (lb) | 2nd Cycle Δ @ Pmax (in) | 2nd Cycle Ke (lb/in) | 3rd Cycle Pmax (lb) | 3rd Cycle Δ @ Pmax (in) | 3rd Cycle Ke (lb/in) | Total Energy Absorbed (lb-in) |
|---|---|---|---|---|---|---|---|---|---|---|---|---|
| 1 | 2 | 3 | 4 | 5 | 6 | 7 | 8 | 9 | 10 | 11 | 12 | 13 |
| Static_4R_001 | 8478 | 4.04 | 3000 | 0.49 | 6.11 | 6000 | 1.11 | 7.60 | 8478 | 4.04 | 4.06 | 40277 |
| Static_4R_002 | 9974 | 4.10 | 3000 | 0.32 | 9.29 | 6000 | 0.98 | 7.73 | 9974 | 4.10 | 2.94 | 50404 |
| Static_4R_003 | 8759 | 3.26 | 3000 | 0.22 | 13.82 | 6000 | 0.775 | 9.02 | 8759 | 3.26 | 3.15 | 42117 |
| **Average** | 9070 | 3.80 | 3000 | 0.34 | 9.74 | 6000 | 0.95 | 8.12 | 9070 | 3.80 | 3.38 | 44266 |
| **St. Dev.** | 794.83 | 0.47 | 0.00 | 0.14 | 3.88 | 0.00 | 0.17 | 0.78 | 794.83 | 0.47 | 0.60 | 5395 |
| **COV (%)** | 9% | 12% | 0% | 40% | 40% | 0% | 18% | 10% | 9% | 12% | 18% | 12% |

**Table B.3 Static Test Results for Conventional OSB Shear Walls with 6 in. Nail Spacing at the Panel Edges**

| Specimen | Pult (lb) | Δ @ Pult (in) | 1st Cycle | | | 2nd Cycle | | | 3rd Cycle | | | Total Energy Absorbed (lb-in) |
|---|---|---|---|---|---|---|---|---|---|---|---|---|
| | | | Pmax (lb) | Δ @ Pmax (in) | Ke lb/in | Pmax (lb) | Δ @ Pmax (in) | Ke (lb/in) | Pmax (lb) | Δ @ Pmax (in) | Ke (lb/in) | |
| 1 | 2 | 3 | 4 | 5 | 6 | 7 | 8 | 9 | 10 | 11 | 12 | 13 |
| Static_6C_1 | 6356.3 | 2.94 | 2000 | 0.21 | 9.76 | 4000 | 0.83 | 5.46 | 6356.3 | 2.94 | 2.61 | 23377 |
| Static_6C_2 | 5330.7 | 2.89 | 2000 | 0.27 | 7.52 | 4000 | 1.15 | 3.96 | 5330.7 | 2.89 | 2.63 | 21382 |
| Static_6C_3 | 6037.3 | 3.44 | 2000 | 0.20 | 9.90 | 4000 | 0.85 | 5.23 | 6037.3 | 3.44 | 2.06 | 24297 |
| **Average** | 5908.1 | 3.1 | 2000 | 0.22 | 9.06 | 4000 | 0.94 | 4.88 | 5908.1 | 3.09 | 2.43 | 23018 |
| **St. Dev.** | 524.90 | 0.30 | 0.00 | 0.04 | 1.34 | 0.00 | 0.18 | 0.80 | 524.90 | 0.30 | 0.32 | 1490 |
| **COV (%)** | 9% | 10% | 0% | 16% | 15% | 0% | 19% | 16% | 9% | 10% | 13% | 6% |

**Table B.4 Static Test Results for AOSB Shear Walls with 6 in. Nail Spacing at the Panel Edges**

| Specimen | Pult (lb) | Δ @ Pult (in) | 1st Cycle | | | 2nd Cycle | | | 3rd Cycle | | | Total Energy Absorbed (lb-in) |
|---|---|---|---|---|---|---|---|---|---|---|---|---|
| | | | Pmax (lb) | Δ @ Pmax (in) | Ke lb/in | Pmax (lb) | Δ @ Pmax (in) | Ke (lb/in) | Pmax (lb) | Δ @ Pmax (in) | Ke (lb/in) | |
| 1 | 2 | 3 | 4 | 5 | 6 | 7 | 8 | 9 | 10 | 11 | 12 | 13 |
| Static_6R_001 | 6545.0 | 3.89 | 2000 | 0.139 | 14.39 | 4000 | 0.650 | 6.71 | 6545.0 | 3.89 | 1.91 | 31309 |
| Static_6R_002 | 5582.8 | 4.26 | 2000 | 0.305 | 6.56 | 4000 | 0.879 | 5.24 | 5582.8 | 4.264 | 1.51 | 27842 |
| Static_6R_003 | 5490.2 | 3.63 | 2000 | 0.304 | 6.58 | 4000 | 0.806 | 6.24 | 5490.2 | 3.63 | 1.85 | 28477 |
| **Average** | 5872.7 | 3.9 | 2000 | 0.25 | 9.17 | 4000 | 0.78 | 6.06 | 5872.7 | 3.93 | 1.76 | 29209 |
| **St. Dev.** | 584.10 | 0.32 | 0.00 | 0.10 | 4.52 | 0.00 | 0.12 | 0.75 | 584.10 | 0.32 | 0.21 | 1846 |
| **COV (%)** | 10% | 8% | 0% | 38% | 49% | 0% | 15% | 12% | 10% | 8% | 12% | 6% |

**Table B.5 Cyclic Test Results for Conventional OSB Shear Walls with 4 in. Nail Spacing at the Panel Edges**

| Specimen ID | Max Load | Disp @ Max Load | Min Load | Disp @ Min Load | Energy |
|---|---|---|---|---|---|
| | lb | in | lb | in | lb-in |
| Cyclic_4C_1 | 6744 | 2.23 | -6351 | -2.23 | 106800 |
| Cyclic_4C_2 | 7582 | 2.38 | -6267 | -2.21 | 123034 |
| Cyclic_4C_3 | 7391 | 2.32 | -6323 | -2.32 | 120729 |
| **Average** | **7239** | **2.31** | **-6314** | **-2.25** | **116854** |
| **STDEV** | **439** | **0.08** | **42** | **0.06** | **8783** |
| **COV (%)** | **6%** | **3%** | **1%** | **3%** | **8%** |

**Table B.6 Cyclic Test Results for AOSB Shear Walls with 4 in. Nail Spacing at the Panel Edges**

| Specimen ID | Max Load | Disp @ Max Load | Min Load | Disp @ Min Load | Energy |
|---|---|---|---|---|---|
| | lb | in | lb | in | lb-in |
| Cyclic_4R_001 | 9459 | 3.14 | -8902 | -2.27 | 203250 |
| Cyclic_4R_002 | 8633 | 2.23 | -7835 | -2.24 | 199124 |
| Cyclic_4R_003 | 8610 | 2.05 | -8357 | -2.34 | 205465 |
| **Average** | **8901** | **2.47** | **-8365** | **-2.28** | **202613** |
| **STDEV** | **483** | **0.58** | **533** | **0.05** | **3218** |
| **COV (%)** | **5%** | **23%** | **6%** | **2%** | **2%** |

**Table B.7 Cyclic Test Results for Conventional OSB Shear Walls with 6 in. Nail Spacing at the Panel Edges**

| Specimen ID | Max Load | Disp @ Max Load | Min Load | Disp @ Min Load | Energy |
|---|---|---|---|---|---|
| | lb | in | lb | in | lb-in |
| Cyclic_6C_1 | 4766 | 1.71 | -4828 | -2.15 | 83735 |
| Cyclic_6C_2 | 5176 | 2.26 | -4423 | -2.9 | 94710 |
| Cyclic_6C_3 | 5609 | 2.32 | -4805 | -2.35 | 88685 |
| **Average** | **5184** | **2.10** | **-4685** | **-2.47** | **89043** |
| **STDEV** | **421** | **0.34** | **227** | **-0.39** | **5496** |
| **COV (%)** | **8%** | **16%** | **5%** | **16%** | **6%** |

**Table B.8 Cyclic Test Results for AOSB Shear Walls with 6 in. Nail Spacing at the Panel Edges**

| Specimen ID | Max Load | Disp @ Max Load | Min Load | Disp @ Min Load | Energy |
|---|---|---|---|---|---|
| | lb | in | lb | in | lb-in |
| Cyclic_6R_001 | 5193 | 2.32 | -5530 | -2.03 | 136549 |
| Cyclic_6R_002 | 6081 | 2.19 | -4968 | -2.39 | 135730 |
| Cyclic_6R_003 | 5755 | 2.33 | -5300 | -2.06 | 135166 |
| **Average** | **5676** | **2.28** | **-5266** | **-2.16** | **135815** |
| **STDEV** | **449** | **0.08** | **-282** | **0.20** | **695** |
| **COV (%)** | **8%** | **3%** | **5%** | **9%** | **1%** |

**Table B.9 Moisture Content Variation Between Time of Fabrication and Time of Testing for Cyclic Shear Wall Specimens**

| Specimen ID | Avg. Moisture Content of Framing Members (%) | |
|---|---|---|
| | When Built | When Tested |
| Cyclic_4C_1 | 12.6 | 6.1 |
| Cyclic_4C_2 | 12.2 | 5.4% |
| Cyclic_4C_3 | 12.2 | 6.1 |
| Cyclic_4R_001 | 12.0 | 6.0 |
| Cyclic_4R_002 | 9.6 | 6.0 |
| Cyclic_4R_003 | 10.2 | 6.1 |
| Cyclic_6C_1 | 10.8 | 6.0 |
| Cyclic_6C_2 | 10.5 | 6.0 |
| Cyclic_6C_3 | 10.6 | 6.1 |
| Cyclic_6R_001 | 10.1 | 6.0 |
| Cyclic_6R_002 | 10.5 | 6.0 |
| Cyclic_6R_003 | 10.3 | 6.0 |

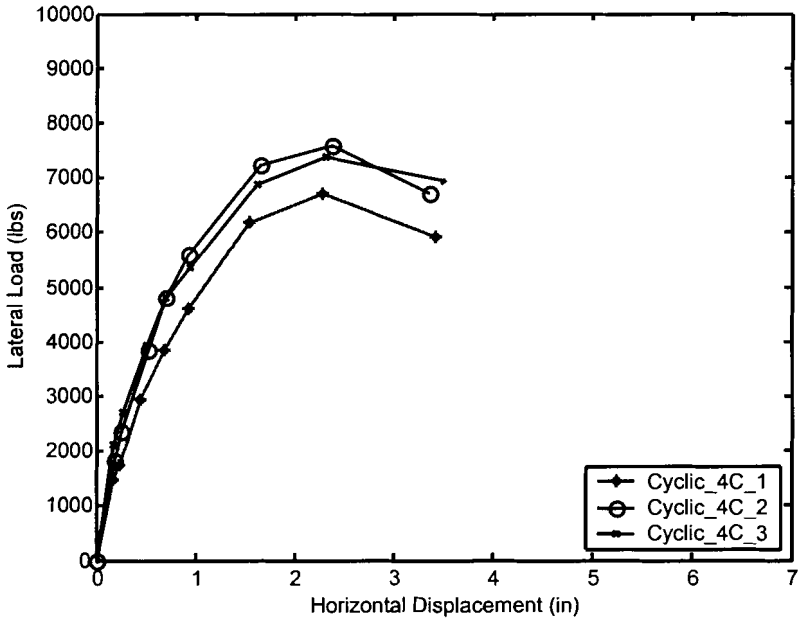


**Figure B.1 First Cycle Envelope Curves for Conventional OSB Shear Walls with 4in. Nail Spacing at the Panel Edges**

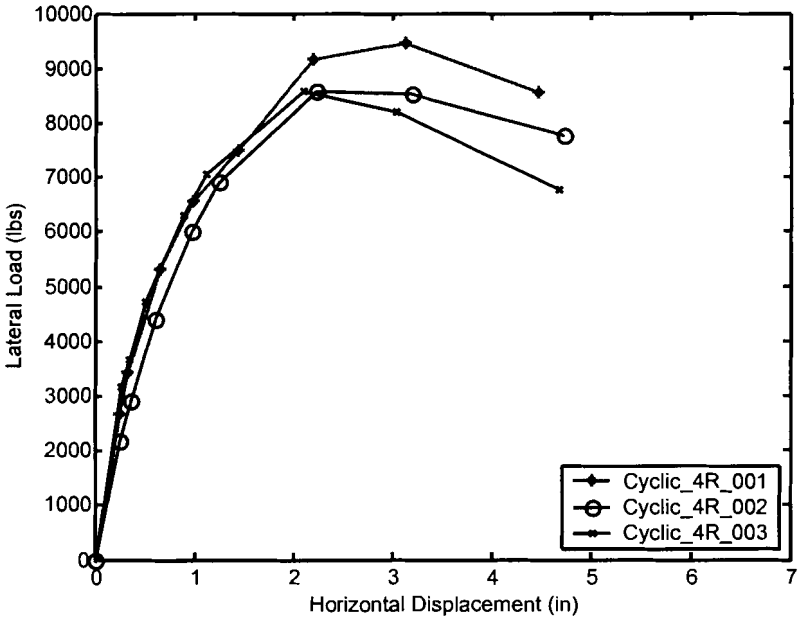


**Figure B.2 First Cycle Envelope Curves for AOSB Shear Walls with 4in. Nail Spacing at the Panel Edges**

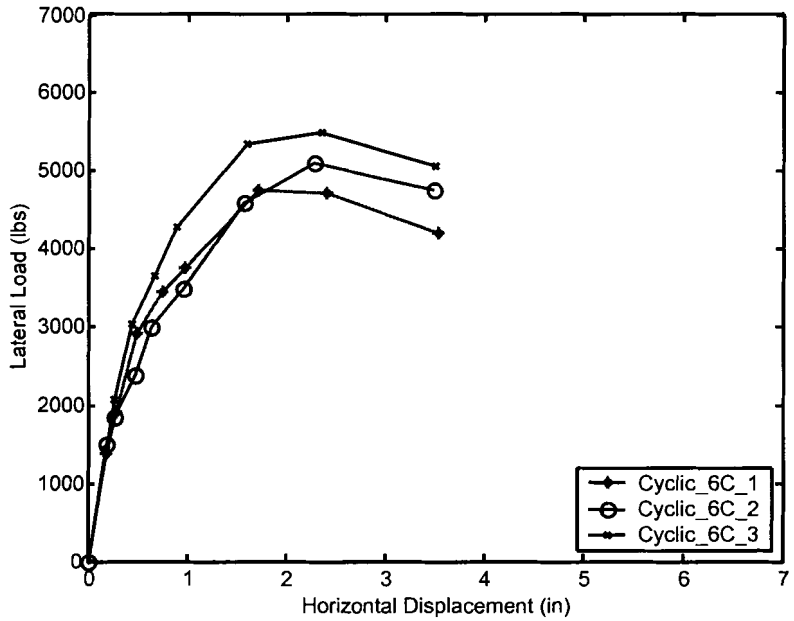


**Figure B.3 First Cycle Envelope Curves for Conventional OSB Shear Walls with 6in. Nail Spacing at the Panel Edges**

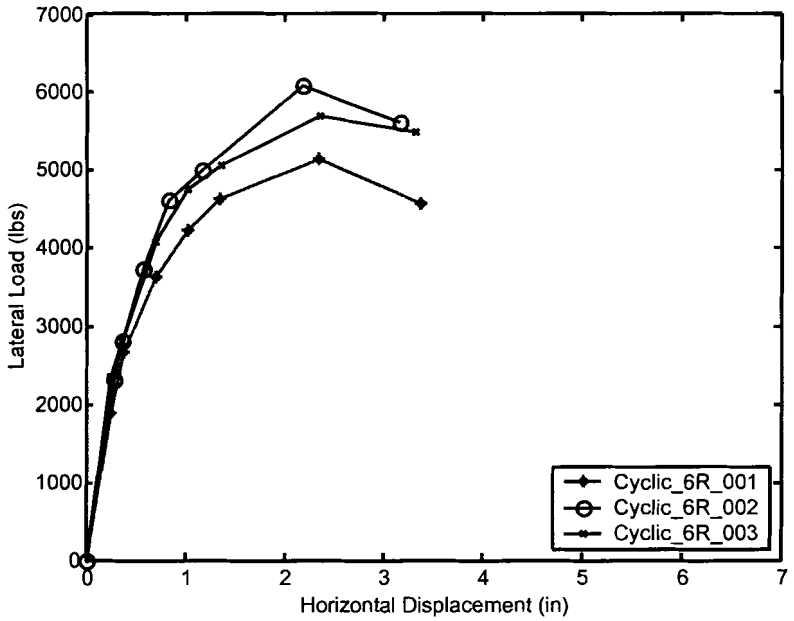


**Figure B.4 First Cycle Envelope Curves for Conventional AOSB Shear Walls with 6in. Nail Spacing at the Panel Edges**

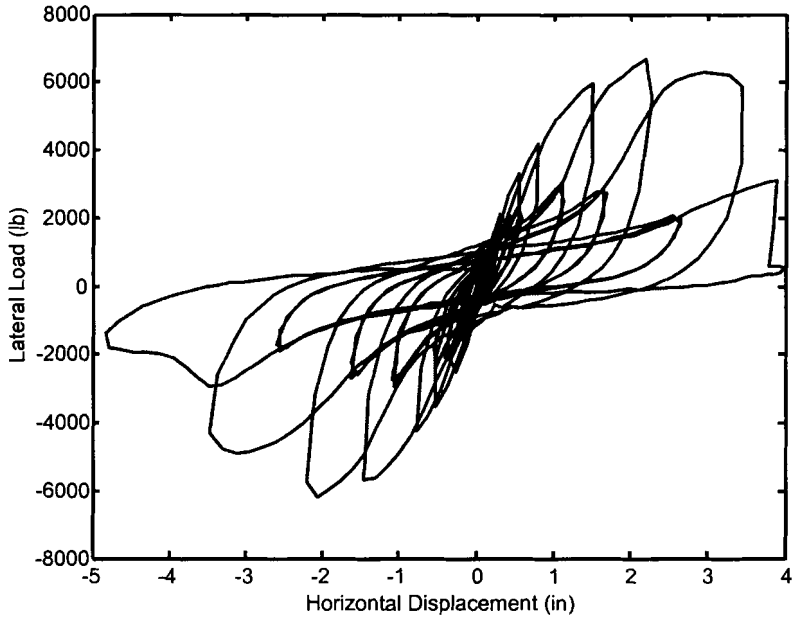


**Figure B.5 Hysteretic Response; Specimen ID:Cyclic_4C_1**

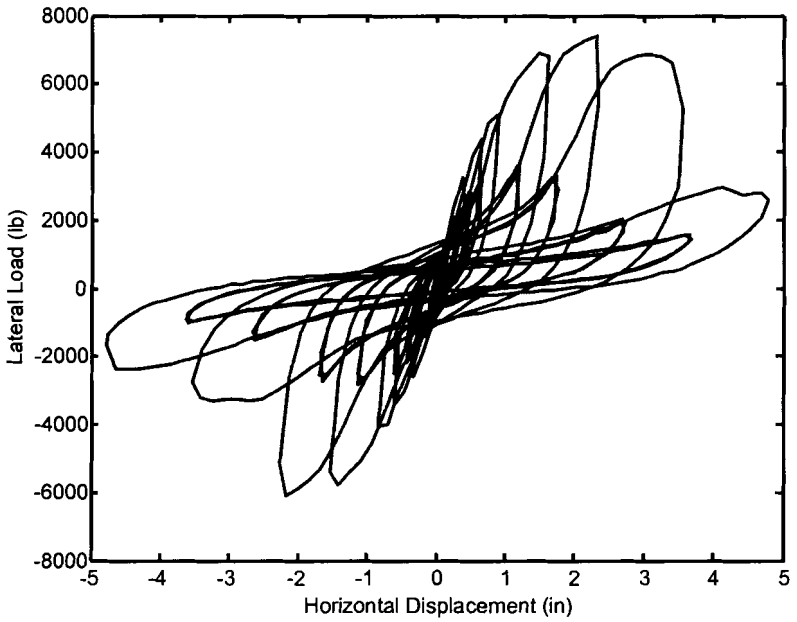


**Figure B.6 Hysteretic Response; Specimen ID:Cyclic_4C_2**

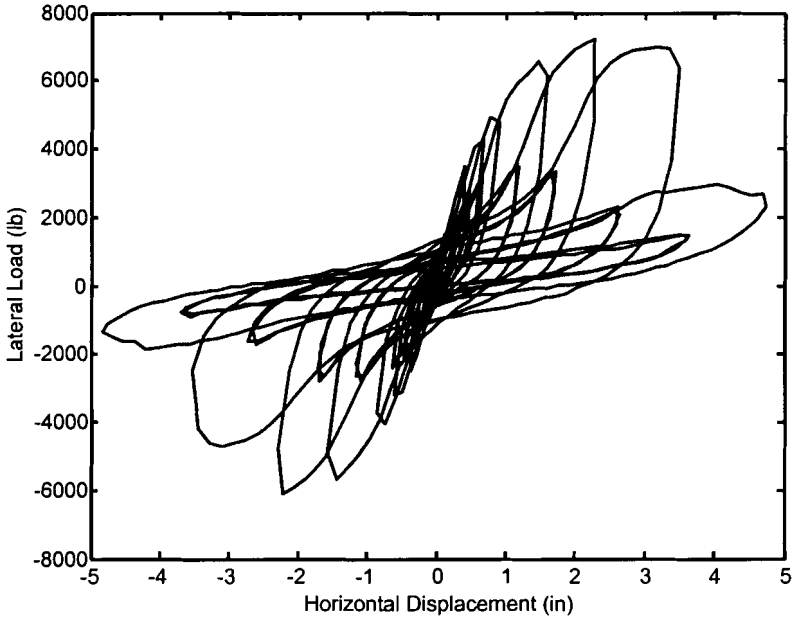


**Figure B.7 Hysteretic Response; Specimen ID:Cyclic_4C_3**

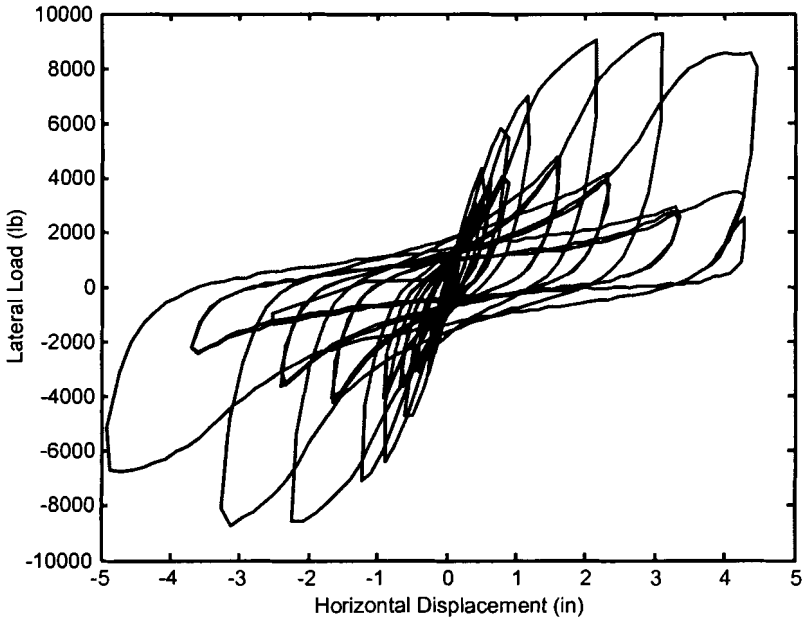


**Figure B.8 Hysteretic Response; Specimen ID:Cyclic_4R_001**

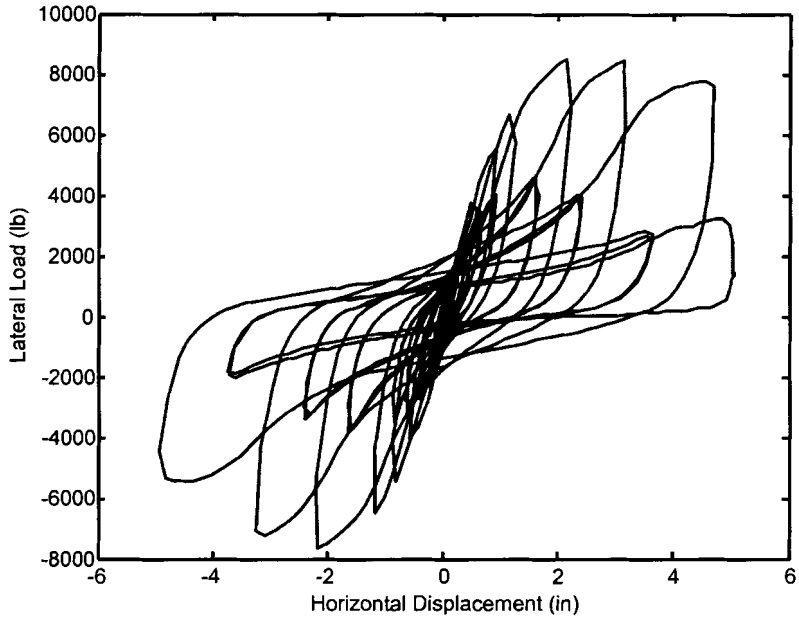


**Figure B.9 Hysteretic Response; Specimen ID:Cyclic_4R_002**

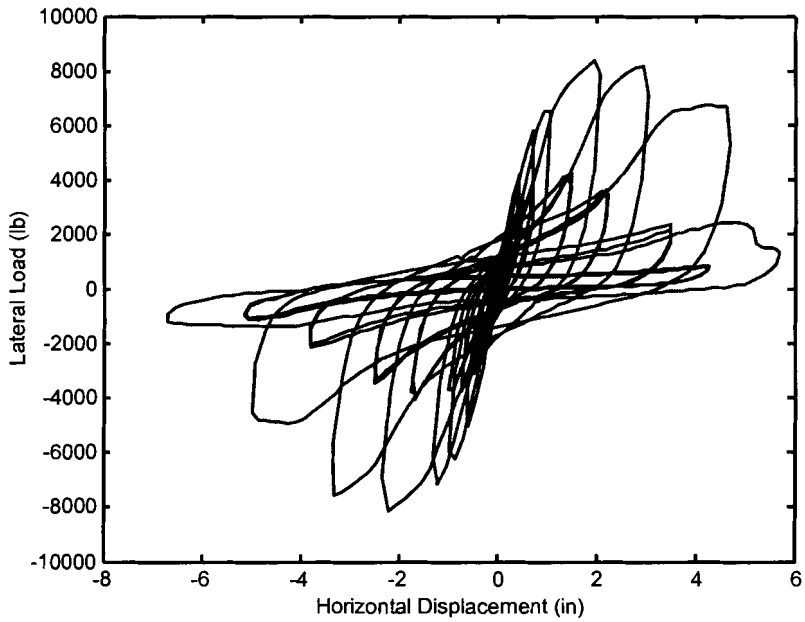


**Figure B.10 Hysteretic Response; Specimen ID:Cyclic_4R_003**

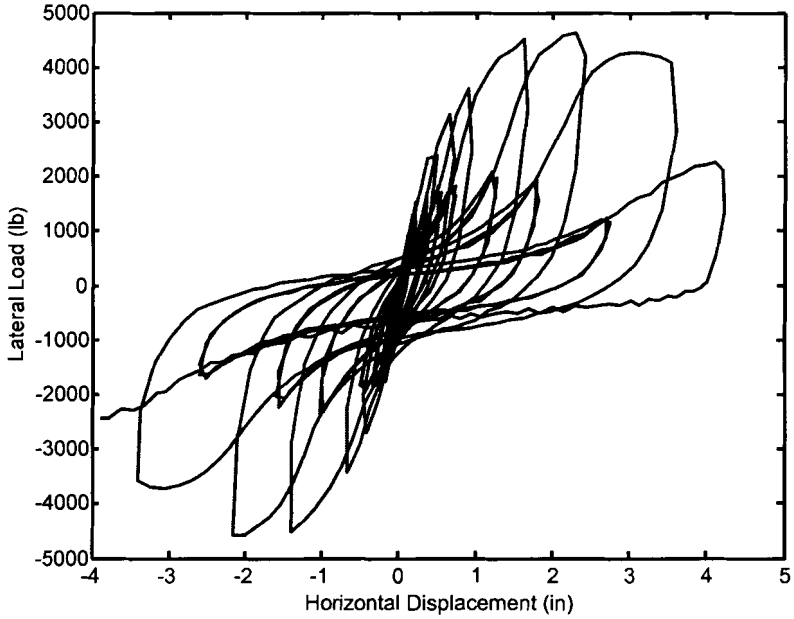


**Figure B.11 Hysteretic Response; Specimen ID:Cyclic_6C_1**

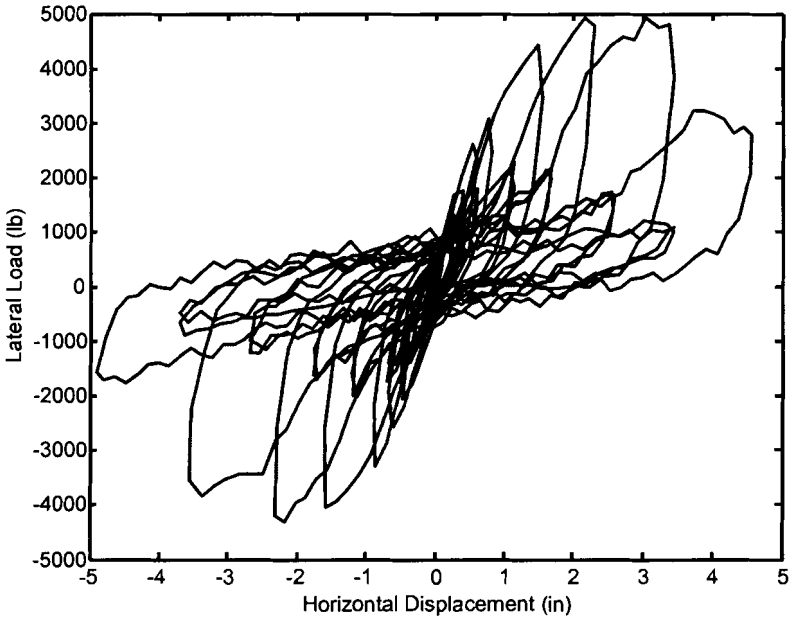


**Figure B.12 Hysteretic Response; Specimen ID:Cyclic_6C_2**

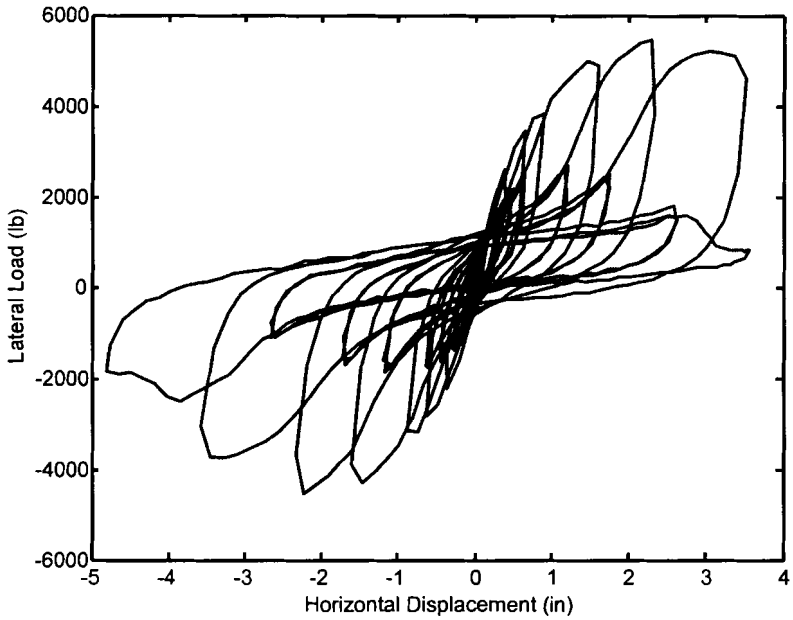


**Figure B.13 Hysteretic Response; Specimen ID:Cyclic_6C_3**

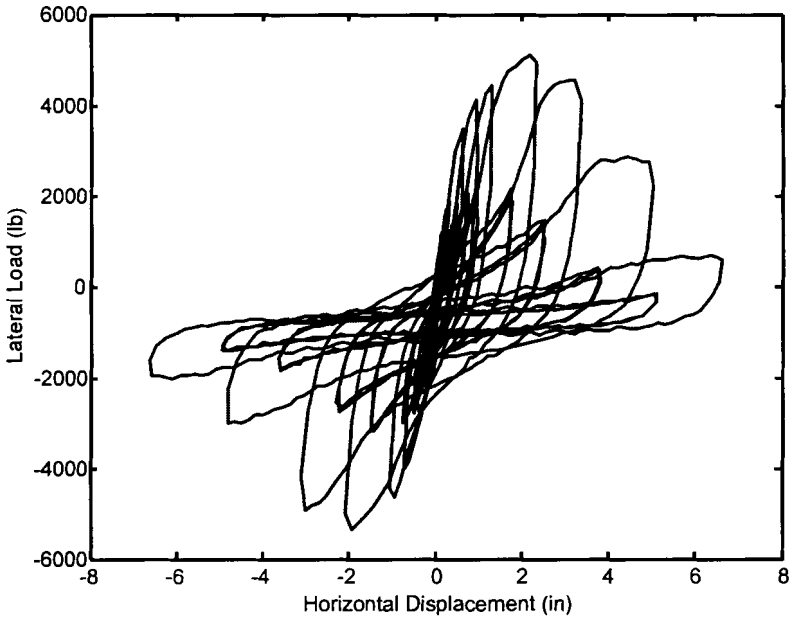


**Figure B.14 Hysteretic Response; Specimen ID:Cyclic_6R_001**

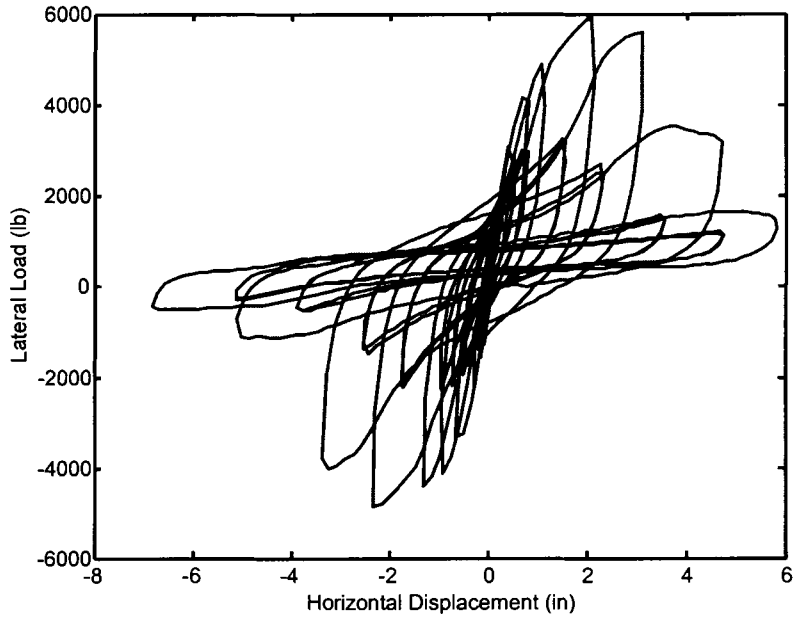


**Figure B.15 Hysteretic Response; Specimen ID:Cyclic_6R_002**

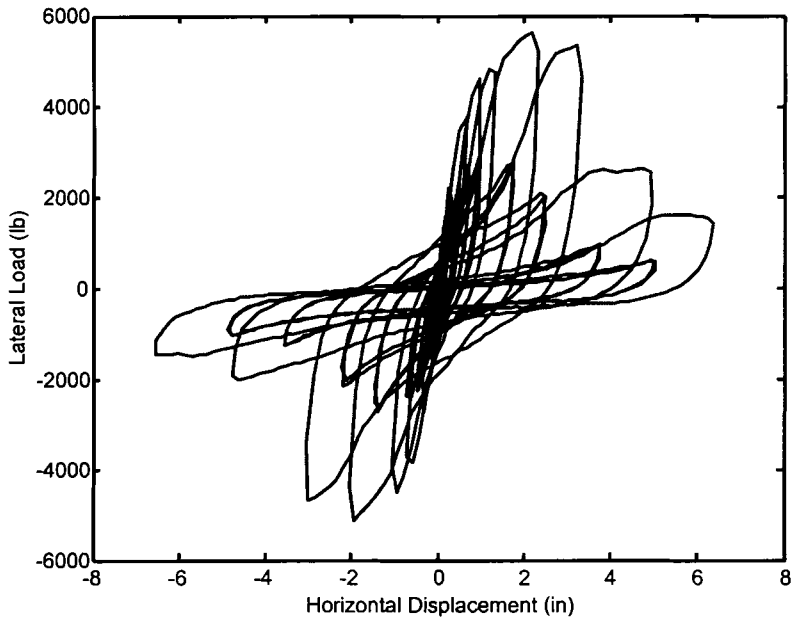


**Figure B.16 Hysteretic Response; Specimen ID:Cyclic_6R_003**

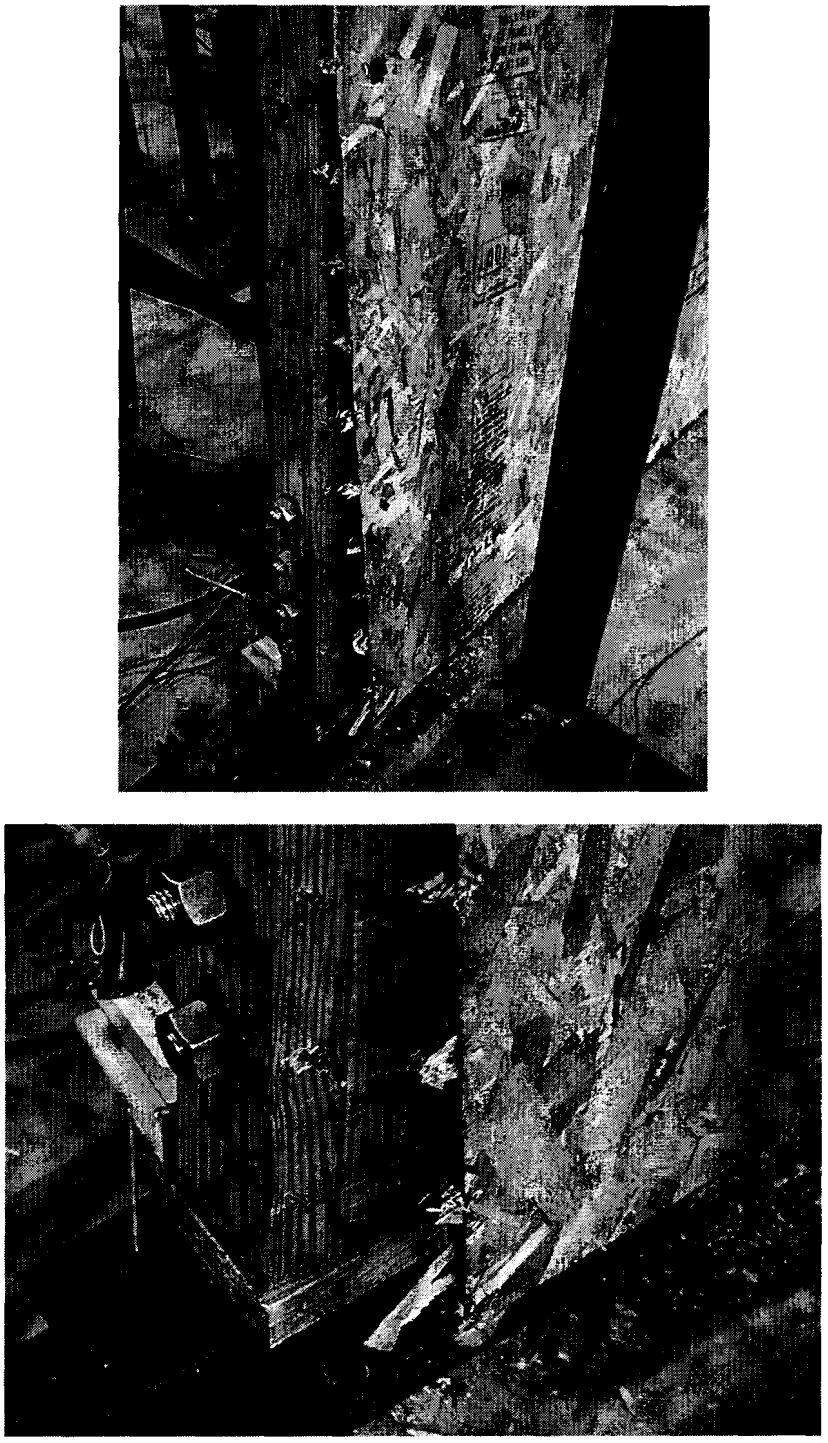

**Figure B.17 Edge Tear Failures Commonly Observed in Static Tests of Conventional OSB Walls**

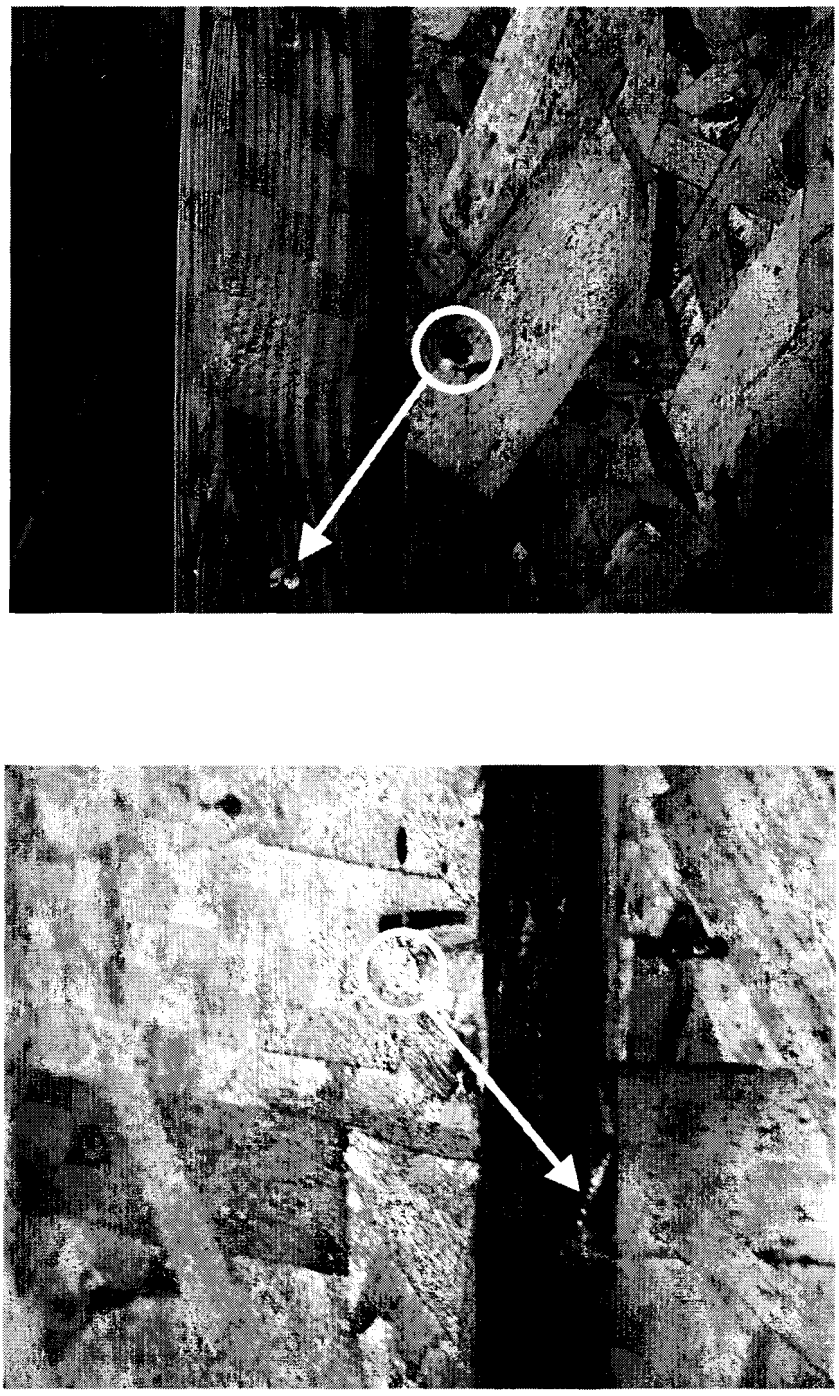

**Figure B.18 Nail Head Pull-Through Failures Commonly Observed in Static Tests of Conventional OSB Walls**

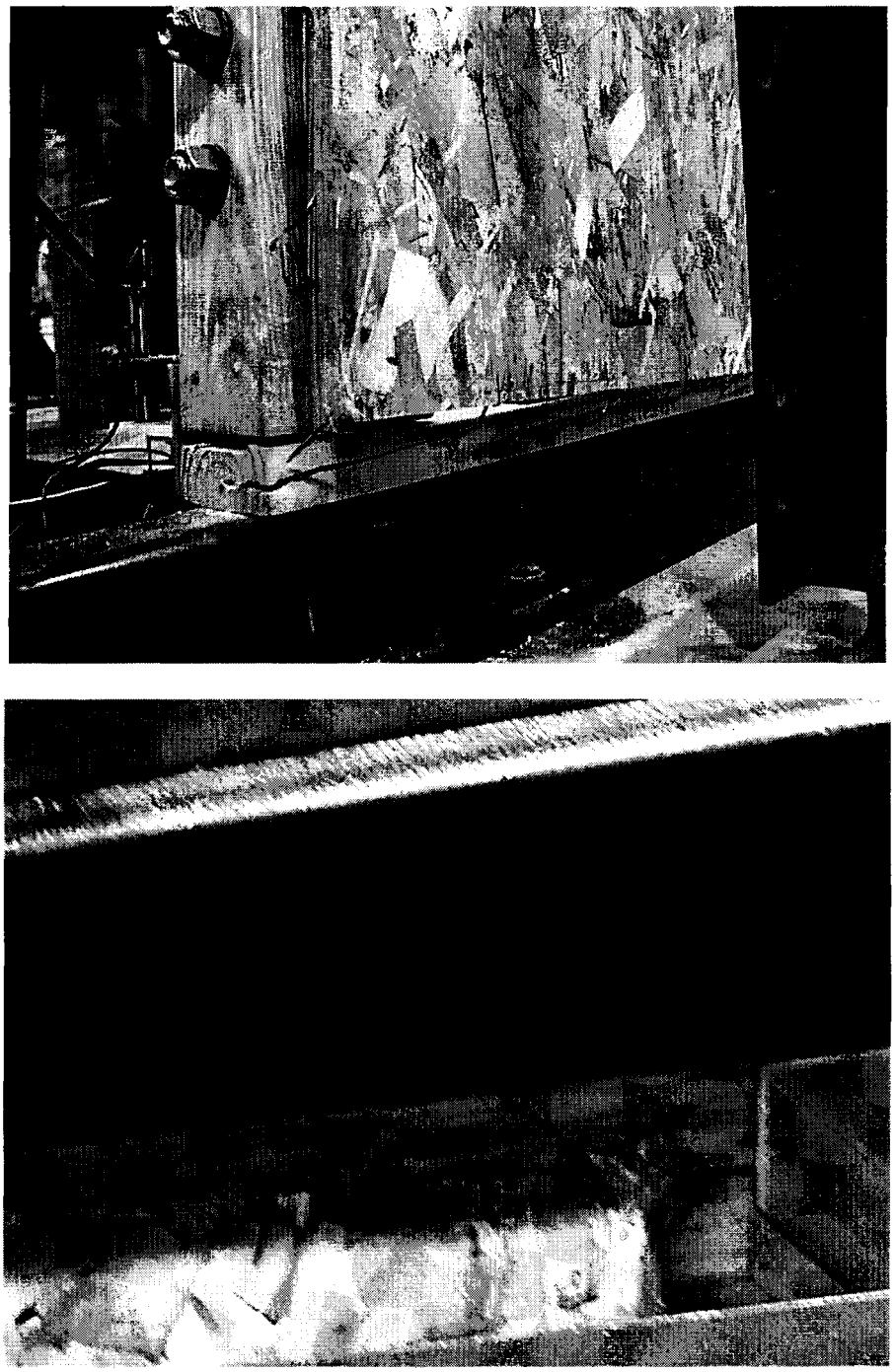

**Figure B.19 Typical Failures Observed in Static Tests of AOSB Shear Walls (Top: nail pull-out; Bottom: edge tear with increased withdrawal)**

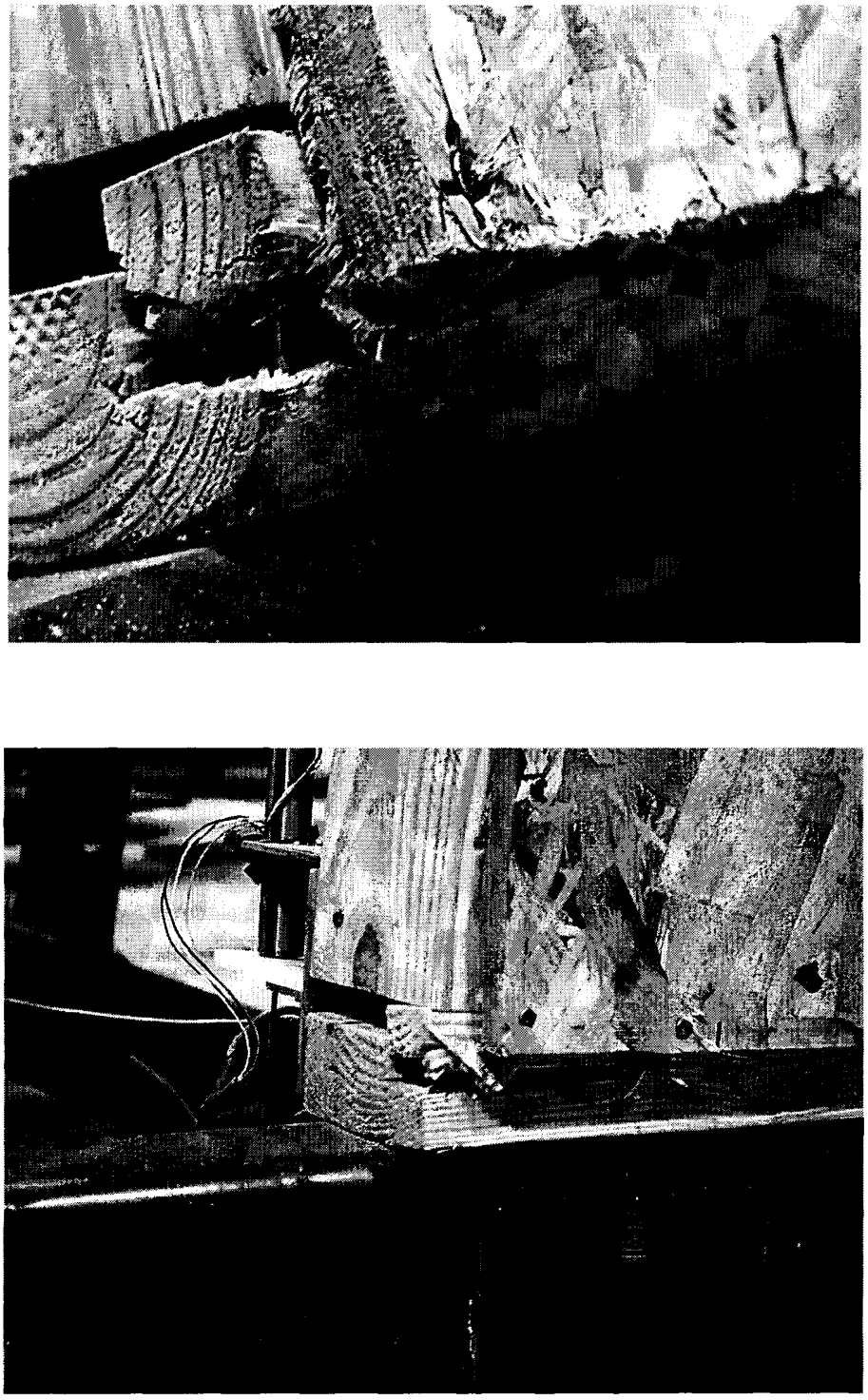

**Figure B.20 Splitting of Bottom Plate at the Tension Corner (Commonly Observed in Static Tests of AOSB Shear Walls)**

**Figure B.21 Typical Failures Observed in Cyclic Tests of Conventional OSB Shear Walls (Top: nail head pull-through; Bottom: edge tear )**

**Figure B.22 Typical Failures Observed in Cyclic Tests of AOSB Shear Walls (Top: nail fatigue; Bottom: nail pull-out )**

**Figure B.23 Nail Extraction Under Load Cycling (Commonly Observed in AOSB Shear Walls)**

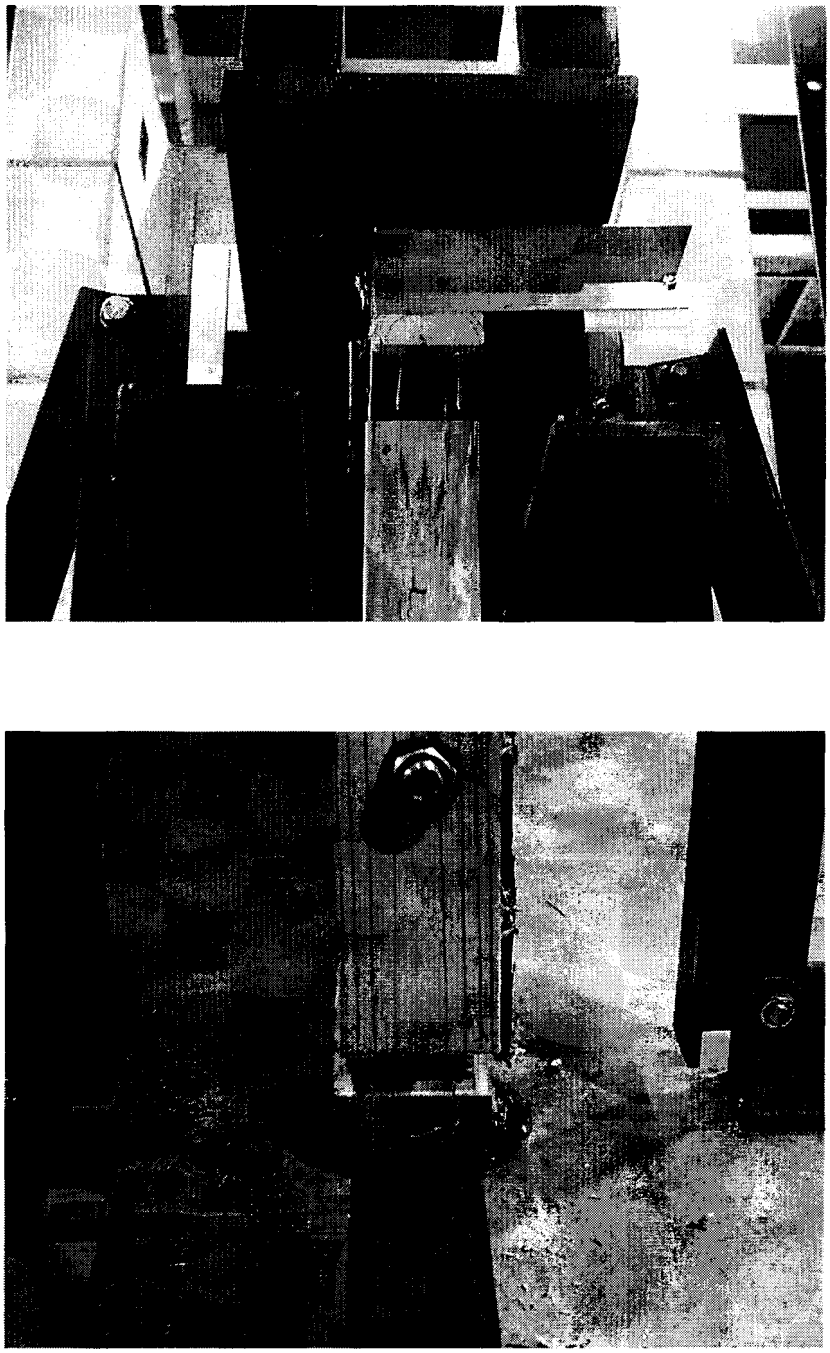

**Figure B.24 Failures Common in Static and Cyclic Tests of both Conventional and AOSB Shear Walls (Top: top plate lifting off; Bottom: separation of tension post and bottom plate)**

## BIOGRAPHY OF THE AUTHOR

Eric Dana Cassidy was born in Presque Isle, Maine on March 12, 1978. He graduated from Presque Isle High School in 1996. He attended the University of Maine and graduated cum laude in 2000 with a Bachelor's degree in Civil Engineering. He entered the Civil Engineering graduate program at the University of Maine in the spring of 2001. Eric is a candidate for the Master of Science degree in Civil Engineering from The University of Maine in December, 2002.